SAPIENZA
UNIVERSITÀ DI ROMA

Facoltà di Ingegneria Civile e Industriale
Dipartimento di Ingegneria Meccanica e Aerospaziale

A flamelet approach for the simulation of swirling turbulent non-premixed flames

THESIS ADVISOR:
Prof. Francesco Creta

AUTHOR:
Sebastián Sánchez Riera

CO-ADVISORS:
Dr. Pasquale Lapenna
Dr. Giuseppe Indelicato
Dr. Rachele Lamioni

Academic Year 2018/2019

Acknowledgements

Este Trabajo Final de Grado supone la culminación a cuatro años de esfuerzo y trabajo duro. Por ello, me gustaría aprovechar esta oportunidad para dar las gracias a todos aquellos que me han acompañado durante este tiempo, especialmente mis padres y hermano.

Agradecer también a la Universitat Politècnica de València y a la Escuela Técnica Superior de Ingeniería del Diseño por darme la oportunidad de cursar el Grado en Ingeniería Aeroespacial, así como a su profesorado.

Otra parte fundamental en todo este camino han sido los compañeros de la universidad, con quienes he tenido el placer de emprender, compartir y finalizar esta aventura.

Por último, pero no por ello menos importante, agradezco especialmente al Prof. Francesco Creta junto a Dr. Pasquale Lapenna, Dr. Giuseppe Indelicato y Dr. Raquele Lamioni por brindarme la oportunidad de trabajar en este Trabajo Final de Grado, depositando así toda su confianza en mí.

GRACIAS

Aquest Treball Final de Grau suposa la culminació a quatre anys d'esforç i treball dur. Per això, m'agradaria aprofitar aquesta ocasió per a donar les gràcies a tots aquells que m'han acompanyat al llarg d'aquest temps, especialment els meus pares i germà.

Agrair també a la Universitat Politècnica de València i a l'Escola Tècnica Superior d'Enginyeria del Disseny per brindar-me l'oportunitat de cursar el Grau en Enginyeria Aeroespacial, així com al professorat.

Una altra part fonamental en tot aquest camí han sigut els companys de la universitat, amb qui he tingut el plaer d'emprendre, compartir i finalitzar aquesta aventura.

Per últim, però no per això menys important, agraïsc especialment al Prof. Francesco Creta junt amb Dr. Pasquale Lapenna, Dr. Giuseppe Indelicato i Dr. Raquele Lamioni per brindar-me l'oportunitat de treballar en aquest Treball Final de Grau, depositant així tota la seua confiança en mi.

GRÀCIES

Abstract

Aerospace industry and its continuous seek for technological improvements are responsible for the innovations experienced during the last decades. In this sense, swirling flames constitute a point of interest for the combustion field, and its study is what has motivated this thesis project. In particular, the main objective of this work is to implement a swirling flow in OpenFOAM environment by setting a new boundary condition, named *swirl*. Then, both non-reactive and reactive flow simulations are carried out, whose analysis is done by comparing and validating them with experimental data.

Focusing onto the reactive case (swirling non-premixed flame), the methodology used is based on Computational Fluid Dynamics techniques which allow solving turbulent combustion problems through the implementation of a numerical approach known as Flamelet approach. It consists on decoupling the combustion process into two subsets: mixing and flame structure. This method is attainable thanks to the introduction of a passive scalar: the mixture fraction z.

La costante ricerca di miglioramenti tecnologici nell'ambito dell'industria aerospaziale è la principale responsabile delle innovazioni nel settore delle ultime decadi. In questo senso le $swirling\ flames$ costituiscono un punto di grande interesse nel mondo della combustione, la volontà di studiarle motiva la realizzazione di questa tesi. Nello specifico, l'obiettivo del lavoro riguarda l'implementazione di uno $swirling\ flow$ nell'ambiente di lavoro OpenFOAM attraverso la creazione di una nuova condizione di contorno chiamata swirl. Oltre a ciò sono effettuate sia simulazioni del flusso non reattivo che del flusso reattivo, queste sono poi analizzate e validate tramite il confronto dei risultati con dati sperimentali.

Concentrandosi sul caso del flusso reattivo ($swirling\ non-premixed\ flame$), la metodologia usata è basata sulle tecniche della Meccanica dei Fluidi Computazionale, le quali permettono di risolvere problemi di combustione turbolenta mediante l'uso di un approccio numerico chiamato *Flamelet approach*. Questo permette di disaccoppiare il processo di combustione in due parti: mescolamento e struttura della fiamma. Tale metodo è possibile grazie all'introduzione di uno scalare passivo: la frazione di miscela z.

La industria aeroespacial junto a su continua búsqueda de mejoras a nivel tecnológico son las principales responsables de las innovaciones experimentadas en el sector durante las últimas décadas. En esta línea, las *swirling flames* constituyen un punto de gran interés en el campo de la combustión, y su estudio es lo que ha motivado la realización de esta Trabajo Final de Grado. Específicamente, el objetivo de este proyecto es implementar un *swirling flow* en el ambiente de trabajo OpenFOAM a través de la creación de una nueva condición de contorno, llamada *swirl*. A continuación, tanto las simulaciones de flujo no reactivo como de flujo reactivo son llevadas a cabo, cuyo análisis consiste en la comparación y validación de los resultados con datos experimentales.

Centrándonos en el caso del flujo reactivo (*swirling non − premixed flame*), la metodología usada se basa en las técnicas de la Mecánica de Fluidos Computacional, las cuales permiten resolver problemas de combustión turbulenta mediante el uso de un enfoque numérico llamado *Flamelet approach*. Este permite desacoplar el proceso de combustión en dos partes: mezclado y estructura de la llama. Este método es posible gracias a la introducción de un escalar pasivo: la fracción de mezcla z.

La indústria aeroespacial i la seua continua recerca de millores a nivell tecnològic son les principals responsables de les innovacions experimentades en el sector durant les últimes dècades. En esta línia, les *swirling flames* constituïxen un punt de gran interès en el camp de la combustió, i el seu estudi es el que ha motivat la realització d'aquest Treball Final de Grau. De manera específica, l'objectiu d'aquest projecte és la implementació d'una nova condició de contorno, denominada *swirl*. A continuació, tant les simulacions de fluxos no reactius com reactius son dutes a terme, l'anàlisi de les quals es basa en la comparació i validació dels resultats amb dades experimentals.

Centrant-se en el cas del flux reactiu (*swirling non − premixed flame*), la metodologia usada es troba basada en les tècniques de la Mecànica de Fluids Computacional, les quals permeten resoldre problemes de combustió turbulenta mitjançant l'ús d'un enfocament numèric nomenat *Flamelet approach*. Aquest permet desacoblar el procés de combustió en dues parts: mesclat i estructura de la flama. Aquest mètode és possible gràcies a la introducció d'un escalar passiu: la fracció de mescla z.

Key words

Swirling non-premixed flames

Turbulent combustion

Flamelet approach

OpenFOAM environment

Contents

List of Figures

List of Tables

Nomenclature

Abbreviations

C_p	—	Constant pressure heat capacity	[J/(K · kg)]
D	—	Pipe diameter	[m]
D_{eq}	—	Equivalent pipe diameter	[m]
D_i	—	Internal pipe diameter	[m]
D_k	—	Molecular diffusivity of the k-th species	[mol/m^3]
D_o	—	Outer pipe diameter	[m]
Da	—	Damköhler number	[-]
Da_{ig}	—	Ignition Damköhler number	[-]
Da_q	—	Quenching Damköhler number	[-]
f_m	—	Body forces	[m/s^2]
h_s	—	Sensible enthalpy	[J/kg]
$K(T)$	—	Equilibrium constant	[-]
k	—	Turbulent kinetic energy	[J/kg]
L_0	—	Integral turbulence scale	[m]
Le	—	Lewis number	[-]
p	—	Pressure	[Pa]
$\dot{Q}$	—	Heat source per unit volume	[J/(m^3 · s)]
R	—	Air ideal gas constant	[J/(kg · K)]
Re	—	Reynolds number	[-]
r	—	Radial coordinate	[m]
S	—	Swirl number	[-]
S_g	—	Geometric Swirl number	[-]
T	—	Temperature	[K]
t	—	Time	[s]
t_c	—	Chemical time scale	[s]
t_f	—	Flow time scale	[s]
U	—	Mean axial velocity	[m/s]
u	—	Axial velocity	[m/s]
u'	—	Fluctuating axial velocity	[m/s]
V	—	Mean radial velocity	[m/s]
V_k	—	Diffusion velocity of k-th species	[m/s]
v	—	Radial velocity	[m/s]
v'	—	Fluctuating radial velocity	[m/s]
$\underline{v}$	—	Velocity vector	[m/s]
W	—	Mean tangential velocity	[m/s]
w	—	Tangential velocity	[m/s]
w'	—	Fluctuating tangential velocity	[m/s]

x	—	Longitudinal coordinate	[m]
Y	—	Mass fraction	[-]
Z	—	Passive scalar	[-]
z	—	Mixture fraction	[-]

Greek letters

ϵ	—	Eddy dissipation rate	$[m^2/s^3]$
λ	—	Thermal conductivity	$[W/(m \cdot K)]$
μ	—	Kinematic viscosity	$[Pa \cdot s]$
ν	—	Dynamic viscosity	$[m^2/s]$
ω	—	Angular velocity	[rad/s]
$\dot{\omega}_k$	—	Mass reaction rate of k-th species	$[kg/s \cdot m^3]$
$\dot{\omega}'_T$	—	Thermal reaction rate	$[J/(m^3 \cdot s)]$
ρ	—	Density	$[kg/m^3]$
σ	—	Stress	[Pa]
τ_{ij}	—	Viscous stress tensor	[Pa]
φ	—	Azimuthal angle	[°]
χ	—	Scalar dissipation	[1/s]
χ_{st}	—	Stoichiometric scalar dissipation	[1/s]

Acronyms

CFD	—	Computational Fluid Dynamics
DNS	—	Direct Numerical Simulations
FVM	—	Finite Volume Method
LES	—	Large Eddy Simulations
pdf	—	Probability density function
PVC	—	Precessing Vortex Core
RANS	—	Reynolds Averaged Navier-Stokes
SRS	—	Scale Resolving Simulations
VB	—	Vortex Breakdown

Chapter 1

Introduction

1.1 Motivation

For recent years, the use of swirling flows has become a common trend in a wide range of applications. The development experienced by the aerospace industry, which is continuously seeking for better performances while reducing costs, has motivated the introduction of swirling flows in an innovative way. Turbomachinery, large pipeline systems or combustion chambers are some good examples. In the past decades, most of the studies were focused on internal swirling flows, particularly flow in pipes, but recent investigations are pointing into a new direction, which is swirl injectors. During the development of this thesis, we will focus on this last application.

In this sense, swirling flames constitute a point of interest for the combustion field. They offer a wide range of advantages such as flame stabilization, reduction of unburned gases and mixing enhancement. These features are due to the creation of a recirculation bubble, which is related to a complex flow structure derived from the swirl motion. It is the so called Vortex Breakdown (VB) and it constitutes the dominant flame stabilisation mechanism thanks to its characteristic reverse flows (recirculation). This structure can eventually develop into a Precessing Vortex Core (PVC), whose oscillation contributes to the improvement in combustion efficiency and mixing.

1.2 Objectives

The main objective of this thesis project is to implement a swirling flow in OpenFOAM environment by setting a new boundary condition, named *swirl*. Once it is achieved, an intensive validation process is carried out by simulating both non reactive and reactive flow well known cases. In this way, the numerical results are compared with experimental data.

Focusing onto the reactive case (swirling flame), the methodology used is based on Computational Fluid Dynamics techniques which allow solving turbulent combustion problems through the implementation of a numerical approach known as Flamelet approach. It consists on decoupling the combustion process into two subsets: mixing and flame structure. This method is attainable thanks to the introduction of a passive scalar: the mixture fraction z. The solver used is flameletPimpleSMOKE, which is a solver belonging to Dipartamento di Ingegneria Meccanica e Aerospaziale of Sapienza University of Rome.

Regarding the simulations, Realizable $k - \epsilon$ (RANS) model is used for turbulence modelling due to its reduced computational cost. As a consequence, the suitability of this model will be also analysed.

So, to sum up, the objectives of the present work are to introduce a swirl motion in OpenFOAM environment as well as, to analyse the requirements imposed by swirling flames in terms of turbulence modelling.

Chapter 2

Theoretical framework

The aim of this chapter is to set the theoretical basics needed to develop this thesis project. As starting point, a brief comment about combustion is done in order to introduce the main general concepts and the different types of combustion. After that, the focus is pointed into non-premixed flames, whose study through computational fluid dynamics techniques constitutes our scope.

To fully describe non-premixed flames, laminar diffusion flames are explained before moving to the turbulent ones. A fundamental part of this chapter is given by the description and characterization of the computational approach used, which is based on the flamelet assumption.

Finally, swirling flames are explained by characterising a swirling flow as well as introducing its applications in the combustion field.

2.1 Introduction to combustion

A commonly extended academic definition of combustion is: " Combustion is a high temperature exothermic redox (reduction-oxidation) chemical reaction between a **fuel** (the reductant which is oxidized) and an **oxidizer** (which is reduced), usually atmospheric oxygen ".

A more useful definition is: " Combustion is the rearrangement of atoms and, thus, of chemical covalent bonds between reactants and products " . It means that nuclear reactions are not involving a combustion process, since atoms are changed. However, chemical reactions, which may involve a combustion process if a fuel and oxidizer are present, only rearrange the atoms (elements) to form new molecules (species), i.e. atoms are conserved. Then, combustion involves two process: chemical reactions with its consequent production of heat and the convective/diffusive transport of heat and molecules. [1]

One forward step can be done by introducing the two types of combustion. They can be classified into: [2]

- Premixed combustion: It is characterised by the presence of a combustable mixture of fuel and oxidizer. Once ignition occurs, the resulting premixed flame tends to act as a sink for reactants and a source of products. Thus, it will tend to propagate into the unburned mixture. Then, premixed combustion is a wave phenomenon that implies propagation. Depending on the velocity of the combustion wave, premixed combustion

can be classified into deflagrations (flames) and detonations. While flames are subsonic and controlled, detonations are subsonic and uncontrolled.

– Non-premixed (diffusive) combustion: It is a typical flame for most combustion systems where fuel and oxidizer are initially separated. For example, a coaxial burner having a central fuel nozzle and an outer oxidizer nozzle will give rise to a non-premixed flame. This is the case studied in this thesis project. In addition, candle flame and droplet combustion also constitute good examples of non-premixed combustion.

2.2 Laminar diffusion flames

Diffusion flames constitute a specific class of combustion problems where fuel and oxidizer are not mixed before they enter the combustion chamber: for these flames, mixing must bring reactants into reaction zone fast enough for combustion to proceed. Then, **mixing** becomes one of the main issues in diffusion flames.

2.2.1 Main characteristics

Diffusion flame structure is reported in Fig. (2.1). (Ref. [3])

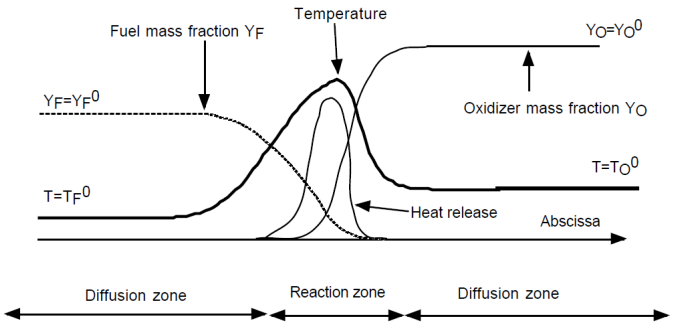

Figure 2.1: Laminar diffusion flames - Flame structure

From Fig. (2.1), two different boundary states are considered: fuel on the left and oxidizer on the right, which may be diluted or not. They diffuse towards the reaction zone where they burn and, thus, generate heat. As a consequence, temperature is maximum in this zone and diffuses away from the flame front towards the fuel and oxidizer streams. Additionally, the main characteristics of a laminar diffusive flame are defined:

– Far away on each side of the flame, the gas is either too rich or too lean to burn. Chemical reactions can only proceed in a limited region, where fuel and oxidizer are properly mixed. A diffusion flame usually lies along the points where mixture is found in an approximately stoichiometric proportion. At this region, heat release occurs (Fig. (2.1)).

  This means that a diffusion flame does not exhibit a reference speed (as premixed flames) since it is unable to propagate towards fuel because of the lack of oxidizer and, in an analogous way, it cannot propagate towards oxidizer due to insufficient amount of fuel.

– The flame structure is steady only when strain if applied to the flame, i.e. when fuel and oxidizer streams are pushed against each other at a given speed. In this way, a stationary plane where reaction occurs is formed, as shown in Fig. (2.2) (Ref. [4]).

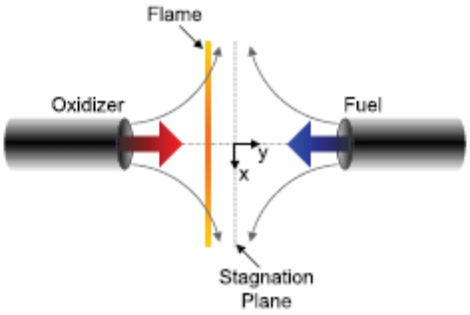

Figure 2.2: Laminar diffusion flames - Stretched flame

- It does not have a reference thickness: this is different from premixed flames where a thickness may be introduced and depends on the fluid properties and the flame speed.
- As previously commented, mixing is the key characteristic of diffusion flames. These flames are simpler to design and to build: no premixing, with a given equivalence ratio, is required. They are also safer to operate because they do not propagate. However, their burning efficiency is reduced compared to premixed flames because mixing reduces the speed at which chemical reactions may proceed.

In diffusion flames, fluid dynamics and combustion are strictly connected, each concurring with proper and different time-scales: this is cause of discretization problems in time and space and of an inherent stiffness in the numerical solution of the governing Navier-Stokes equations for a reactive and compressible mixture. Then, to limit the computational cost, a conserved scalar model is introduced: the use of a passive (non reacting) scalar as independent variable allows decoupling the original problem into two subsets: **mixing** and **flame structure**.

Taking advantage of this fact, the numerical solution of turbulent flow is separated from the solution of the chemistry [5], which can be stored in appropriate libraries without affecting the run time solution. During this thesis project, it is explained how to exploit this capability by introducing a combustion model known as **flamelet model**.

2.2.2 Governing equations

To describe a diffusion laminar flame, it is appropriate to consider the Navier-Stokes equations for a compressible and reactive mixture composed by N species as starting point. The conservation equations, described using the Einstein notation, are written as:

- Mass conservation:

$$\frac{\partial \rho}{\partial t} + \frac{\partial \rho u_i}{\partial x_i} = 0 \tag{2.2.1}$$

- Momentum conservation:

$$\frac{\partial}{\partial t}\left(\rho u_i\right) + \frac{\partial}{\partial x_j}\left(\rho u_i u_j\right) = \frac{\partial \sigma_{ij}}{\partial x_j} + \rho \sum_{k=1}^{N} Y_k f_{k,j} \tag{2.2.2}$$

– Mass fraction conservation for the k-th species:

$$\frac{\partial \rho Y_k}{\partial t} + \frac{\partial}{\partial x_i}\left(\rho(u_i + V_{k,i})Y_k\right) = \dot{\omega}_k \tag{2.2.3}$$

– Energy equation in terms of sensible enthalpy h_s:

$$\rho C_p \frac{DT}{Dt} = \frac{Dp}{Dt} + \frac{\partial}{\partial x_j}\left(\lambda \frac{\partial T}{\partial x_j}\right) + \tau_{ij}\frac{\partial u_i}{\partial x_j} + \dot{Q} + \rho \sum_{k=1}^{N} Y_k f_{k,i} V_{k,i} + \dot{\omega}'_T - \left(\rho \sum_{k=1}^{N} Y_k C_{p,k} V_{k,i}\right)\frac{\partial T}{\partial x_j} \tag{2.2.4}$$

where the terms $V_{k,i}$ are the species diffusion velocities, $f_{k,j}$ the body forces and σ_{ij} a tensor given from the combination of the viscous tensor τ_{ij} and pressure $p\delta_{ij}$. It is defined in the following way:

$$\sigma_{ij} = \tau_{ij} - p\delta_{ij} \qquad \tau_{ij} = -\frac{2}{3}\mu \frac{\partial u_k}{\partial x_k}\delta_{ij} + \mu\left(\frac{\partial u_i}{\partial x_j} + \frac{\partial u_j}{\partial x_i}\right) \tag{2.2.5}$$

Note that $i = 1, ..., 3$, $j = 1, ..., 3$ and $k = 1, ..., N$ for Eqs. (2.2.1), (2.2.2), (2.2.3) and (2.2.4); while $k = 1, ..., 3$ for Eq. (2.2.5).

At this point, three simplifying hypothesis are introduced [5]:

H1. Equal diffusion coefficients ($D_k = D$) are assumed, while Fick's law, without velocity correction, is used for molecular diffusion velocities. Then:

$$\frac{\partial}{\partial x_i}\left(\rho V_{k,i} Y_k\right) = -\frac{\partial}{\partial x_i}\left(\rho D \frac{\partial Y_k}{\partial x_i}\right) \tag{2.2.6}$$

H2. Equal specific heat capacities ($C_{p,k} = C_p$), which do not depend on temperature, are assumed. This means that Lewis number, which expresses the relation between thermal and molecular diffusion, is also equal ($Le_k = \frac{\lambda}{\rho C_p D_k} = Le$, with $k = 1, ..., N$).

H3. Thermodynamic pressure ($p_0 = \rho RT$) is constant and Mach numbers are small.

H1 and H2 assumptions allow to simplify the flame analysis while introducing very small errors, which are negligible since fluxes due to turbulent transport are of higher order with respect to species and heat diffusion terms.

Further comments about the conservation equations can be done:

– Under H2 assumption and being the term $\sum_{k=1}^{N} Y_k V_{k,i} = 0$ by definition, also the term $\rho \sum_{k=1}^{N}(Y_k C_{p,k} V_{k,i})$ is null (Eq. (2.2.4)).

– In Eq. (2.2.2), the divergence of the term σ_{ij} tensor appears: when applied to the pressure term $p\delta_{ij}$, in the low Mach number formulation, it returns only the derivatives of the hydrodynamic pressure p_i, being the thermodynamic pressure p_0 homogeneous in space and also constant in time for open domains. [5]

– The heat source $\dot{Q}$ in Eq. (2.2.4) does not include the heat released by reaction, i.e $\dot{\omega}_T = -\sum_{k=1}^{N} \Delta h^0_{f,k} \dot{\omega}_k$, which is equal to $\dot{\omega}'_T = -\sum_{k=1}^{N} h^0_k \dot{\omega}_k$ having the species involved the same sensible enthalpies and being $\sum_{k=1}^{N} \dot{\omega}_k = 0$ by definition.

– Low Mach number formulation allows also to neglect the variations of pressure, i.e. $\frac{Dp}{DT}$, as well as the heating viscous term $\tau_{ij}\frac{\partial u_i}{x_j}$. Both of them are contained in Eq. (2.2.4).

– Additionally, body forces $f_{k,i}$ can be neglected due to the low densities characterising the combustion gases. A term associated to body forces is present in Eqs. (2.2.2) and (2.2.4)

Then, by considering all the previous assumption, the conservation equations read as:

– Mass conservation:

$$\frac{\partial \rho}{\partial t} + \frac{\partial \rho u_i}{\partial x_i} = 0 \tag{2.2.7}$$

– Momentum conservation:

$$\frac{\partial}{\partial t}\left(\rho u_i\right) + \frac{\partial}{\partial x_j}\left(\rho u_i u_j\right) = \frac{\partial \sigma_{ij}}{\partial x_j} \tag{2.2.8}$$

– Mass fraction conservation for the k-th species:

$$\frac{\partial \rho Y_k}{\partial t} + \frac{\partial}{\partial x_i}\left(\rho u_i Y_k\right) = \frac{\partial}{\partial x_i}\left(\rho D \frac{\partial Y_k}{\partial x_i}\right) + \dot{\omega}_k \tag{2.2.9}$$

– Energy equation in terms of sensible enthalpy h_s:

$$\rho C_p \frac{DT}{Dt} = \frac{\partial}{\partial x_j}\left(\lambda \frac{\partial T}{\partial x_j}\right) + \dot{Q} + \dot{\omega}'_T \tag{2.2.10}$$

2.2.3 Passive scalars and mixture fraction

The starting point of the diffusion flames analysis is to assume idealised situations using a passive scalar (or mixture fraction z).

Considering a single-step chemical reaction (M=1), which only involves fuel (F), oxidizer (O) and products (P), the chemical system is written as follows:

$$\sum_{k=1}^{N} \nu'_k M_k \rightleftharpoons \sum_{k=1}^{N} \nu''_k M_k \quad \Rightarrow \quad \nu_F F + \nu_O O \rightleftharpoons \nu_P P \tag{2.2.11}$$

where ν_k is the stoichiometric coefficient corresponding to the k-th species.

Next, the definition of $\dot{\omega}_k$ can be introduced by relating it to the single-step reaction rate $\mathbb{Q}$:

$$\dot{\omega}_k = W_k \nu_k \mathbb{Q} \tag{2.2.12}$$

Note that molecular weight of k-th species (W_k) is introduced to satisfy the units equality. As known, the reaction rate $\dot{\omega}_k$ is expressed as a variation of density with time, while $\mathbb{Q}$ refers to the variation of molar concentration in time.

Moreover, $\dot{\omega}_k$ allows to link temperature, oxidizer and fuel reaction rates thanks to the heat term Q and the mass stoichiometric ratio s:

$$\begin{cases} \dot{\omega}_O = s\dot{\omega}_F \ ; \quad with \ \ s = \frac{\nu_O W_O}{\nu_F W_F} \\ \dot{\omega}_T = -Q\dot{\omega}_F \ ; \quad with \ \ Q = \frac{Q^m}{W_F} \end{cases} \tag{2.2.13}$$

In particular, Q^m is the heat released by the combustion of 1 mol of fuel.

Using Eq. (2.2.13), the conservation equations for fuel and oxidizer mass fractions and temperature become:

$$\frac{\partial \rho Y_F}{\partial t} + \frac{\partial}{\partial x_i}\left(\rho u_i Y_F\right) = \frac{\partial}{\partial x_i}\left(\rho D \frac{\partial Y_F}{\partial x_i}\right) + \dot{\omega}_F \tag{2.2.14}$$

$$\frac{\partial \rho Y_O}{\partial t} + \frac{\partial}{\partial x_i}\left(\rho u_i Y_O\right) = \frac{\partial}{\partial x_i}\left(\rho D \frac{\partial Y_O}{\partial x_i}\right) + s\dot{\omega}_F \tag{2.2.15}$$

$$\frac{\partial \rho T}{\partial t} + \frac{\partial}{\partial x_i}(\rho u_i T) = \frac{\partial}{\partial x_j}\left(\frac{\lambda}{C_p}\frac{\partial T}{\partial x_j}\right) - \frac{Q}{C_p}\dot{\omega}_F \tag{2.2.16}$$

In Eq. (2.2.16), the heat source term $\dot{Q}$ has been neglected because the radiative heat fluxes represents a small percentage.

Now, it is pretended to obtain fuel, oxidizer and temperature equations as independent from fuel reaction rate $\dot{\omega}_F$. This can be done by combining Eqs. (2.2.14), (2.2.15) and (2.2.16) two by two. These are:

1. { $s \cdot$ (Eq. (2.2.14)) - (Eq. (2.2.15)) }
2. { (Eq. (2.2.14)) + $\frac{C_p}{Q} \cdot$ (Eq. (2.2.16)) }
3. { (Eq. (2.2.15)) + $\frac{sC_p}{Q} \cdot$ (Eq. (2.2.16)) }

Performing these three mathematical operations, the following equations are obtained:

$$\frac{\partial \rho(sY_F - Y_O)}{\partial t} + \frac{\partial \rho u_i(sY_F - Y_O)}{\partial x_i} = \frac{\partial}{\partial x_i}\left(\rho D \frac{\partial (sY_F - Y_O)}{\partial x_i}\right) \tag{2.2.17}$$

$$\frac{\partial \rho(Y_F + \frac{C_p T}{Q})}{\partial t} + \frac{\partial \rho u_i(Y_F + \frac{C_p T}{Q})}{\partial x_i} = \frac{\partial}{\partial x_i}\rho D\left(\frac{\partial Y_F}{\partial x_i} + Le\frac{\partial \frac{C_p T}{Q}}{\partial x_i}\right) \tag{2.2.18}$$

$$\frac{\partial \rho(Y_O + \frac{sC_p T}{Q})}{\partial t} + \frac{\partial \rho u_i(Y_O + \frac{sC_p T}{Q})}{\partial x_i} = \frac{\partial}{\partial x_i}\rho D\left(\frac{\partial Y_O}{\partial x_i} + Le\frac{\partial \frac{sC_p T}{Q}}{\partial x_i}\right) \tag{2.2.19}$$

It can be observed that these last three transport equations are independent from the reaction rates, as it was intended. Additionally, a new hypothesis can be considered:

H4. It is assumed that Le=1, i.e. molecular diffusion of species is of the same order of thermal diffusion. In turbulent flows, molecular species diffusion become relevant only close to the injection zone, where the scalar dissipation is higher and, thus, the mixing region is laminar, being so thin that vortices do not enter. Downstream, the flame structures broadens and the enhanced turbulent transport satisfies the hypothesis on the unitary Lewis number.

H4 assumption allows to define three different passive scalars. These are:

$$Z_1 = sY_F - Y_O \quad ; \quad Z_2 = Y_F + \frac{C_p T}{Q} \quad ; \quad Z_3 = Y_O + \frac{sC_p T}{Q} \tag{2.2.20}$$

Note that the three passive scalars follow the same balance equation, which is not containing any source term, and then it is **independent from the reaction**. The passive scalar Z_j only varies due to diffusion and convection. By introducing passive scalars definition, given by Eq. (2.2.20), into Eqs. (2.2.17), (2.2.18) and (2.2.19), the following expression is obtained.

$$\frac{\partial \rho Z_j}{\partial t} + \frac{\partial \rho u_i Z_j}{\partial x_i} = \frac{\partial}{\partial x_i}\left(\rho D \frac{\partial Z_j}{\partial x_i}\right) \tag{2.2.21}$$

Although reaction rates are not present in Eq. (2.2.21), boundary conditions are depending on the passive scalar, i.e. Z_1, Z_2 and Z_3. To solve this issue, Z_j can be normalised. So, a new variable is defined z_j.

$$z_j = \frac{Z_j - Z_{j,O}}{Z_{j,F} - Z_{j,O}} \tag{2.2.22}$$

Due to the normalisation $z_1 = z_2 = z_3 = z$, which is the so-called **mixture fraction**. It measures the local fuel/oxidizer ratio. Then, Eq. (2.2.21) can be rewritten as:

$$\frac{\partial \rho z}{\partial t} + \frac{\partial \rho u_i z}{\partial x_i} = \frac{\partial}{\partial x_i}\left(\rho D \frac{\partial z}{\partial x_i}\right) \tag{2.2.23}$$

with $z = 1$ at the fuel side and $z = 0$ at the oxidizer side as boundary conditions. If Z_1 is substituted into Eq. (2.2.22), a new definition for z can be found, where the equivalence ratio ϕ is introduced.

$$z = \frac{sY_F - Y_O + Y_O^0}{sY_F^0 + Y_O^0} = \frac{1}{1+\phi}\left(\phi \frac{Y_F}{Y_F^0} - \frac{Y_O}{Y_O^0} + 1\right) \quad with \quad \phi = s\,\frac{Y_F^0}{Y_O^0} \tag{2.2.24}$$

Once the new transport equation for z has been defined, it is possible to express the flame structure in terms of the mixture fraction z and time t only:

$$Y_k = Y_k(z,t) \quad ; \quad T = T(z,t) \tag{2.2.25}$$

This allow separating the chemistry problem from the solution of the transport equation for the new variable z: this is done by using the Laminar Flamelet Model, described in detail in the next section.

2.2.4 Laminar Flamelet Model

Laminar Flamelet Model is based on a new assumption: the **flamelet assumption**, which is the basis of many models for turbulent combustion. It is:

H5. The flame is assumed to be thin compared to other flow and turbulence scales, which implies that the chemical time scales are much smaller than the characteristic flow time scales (i.e. large Damköhler number).

$$Da = \frac{t_f}{t_c} \tag{2.2.26}$$

This assumption means that, if $t_f >> t_c$ (flow time scale $>>$ chemical time scale), the reactions happen within times and zones so small that they have no means of interacting with turbulent phenomena and therefore the flame structure remains laminar. Each element of the flame front is viewed as a small laminar flame also called $flamelet$. Formally, this new assumption is a variable change in the species equation from (x_1, x_2, x_3, t) to (z, y_2, y_3, t), where y_2, y_3 are the spatial variables in planes parallel to the iso-z surfaces. In the resulting equations, terms corresponding to gradients along the flame front, i.e. along y_2 and y_3, are neglected in comparison to terms normal to the flame, i.e. along z.

On the basis of the flamelet assumption, the structure of the diffusion flame only depends on the mixture fraction z and on time t, as already noted in Eq. (2.2.25). Under this hypothesis, the species mass fractions and temperature balance equations may be rewritten:

$$\rho \frac{\partial Y_k}{\partial t} = \rho D \left(\frac{\partial z}{\partial x_i} \frac{\partial z}{\partial x_i} \right) \frac{\partial^2 Y_k}{\partial z^2} + \dot{\omega}_k \tag{2.2.27}$$

$$\rho \frac{\partial T}{\partial t} = \rho D \left(\frac{\partial z}{\partial x_i} \frac{\partial z}{\partial x_i} \right) \frac{\partial^2 T}{\partial z^2} + \dot{\omega}_T \tag{2.2.28}$$

Now, a new variable is introduced: the Scalar Dissipation χ, which has the dimension of an inverse time [$1/s$ or Hz], like the strain. It measures the gradients of mixture fraction and the molecular fluxes of species towards the flame.

It is directly influenced by the strain: in fact, when the flame strain rate increases, χ also increases. It is defined as:

$$\chi = 2D \left(\frac{\partial z}{\partial x_i} \frac{\partial z}{\partial x_i} \right) \tag{2.2.29}$$

Once χ is introduced, Eqs. (2.2.27) and (2.2.28) can be expressed as:

$$\rho \frac{\partial Y_k}{\partial t} = \frac{1}{2} \rho \chi \frac{\partial^2 Y_k}{\partial z^2} + \dot{\omega}_k \tag{2.2.30}$$

$$\rho \frac{\partial T}{\partial t} = \frac{1}{2} \rho \chi \frac{\partial^2 T}{\partial z^2} + \dot{\omega}_T \tag{2.2.31}$$

Eqs. (2.2.30) and (2.2.31) are the *Flamelet Equations*, which are key elements in many diffusion flame theories. In these equations, the only term depending on spatial variables (x_i) is just χ, which controls the mixing. Once χ is specified, the flamelet equations can be entirely solved in z-space to provide the flame structure, i.e. temperature T and species mass fractions Y_k as functions of z and time t.

This means that diffusion flame computations, whose objective is to find $T(x_i, t)$ and $Y_k(x_i, t)$, are split into two problems, as initially intended:

- A mixing problem where Eq. (2.2.23) must be solved to obtain the mixture fraction field $z(x_i, t)$ as a function of spatial coordinates x_i and time t.
- A flame structure problem where flame variables are found. They are the species mass fractions $Y_k(z)$ and temperature $T(z)$, which are solutions of Eqs. (2.2.30) and (2.2.31), respectively.

Later, the link between flames variables and z are used to construct all the flame variables ($Y_k(x_i,t)$ and $T(x_i,t)$). The procedure followed is summarise in Fig. (2.3) (Ref. [3]). Finally, note that T and Y_k are parametrised by the scalar dissipation χ: different values of χ lead to different flame structures.

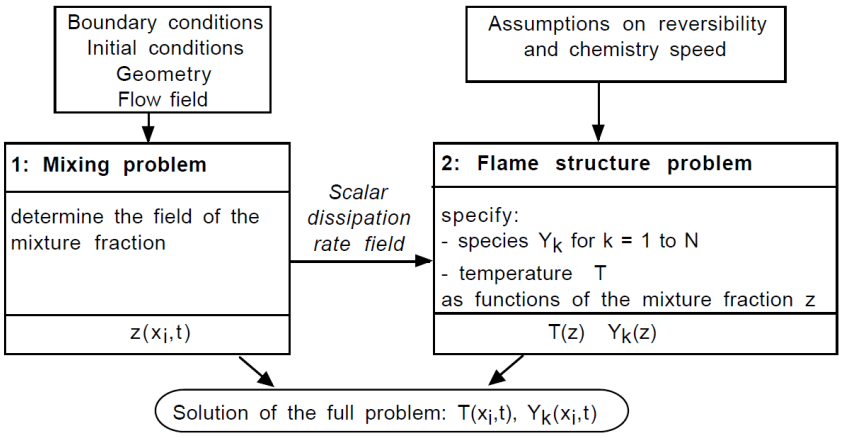

Figure 2.3: Laminar diffusion flames - Problem decoupling

2.2.5 Diffusion flame structures

It is possible to predict different diffusion flames structures by doing some assumptions on the chemistry mechanism, such as:

- Equilibrium condition (Infinitely Fast Chemistry): chemical reactions proceed locally so fast that equilibrium is instantaneously reached. The fast chemistry is controlled by Da number, which has been already introduced when studying the flamelet laminar model.
- Irreversible condition: chemical reactions only proceed from reactants to products side (unidirectional).

Combining these two assumptions leads to four possible solutions:

· For infinitely fast and irreversible chemistry, fuel and oxidizer cannot coexist at the same time: once mixing is achieved, the reactants are instantaneously depleted and an infinitely thin flame separates F and O. This simplest "equilibrium" assumption is called *irreversible fast chemistry*, in which $T(z)$ and $Y_k(z)$ functions are independent from scalar dissipation rate.

· For infinitely fast but reversible chemistry, fuel, oxidizer and products mass fractions are linked by the equilibrium relation (being $K(T)$ the equilibrium constant at temperature T):

$$K(T) = \frac{Y_F^{\nu_F} \cdot Y_O^{\nu_O}}{Y_P^{\nu_P}} \tag{2.2.32}$$

For this case, the flame structure is still independent of the flow condition. In other words, scalar dissipation rate χ is not playing any role when infinitely fast chemistry is considered. In particular, $\chi = 0$ for reversible and fast chemistry. In this case, fuel and oxidizer may be found simultaneously at the same location and time.

· For irreversible but not infinitely fast chemistry, fuel and oxidizer may also exist simultaneously, but their concentration now depends on the scalar dissipation rate χ. Temperature and mass fractions must be parametrised by χ.

· For reversible and not infinitely fast chemistry, which is the general case, there are no simple models to express the dependency of $T(z)$ and $Y_k(z)$ on χ.

Further comments can be done for all the equilibrium cases (fast chemestry, i.e. $\dot{\omega}_k = 0$) if the steady flamelet equation is considered. It is obtained from Eq. (2.2.30) and it reads as:

$$\dot{\omega}_k = -\frac{1}{2}\rho\chi\frac{\partial^2 Y_k}{\partial z^2} = 0 \tag{2.2.33}$$

This equation can be satisfied if:

$$\begin{cases} \frac{\partial^2 Y_k}{\partial z^2} = 0 \quad (1) \\ \chi = 0 \quad (2) \end{cases} \tag{2.2.34}$$

Relation (1) refers to two different sub-problems:

– A pure mixing problem, where oxidizer and fuel mix without reacting. This process is known as **frozen chemistry**.

– An infinitely fast chemistry problem for irreversible reactions, where infinitely thin flame separates fuel and oxidizer. In fact, there are not coexisting zones of fuel and oxidizer, being reactants instantaneously depleted once supplied to the reaction zone. This phenomena is reported in Fig. (2.4) (Ref. [3]), which describes Burke-Schumann solution for the flame structure. [6]

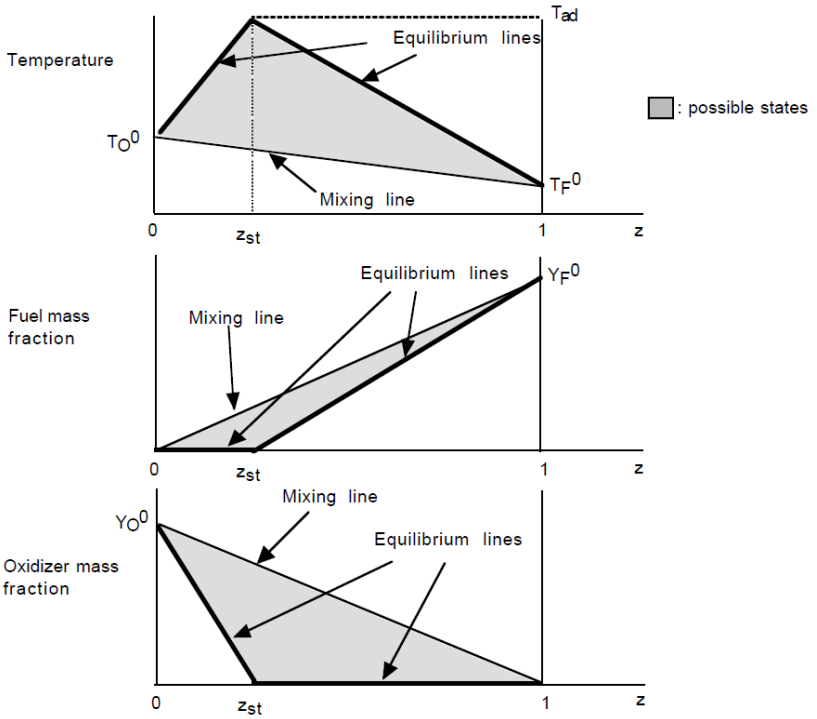

Figure 2.4: Laminar diffusion flames - Burke-Schumann solution for fast and irreversible reactions

On the other hand, relation (2) allows to relax the strong constraint on irreversible chemistry. Then, it considers the more general context of reversible reactions, for which a full equilibrium calculation is required. It is governed by Eq. (2.2.32).

All the described situations are summarised in terms of temperature plots in the z-space in Fig. (2.5) (Ref. [3]). It can be observed that chemistry effects are only important in the zone where reaction takes place and this zones usually remains small. Outside this region, combustion is zero and the behaviour of the thermofluid properties is independent from the chemistry.

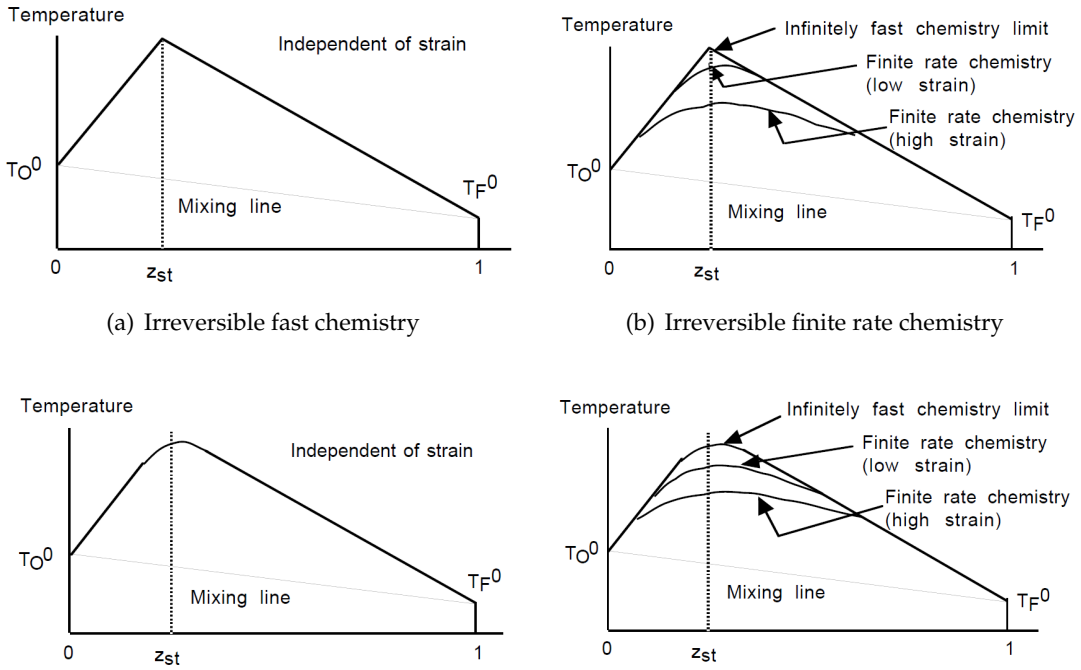

(a) Irreversible fast chemistry

(b) Irreversible finite rate chemistry

(c) Reversible fast chemistry

(d) Reversible finite rate chemistry

Figure 2.5: Laminar diffusive flames - Chemistry processes

Additionally, the main properties of the chemistry processes described are grouped in Table (2.1).

Chemistry Mechanism	Fast chemistry (equilibrium): $\dot{\omega}_k = 0$	Finite rate mechanism (non equilibrium): $\dot{\omega}_k \neq 0$
Irreversible chemestry	F and O cannot coexist (independently of χ)	F and O may overlap in reaction zone (depending on χ)
Reversible chemestry	F, O and P are in equilibrium ($\chi = 0$)	No simple model for this case (depending on χ)
Frozen (pure mixing)	F and O mix but do not burn	Not applicable

Table 2.1: Laminar diffusion flames - Chemistry mechanism

To conclude, it is possible to analyse the effect of the scalar dissipation χ on the flame by introducing the S-shaped diagram (Fig. (2.6)) (Ref. [3]).

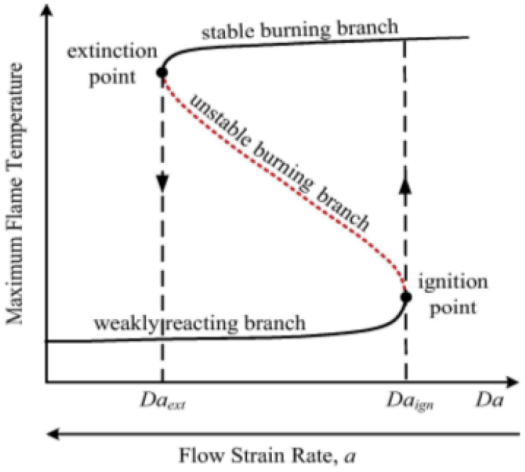

Figure 2.6: Laminar diffusion flames - Burke-Schumann solution for fast and irreversible reactions

Fig. (2.6) shows the maximum flame temperature profile as a function of the Damköhler number Da or the strain rate a. Note that a is equivalent to the stoichiometric scalar dissipation χ_{st} value.

Each point of this curve represents a thermochemical state of a diffusion flame as obtained by solving the flamelet equations. In particular, laminar flame solutions proceed along the burning branch of the S-shaped flame-response curve, moving from near-equilibrium solutions towards the extinction point. The unstable branch of this curve goes from the extinction point down to the mixing/non-reacting branch. At the quenching scalar dissipation value, large scalar gradients drive cold reactants to rapidly diffuse into the inner reactive layer of the flame and dilute the hot products. The resulting cooling overwhelms the Arrhenius reaction rates and the flame extinguishes. The lower branch represents adiabatic mixing of the fresh mixture. Consequently, the collection of laminar flame solution on the S-shaped curve provides insights into how the chemistry would interact with the strained mixing fields in a turbulent flow.

By increasing the χ_{st} value, the flame strain increases until the flow speed becomes large enough to supply reactants in the reaction zone and then let reactions proceed: the value at which the flame ignites is χ_{st} (i.e. Da_{ig}). Considering the flame burning and further increasing the strain, moving to the left of the diagram in the upper branch, the heat conduction from the reaction to the mixing zones increases until it exceeds the heat released: under these conditions the maximum temperature decreases, until the quenching scalar dissipation χ_q (i.e. Da_q) is achieved and the extinction flame occurs.

2.3 Introduction to turbulent combustion

Once the bases of laminar combustion applied to diffusion flames have been set, turbulent combustion is introduced. Before moving to turbulent non-premixed flames (i.e. diffusion flames), turbulent flows should be described. In particular, to focus on the interaction between turbulence and combustion is of utmost importance, as well as to introduce the computational approaches used to solve turbulent combustion.

2.3.1 Turbulent flows

By definition, turbulence is not a flow property (such as density or viscosity). Turbulence is considered a flow state, since it is not depending on its origin and it is characterised by sudden and irregular fluctuations in the flow properties (for example, velocity or pressure). In addition, a turbulent flow is irrotational (vortices) and highly diffusive and dissipative.

This last characteristic is what holds Richarson's definition of turbulence: "Big whirls have little whirls that feed on their velocity, and little whirls have lesser whirls and so on to viscosity". So, turbulence is constituted by an initial production of energy, which is dissipated by breaking big vortices into smaller ones until viscosity fully dissipates these smaller vortices. This phenomenon is known as **energy cascade** [7], which describes the transfer of energy between the different turbulence length scales. These are: [7]

- **Integral scale** (L_0). Turbulent flows always occur for high Reynolds numbers. For high Re, the energy cascade model of Kolmogorov establishes a transport of kinetic energy from the main flow to the bigger vortices or eddies. These eddies are characterised by length scales with the same order of magnitude of the main flow, with a high level of anisotropy and with low fluctuation frequencies. Then:

$$L_{ref} \sim L_0 \quad ; \quad Re_0 >> 1 \tag{2.3.1}$$

- **Taylor scale (λ)**. A turbulent eddy can be thought of as a local swirling motion, whose characteristic dimension is the local turbulence scale. Eddies overlap in space, where larger ones carry smaller ones. Then, as the turbulence decays, its kinetic energy goes from larger to smaller vortices. Then, an intermediate scale between the largest and the smallest vortices size can be defined. At Taylor scale, inertia and viscosity effects are more or less balanced. This leads to the following characteristic:

$$\frac{\lambda}{L_0} \sim \frac{1}{Re_0^{1/2}} \quad ; \quad Re_\lambda > 1 \tag{2.3.2}$$

- **Kolmogorov scale (μ)**. This is the smallest spatial scale. At this scale, the smaller vortices are dissipated and converted into internal energy by means of the viscous forces (molecular viscosity). Kolmogorov scales are characterised by high fluctuation frequencies and isotropic structures. This scale is defined by:

$$\frac{\mu}{L_0} \sim \frac{1}{Re_0^{3/4}} \quad ; \quad Re_\mu = 1 \tag{2.3.3}$$

Once turbulence scales have been defined, some further comments about the **energy cascade** can be done. Kolmogorov defined a region, known as inertial subrange, in which there is an energy conversion without dissipation from large scales to small scales. Then, he established "**the 5/3 Law**", which describes the slope of the energy cascade in the inertial subrange. The expression found through dimensional analysis (Pi-Buckingham Theorem [8]) is:

$$E(k) \sim Ak^{-5/3}\epsilon^{2/3} \tag{2.3.4}$$

A new concept has been introduced in Eq. (2.3.4), which is the eddy dissipation (ϵ). Additionally, energy cascade phenomenon is summarised in Fig. (2.7) (Ref. [7]). These two concepts become essential when RANS turbulence models are used to carry out CFD simulations.

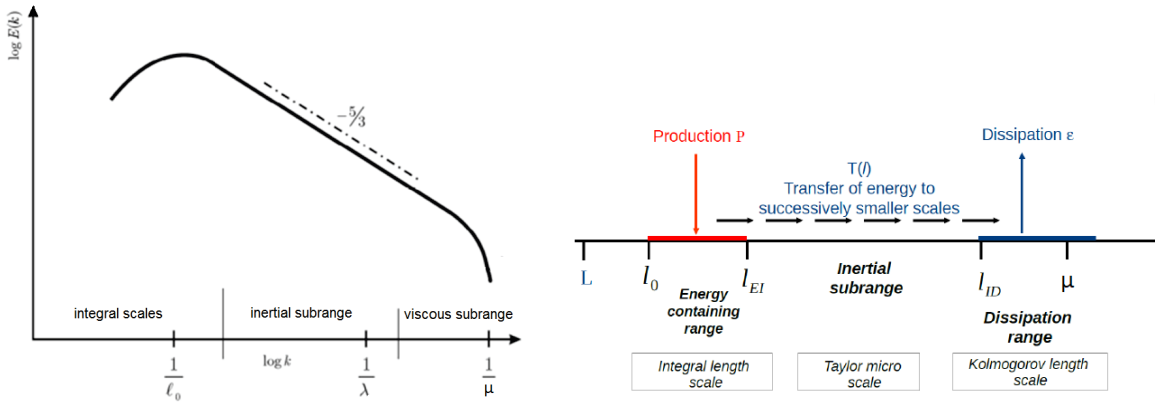

(a) Evolution of the turbulent kinetic energy

(b) Ranges and length scales

Figure 2.7: Introduction to turbulent combustion - Energy Cascade

2.3.2 Interaction between combustion and turbulence

Turbulent combustion results from the two-way interaction of chemistry and turbulence. When a flame interacts with a turbulent flow, turbulence is modified by combustion because of the strong flow accelerations through the flame front induced by heat release, and because of the large changes in kinematic viscosity associated with temperature changes. This mechanism, named flame-generated turbulence, may generate turbulence or damp it (re-laminarization due to combustion). On the other hand, turbulence alters the flame structure, may enhance chemical reactions increasing the reactions rates, but also, in extreme cases, completely inhibit it, leading to flame quenching.

2.3.3 Computational approaches for turbulent combustion

Turbulent combustion occurs in most practical combustion systems and its analysis is an important issue to develop and improve them in terms of efficiency, fuel consumption reduction and pollutant emissions. A combustion process is difficult to handle with analytical techniques and, therefore, numerical simulations of turbulent flame are necessary. The description of turbulent combustion processes using Computational Fluid Dynamics (CFD) may be achieved using three levels of computations:

- Reynolds Averaged Navier-Stokes or RANS: It solves for mean flow fields, where the balance equations for Reynolds or Favre averaged quantities are obtained by averaging the instantaneous balance equations. Here an appropriate turbulence model must me chosen in order to describe the flow dynamics in combination with a turbulent combustion model, which must describe the chemical species conversion and heat release.

- Large Eddy Simulations or LES: This second approach solves larger scales whereas the effects of smaller ones are modelled using a subgrid closure rules. Here the balance equations are obtained by filtering the instantaneous balance equations.

- Direct Numerical Simulations or DNS: It calculates the full Navier-Stokes equations, considering all the characteristic length and time scales.

These approaches can be described in terms of energy spectrum, as reported in Fig. (2.8).

Note the in this figure k refers to the length scale while E(k) is the energy associated to that scale.

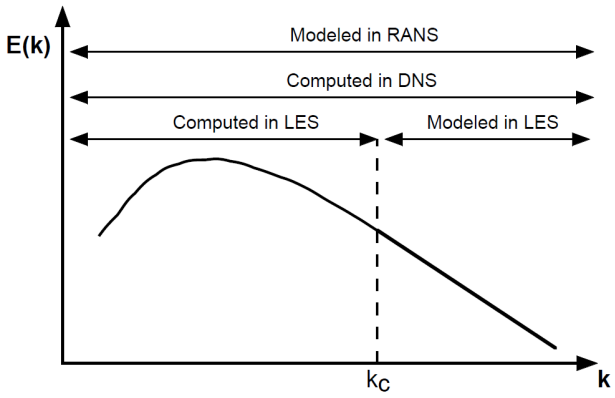

Figure 2.8: Introduction to turbulent combustion - Turbulence models over energy spectrum

The approach used in the present work is **RANS**, which is complemented by **turbulent flamelet model** in order to compute the combustion process. Its main advantage is its reduced computational cost that can be even smaller by introducing geometrical simplifications (2D or 2D axisymmetric models). In addition, it generally offers reliable results if an adequate modelling is done. On the other hand, only mean flow properties are obtained, as previously commented.

Consequently, RANS has become the most extended turbulence model from an engineering point of view. In the following, this approach is deeply explained.

2.3.3.1 Turbulence properties

Due to the irregular behaviour characterising a turbulent flow, a generic property f can be split into two contributions: a mean term ($\overline{f}$) and a fluctuating term (f').

$$f = \overline{f} + f' \Rightarrow Reynolds\ \ average \tag{2.3.5}$$

These two quantities allow to calculate the turbulence intensity I, whose equation reads:

$$I = \frac{\sqrt{\overline{f'^2}}}{\overline{f}} \tag{2.3.6}$$

Typical values of I goes from 0 in a laminar flow to tens of percent in typical wall-bounded flows: this means that the local velocity in a turbulent flow may deviate from its mean value by tens of percent. Turbulence fluctuations are associated with different scales ranging from the integral scale to the Kolmogorov length scale. Note that the weight of these fluctuations has already been defined in section 2.3.1 "Turbulent flows" when introducing the turbulence scales.

2.3.3.2 Reynolds Averages Navier-Stokes equations

The starting point that leads to RANS equations is the instantaneous balance equations for mass, momentum and energy (in terms of sensible enthalpy h_s). In the following, they are recalled.

– Mass conservation:

$$\frac{\partial \rho}{\partial t} + \frac{\partial \rho u_i}{\partial x_i} = 0 \tag{2.3.7}$$

– Momentum conservation:

$$\frac{\partial}{\partial t}\left(\rho u_i\right) + \frac{\partial}{\partial x_j}\left(\rho u_i u_j\right) + \frac{\partial p}{\partial x_i} = \frac{\partial \tau_{ij}}{\partial x_j} \tag{2.3.8}$$

– Mass fraction conservation for the k-th species:

$$\frac{\partial \rho Y_k}{\partial t} + \frac{\partial}{\partial x_i}\left(\rho u_i Y_k\right) = -\frac{\partial}{\partial x_i}(V_{k,i} Y_k) + \dot{\omega}_k \quad for \;\; k = 1, ..., N \tag{2.3.9}$$

– Energy equation in terms of sensible enthalpy h_s:

$$\frac{\partial \rho h_s}{\partial t} + \frac{\partial}{\partial x_i}(\rho u_i h_s) = \frac{Dp}{Dt} + \frac{\partial}{\partial x_i}\left(\lambda \frac{\partial T}{\partial x_i}\right) - \frac{\partial}{\partial x_i}\left(\rho \sum_{k=1}^{N} V_{k,i} Y_k h_{s,k}\right) + \tau_{ij}\frac{\partial u_i}{\partial x_j} + \dot{\omega}_T \tag{2.3.10}$$

Using Reynolds averages with the mass conservation equation leads to some unclosed quantities such as $\overline{\rho' u_i'}$, corresponding to the correlation between density and velocity fluctuations. Thus, modelling is required. Reynolds averaging for variable density flows introduced many other unclosed correlations between any quantity f and density fluctuations ($\overline{\rho' f'}$). To avoid them, mass-weighted averages, known as **Favre averages** are usually introduced:

$$\tilde{f} = \frac{\overline{\rho f}}{\overline{\rho}} \;\; \Rightarrow Favre \;\; averages \tag{2.3.11}$$

Therefore, the quantity f is split now into two new components: the Favre average and its respective variance

$$f = \tilde{f} + f'' \;\; with \;\; \tilde{f''} = 0 \tag{2.3.12}$$

Using this formulation, the averaged balance equations are rewritten as follows:

– Mass conservation:

$$\frac{\partial \overline{\rho}}{\partial t} + \frac{\partial}{\partial x_i}(\overline{\rho}\tilde{u}_i) = 0 \tag{2.3.13}$$

– Momentum conservation:

$$\frac{\partial}{\partial t}(\overline{\rho}\tilde{u}_i) + \frac{\partial}{\partial x_j}(\overline{\rho}\tilde{u}_i\tilde{u}_j) + \frac{\partial \overline{p}}{\partial x_i} = \frac{\partial}{\partial x_j}(\overline{\tau_{ij}} - \overline{\rho}\widetilde{u_i'' u_j''}) \tag{2.3.14}$$

– Mass fraction conservation for the k-th species:

$$\frac{\partial(\overline{\rho}\tilde{Y}_k)}{\partial t} + \frac{\partial}{\partial x_i}(\overline{\rho}\tilde{u}_i\tilde{Y}_k) = -\frac{\partial}{\partial x_i}(\overline{V_{k,i}Y_k} + \overline{\rho}\widetilde{u_i'' Y_k''}) + \overline{\dot{\omega}_k} \quad for \;\; k = 1, ..., N \tag{2.3.15}$$

– Energy equation in terms of sensible enthalpy h_s:

$$\frac{\partial(\overline{\rho}\tilde{h_s})}{\partial t} + \frac{\partial}{\partial x_i}(\overline{\rho}\tilde{u_i}\tilde{h_s}) = \overline{\dot{\omega}_T} + \overline{\frac{Dp}{Dt}} + \frac{\partial}{\partial x_i}\left(\overline{\lambda\frac{\partial T}{\partial x_i}} - \overline{\rho u_i'' h_s''}\right) + \overline{\tau_{ij}\frac{\partial u_i}{\partial x_j}} - \frac{\partial}{\partial x_i}\left(\overline{\rho\sum_{k=1}^{N} V_{k,i}Y_k h_{s,k}}\right) \tag{2.3.16}$$

where:

$$\overline{\frac{Dp}{Dt}} = \frac{\partial\overline{\rho}}{\partial t} + \overline{u_i\frac{\partial p}{\partial x_i}} = \frac{\partial\overline{p}}{\partial t} + \tilde{u_i}\frac{\partial\overline{p}}{\partial x_i} + \overline{u_i''\frac{\partial p}{\partial x_i}} \tag{2.3.17}$$

These equations are formally identical to the classical Reynolds averaged equations for constant density flows. Even though Favre averaging seems to offer a simple and efficient route for reacting flows, some considerations must be done:

▷ There is no simple relation between Favre ($\tilde{f}$) and Reynolds ($\overline{f}$) averages. A relation between these two quantities requires the knowledge, or the modelling, of density fluctuation correlations ($\overline{\rho' f'}$) which remain hidden in Favre average quantities. From Eq. (2.3.11), this relation can be expressed as:

$$\overline{\rho}\tilde{f} = \overline{\rho f} \Rightarrow \overline{\rho}\tilde{f} = \overline{\rho}\overline{f} + \overline{\rho' f'} \tag{2.3.18}$$

▷ Comparisons between numerical simulations, providing Favre averages ($\tilde{f}$), with experimental data are not easy. Most experimental techniques provide Reynolds averages $\overline{f}$, and the difference between $\overline{f}$ and $\tilde{f}$ may be significant.

In the previous Favre averaged equations, **unclosed terms** are present. The objective of turbulent combustion modelling is to propose closures for the unknown quantities found in Eq. (2.3.13) to (2.3.16).

Momentum conservation

· Reynolds stresses ($\widetilde{u_i'' u_j''}$): These terms are closed by a turbulence model. The closure may be directly done or by deriving balance equations for the Reynolds stresses. Most combustion works are based on the classical turbulence models developed for non-reacting flows, such as $k-\epsilon$ model, simply rewritten in terms of Favre averages. Heat release effects are generally not taken into account.

Reynolds stresses can be generally described using the viscous tensor τ_{ij} equation retained for newtonian fluids. In this way, the momentum transport due to vortices is modelled through a turbulent viscosity ($\mu_t = \overline{\rho}\nu_t$). This is the so-called **Boussinesq hypothesis** [9]. It reads as:

$$\overline{\rho u_i'' u_j''} = \overline{\rho}\widetilde{u_i'' u_j''} = -\mu_t\left(\frac{\partial\tilde{u_i}}{\partial x_j} + \frac{\partial\tilde{u_j}}{\partial x_i} - \frac{2}{3}\delta_{ij}\frac{\partial\tilde{u_k}}{\partial x_k}\right) + \frac{2}{3}\overline{\rho}k \tag{2.3.19}$$

where δ_{ij} is the Kronecker symbol and k is the turbulent kinetic energy, whose equation is:

$$k = \frac{1}{2}\sum_{k=1}^{3}\widetilde{u_k'' u_k''} \tag{2.3.20}$$

So, the closure problem now consists in specifying the value of the turbulent viscosity. In this regard three possible turbulent models can be introduced, depending on the number of additional equations used, which are summarised in Table (2.2).

0-Equation Model	1-Equation Model	2-Equations Model
$\mu_t = \overline{\rho} l_m^2 \lvert\tilde{S}\rvert$	$\mu_t = \overline{\rho} C_\mu l_{\rho k} \sqrt{k}$	$\mu_t = \overline{\rho} C_\mu \frac{k^2}{\epsilon}$

Table 2.2: Introduction to turbulent combustion - Turbulence models

In this work, a two-equations model is used, whose selection is justified in next chapter.

Mass fraction conservation for the k-th species

· Species turbulent flux ($\widetilde{\overline{\rho} u_i'' Y_k''}$): It is model by a classical gradient assumption.

$$\widetilde{\overline{\rho} u_i'' Y_k''} = \frac{-\mu_t}{Sc_{kt}} \frac{\partial \tilde{Y}_k}{\partial x_i} \tag{2.3.21}$$

where Sc_{kt} is a turbulent Schmidt number for the k-th species. Schmidt number relates the diffusion of momentum with respect to the molecular diffusion, and its expression reads as follows:

$$Sc = \frac{\nu}{D} \tag{2.3.22}$$

· Species laminar diffusive flux ($\overline{V_{k,i} Y_k}$): As before, a gradient assumption is done.

$$\overline{V_{k,i} Y_k} = -\overline{\rho D_k \frac{\partial Y_k}{\partial x_i}} \approx -\overline{\rho}\,\overline{D_k} \frac{\partial \tilde{Y}_k}{\partial x_i} \tag{2.3.23}$$

where $\overline{D_k}$ is an average species molecular diffusion coefficient.

· Species chemical reaction rates ($\overline{\dot{\omega}_k}$): In this thesis project, the mean reaction rates modelling is carried out through the **turbulent flamelet model**. It is explained in the next section.

Energy equation

· Enthalpy turbulent flux ($\widetilde{u_i'' h_s''}$): It also follows a classical gradient assumption. In this case, no equation is provided by [3].

· Enthalpy laminar diffusive flux ($\overline{\lambda \frac{\partial T}{\partial x_i}}$): It is modelled as a gradient.

$$\overline{\lambda \frac{\partial T}{\partial x_i}} = \overline{\lambda} \frac{\partial \tilde{T}}{\partial x_i} \tag{2.3.24}$$

· Pressure-velocity correlation ($\overline{u_i'' \partial p / \partial x_i}$): This term is simply neglected in most RANS codes.

So, until now the unclosed terms, found in the RANS equation when Favre averages are introduced, have been modelled with the exception of the species reaction rate $\dot{\omega}_k$. To achieve it, the scope of this work should be introduced: turbulent non-premixed flames.

2.4 Turbulent non-premixed flames

Turbulent non-premixed flames are encountered in a large number of industrial systems for two main reasons. First, compared to premixed flames, non-premixed burners are simpler to design and to build because a perfect reactant mixing, in given proportions, is not required. Non-premixed flames are also safer to operate as they don not exhibit propagation speeds and cannot flashback or autoignite in undesired locations. Accordingly, turbulent non-premixed flame modelling is one of the most usual challenges assigned to combustion codes in industrial applications.

As explained for laminar diffusion flames, reactant species have to reach, by molecular diffusion, the flame front before reaction. Hence, non-premixed flames are also called diffusion flames. During this travel, they are exposed to turbulence and their diffusion speeds may be strongly modified by turbulent motions. The overall reaction rate is often limited by the species molecular diffusion towards the flame front. Then, in many models, the chemical reaction is assumed to be fast, or infinitely fast, compared to transport processes.

2.4.1 Main characteristics

Additionally to the characteristics commented for laminar diffusion flames, which are still valid, several points should be remarked (mainly due to the inclusion of turbulence effects):

- Diffusion flames are more sensitive to stretch than turbulent premixed flames: critical stretch values for extinction of diffusion flames are one order of magnitude smaller than for premixed flames. A diffusion flame is more likely to be quenched by turbulent fluctuations.
- Buoyancy effects may be enhanced: pressure gradients or gravity forces induce differential effects on fuel, oxidizer and combustion products streams. For example, pure hydrogen/air flames use reactants having quite different densities. Molecular diffusion may also be strongly affected (differential diffusivity effects).
- The simplest diffusion flame is a fuel jet decharging in ambient air. In this situation, oxidizer is provided to the flame zone through air entrainment and natural convection (Fig. (2.9) (Ref. [3])). Such situations are simple from a technological point of view, but correspond to difficult numerical simulations.

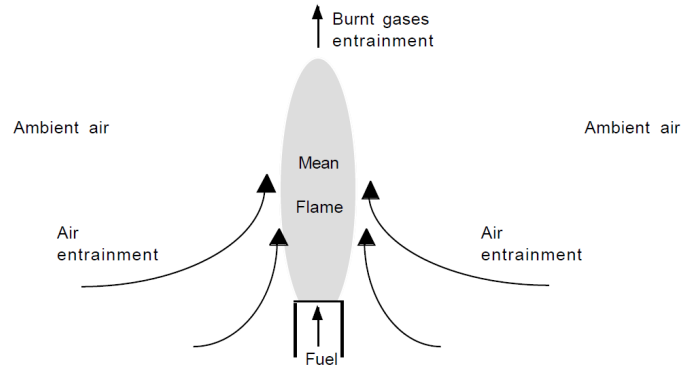

Figure 2.9: Turbulent non-premixed flames - Fuel jet discharging in ambient air

– Non-premixed flame stabilization is also a challenging problem, which requires a deeper discussion.

2.4.1.1 Flame stabilization

In this work, we will focus on two different ways of stabilizing the flame. Both of them are based on creating a recirculation zone, whose objective is to act as a hot burnt gases tank, providing the energy to ignite upcoming reactants. It can be created by:

– Sudden expansion (dump geometries): Recirculation zone is set by the burner geometry: the usual configuration corresponds to the backward facing step. Different configurations are encountered in practice for dump combustors. In the so-called bluff body case (Fig. (2.10) a), fuel and oxidizer are separated by a large step which generate recirculation zones and mixing between fuel and oxidizer. Recirculation zone characteristics strongly depend on relative fuel and oxidizer injection velocities. In other cases, fuel and oxidizer are injected on the same of the bluff body, where a large recirculation of burnt products stabilizes the combustion (Fig. (2.10) b) (Ref. [3]).

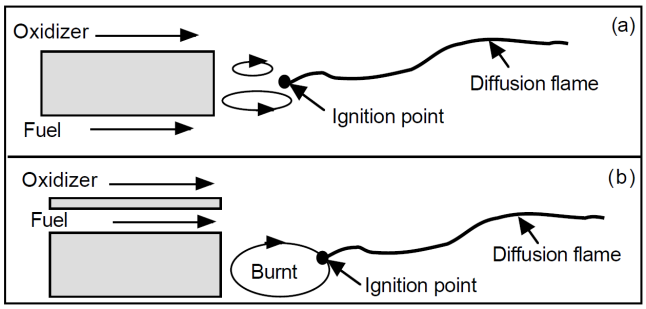

Figure 2.10: Turbulent non-premixed flames - Flame stabilization using bluff-body

– Swirl: In some applications, often for large inlet flow speeds, creating a recirculation zone behind a sudden expansion may not be sufficient to ensure flame stabilization while minimising pressure losses. For such cases, swirl offers another stabilization mechanism. Swirl is introduced upstream of the combustion chamber by vanes or lateral injection in order to create a low-speed region on the combustion chamber axis. Swirling flows are used in most gas turbines. However, their prediction is not simple since it requires a proper description of the flow field. For example, usual turbulence models such as k-ϵ are not very well suited to rotating flows.

  This point will be analysed when introducing the concept of swirl injectors, which constitute one of the fundamental bases of this thesis project.

2.4.1.2 Combustion regimes

The objective is now to identify turbulent non-premixed combustion regimes by comparing characteristic flame scales to characteristic turbulent scales. But, unfortunately, non-premixed flames have no intrinsic length scales and strongly depend on flow condition.

The flame structure and combustion regime depend on the chemical characteristic time τ_c.

– Fast chemistry (low τ_c values and large Damk*öhler* numbers): Flame is very thin and may be identified to a laminar flame element (i.e. **flamelet**).

– Larger values of τ_c: Departures from laminar flame structures to unsteady effects are expected.

– Low Damköhler numbers: Extinction occurs.

Note that Damköhler number (also known as time ratio) is defined as:

$$Da = \frac{\tau_t}{\tau_c} \tag{2.4.1}$$

where τ_t is the shortest turbulent time, corresponding to the worst case, whereas τ_c represents the chemical time. This expression can be modelled in the following way:

$$Da \approx 2\sqrt{Re_t} Da^{fl} \tag{2.4.2}$$

with $Da^{fl} = 1/(\tau_c \chi_{st})$.

Consequently, for sufficient fast chemestry the flame is expected to have a laminar flame (LF) structure. This condition can be written as $Da^{fl} \geq Da^{LFA}$. Extinction occurs for large chemical times, i.e. when $Da^{fl} \leq Da^{ext}$. All these results are summarised in Fig. (2.11) (Ref. [3]).

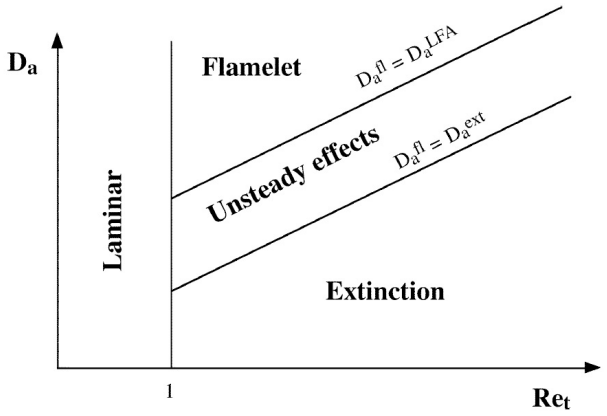

Figure 2.11: Turbulent non-premixed flames - Combustion diagram

To sum up, it has been proved that flamelet model can be extended to the turbulent flow regime if and only if chemistry is sufficiently fast compared to turbulence time scale.

2.4.2 Turbulent Flamelet Model

As known, modelling the reaction rate term $\dot{\omega}_k$ represents the main difficulty in turbulent non-premixed combustion simulations. This goal, as just proved, can be achieved by extending the Laminar Flamelet Model to the turbulent flow regime, where the model hypothesis are equivalent (H1 to H5). In an analogous way to laminar diffusion flames, the turbulent non-premixed problem may be split into two sub-problems, whose characteristics are slightly different:

– A mixing problem providing the average mixture fraction field $\tilde{z}(x_i, t)$ and some of its higher moments (for example, its variance $\widetilde{z''^2}$)

– A flame structure problem, where species mass fractions and temperatures ($\tilde{T}$, $\tilde{Y}_k$) are formulated as functions of conditional expressions ($Y_k|z^*$, $T|z^*$), since they may depend on various parameters in a turbulent flow.

PROBLEMS	**Laminar Flamelet Model**	**Turbulent Flamelet Model**
Mixing	$z(x_j,t)$	$\tilde{z}(z_j,t)$; $\widetilde{z''^2}(x_j,t)$
Flame structure	$T(z,\chi)$; $Y_k(z,\chi)$	$T(z,\chi_{st})$; $Y_k(z,\chi_{st})$
Solution	$T(x_j,t)$; $Y_k(x_j,t)$	$\tilde{T}(x_j,t)$; $\tilde{Y}_k(x_j,t)$

Table 2.3: Turbulent non-premixed flames - Laminar and turbulent flamelet models

The complexity added by turbulence, compared to laminar diffusion flames, comes from the averaging procedures. To determine average values, $\tilde{z}$ is not enough and its first moment, the variance, is needed, together with a full mixture fraction pdf (probability density function). In this regard, the equations of $\tilde{z}$ and $\widetilde{z''^2}$ reads as:

$$\tilde{z} = \int_0^1 z^* \tilde{p}(z^*) dz^* \quad \Rightarrow \quad Mean \;\; Mixture \;\; Fraction \tag{2.4.3}$$

$$\widetilde{z''^2} = \int_0^1 (z^* - \tilde{z})^2 \tilde{p}(z^*) dz^* \quad \Rightarrow \quad Variance \tag{2.4.4}$$

where $\tilde{p}(z)$ is the probability density function that describes the statistical distribution of the mixture fraction in the turbulent flow field. Once the pdf of z is known, any averaged quantity f can be computed as:

$$\overline{\rho}\tilde{f} = \int_0^1 (\overline{\rho f|z^*}) p(z^*) dz^* \tag{2.4.5}$$

where $(\overline{\rho f|z^*})$ represents the conditional average of f for a given value of mixture fraction $z = z^*$, depending on z^* and other quantities such as the scalar dissipation rate.

The method used to solve for $\overline{f}$ is the **primitive variable method**, which is based on Eq. (2.4.5). Assumptions are made on the flame structure to provide conditional quantities $(\overline{\rho Y_k|z^*})$ and $(\overline{\rho T|z^*})$ that are coming from flamelet (laminar flames) libraries. As a consequence, species mass fractions and temperature balance equations are no longer required and mean reaction rates $\overline{\dot{w}_k}$ are not modelled. This means that primitive variable method constitutes a low-time consuming approach. RANS codes only solve for flow variables, such as $\overline{\rho}$ or $\tilde{u}_i$, and mixture fraction variables ($\tilde{z}$ and $\widetilde{z''^2}$) to estimate the probability density function $p(z^*)$. In the following, the steps followed to implement this approach are described.

At first, the mixture problem is calculated. Then, the balance equations for $\tilde{z}$ and its variance $\widetilde{z''^2}$ should be solved. These equations are given by:

$$\frac{\partial \overline{\rho}\tilde{z}}{\partial t} + \frac{\partial}{\partial x_i}(\overline{\rho}\tilde{u}_i\tilde{z}) = \frac{\partial}{\partial x_i}\left(\overline{\rho D \frac{\partial z}{\partial x_i}} - \overline{\rho}\widetilde{u_i'' z''}\right) \tag{2.4.6}$$

$$\frac{\partial \overline{\rho}\widetilde{z''^2}}{\partial t} + \frac{\partial}{\partial x_i}(\overline{\rho}\tilde{u}_i\widetilde{z''^2}) = \frac{\partial}{\partial x_i}\left(\overline{\rho}\frac{\nu_t}{Sc_{t1}}\frac{\partial \widetilde{z''^2}}{\partial x_i}\right) + 2\overline{\rho}\frac{\nu_t}{Sc_{t2}}\frac{\partial \tilde{z}}{\partial x_i}\frac{\tilde{z}}{\partial x_i} - c\overline{\rho}\frac{\epsilon}{k}\widetilde{z''^2} \tag{2.4.7}$$

with c as a model constant of order unity.

Some simplifications can be introduced for these equations. Eq. (2.4.7) can be directly rewritten as:

$$\frac{\partial \overline{\rho}\widetilde{z''^2}}{\partial t} + \frac{\partial}{\partial x_i}(\overline{\rho}\tilde{u}_i\widetilde{z''^2}) = \frac{\partial}{\partial x_i}\left(\frac{\mu_t}{Sc_t}\frac{\partial \widetilde{z''^2}}{\partial x_i}\right) + C_g\overline{\rho}\nu_t\left(\frac{\partial \tilde{z}}{\partial x_i}\right)^2 - C_d\overline{\rho}\frac{\tilde{\epsilon}}{\tilde{k}}\widetilde{z''^2} \tag{2.4.8}$$

where C_g and C_d are model constants equal to 2.86 and 2, respectively, according to [3].

Regarding Eq. (2.4.6), the production term $\overline{\rho}\widetilde{u_i''z''}$ can be expressed as:

$$\overline{\rho}\widetilde{u_i''z''} = -\frac{\mu_t}{Sc_t}\frac{\partial \tilde{z}}{\partial x_i} \tag{2.4.9}$$

Recalling H1 and H2 assumptions (i.e. $Le = 1$), the following property is verified:

$$Sc = Pr \cdot Le \Rightarrow Sc = Pr \quad with \quad \frac{\mu}{\rho D} = Sc \Rightarrow \rho D = \frac{\mu}{Sc} \tag{2.4.10}$$

Note that Prandtl number (Pr) is defining the ratio between momentum diffusion and molecular diffusion.

$$Pr = \frac{\nu\rho C_p}{\lambda} \tag{2.4.11}$$

Consequently, the RHS of Eq. (2.4.6) can be rewritten as:

$$\frac{\partial}{\partial x_i}\left(\frac{\mu}{Sc} + \frac{\mu_t}{Sc_t}\right)\frac{\partial \tilde{z}}{\partial x_i} \tag{2.4.12}$$

In the previous equation, the term in parenthesis represents the effective transport coefficient, which is defined as:

$$\Gamma_{eff} = \frac{\mu}{Sc} + \frac{\mu_t}{Sc_t} \tag{2.4.13}$$

Then:

$$\frac{\partial \overline{\rho}\tilde{z}}{\partial t} + \frac{\partial}{\partial x_i}(\overline{\rho}\tilde{u}_i\tilde{z}) = \frac{\partial}{\partial x_i}\left(\Gamma_{eff}\frac{\partial \tilde{z}}{\partial x_i}\right) \tag{2.4.14}$$

Usually turbulent transport is of order of magnitude higher than its laminar counterpart. Therefore, in many codes the laminar Schmidt number Sc is neglected:

$$\Gamma_{eff} = \frac{\mu_{eff}}{Sc_t} \;\; ; \;\; with \;\; \mu_{eff} = \mu_{lam} + \mu_t \tag{2.4.15}$$

So, after introducing all these simplifications, balance equations for $\tilde{z}$ and $\widetilde{z''^2}$ are given by Eqs. (2.4.8) and (2.4.14).

Once the balance equations required to solve the mixture problem are defined, it is necessary to introduce their corresponding pdf functions. They can be both presumed and

obtained solving for a balance equation. The most widely used presumed pdf for the mixture fraction z is the $\beta - function$, whose dependence is limited to the mean mixture fraction and its variance. Its equation is expressed as:

$$\tilde{p}(z) = \frac{1}{B(a,b)} \cdot z^{a-1} \cdot (1-z)^{b-1} = \frac{\Gamma(a+b)}{\Gamma(a)\Gamma(b)} \cdot z^{a-1} \cdot (1-z)^{b-1} \tag{2.4.16}$$

where $B(a,b)$ is a normalization factor, Γ is a function and a and b are two parameters depending on $\tilde{z}$ and $\widetilde{z''^2}$, whose equations are reported below. [3]

$$B(a,b) = \int_0^1 z^{a-1} \cdot (1-z)^{b-1} dz \tag{2.4.17}$$

$$a = \tilde{z} \cdot \left(\frac{\tilde{z}(1-\tilde{z})}{\widetilde{z''^2}} - 1 \right) \quad ; \quad b = a \cdot \left(\frac{1-\tilde{z}}{\tilde{z}} \right) \tag{2.4.18}$$

$$\Gamma(x) = \int_0^{+\infty} e^{-t} \cdot t^{x-1} dt \tag{2.4.19}$$

In case the chemistry is not infinitely fast, knowing the mixture fraction z is not enough to deduce the local species mass fractions or temperature. A point with equal mixture fraction could correspond to pure mixing, ignited flame or quenched flame, as can be appreciated in Fig. (2.12) (Ref. [3]).

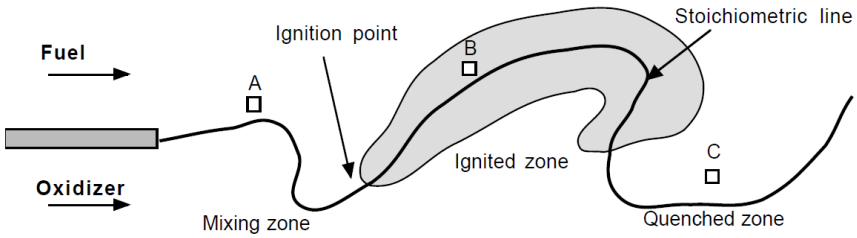

Figure 2.12: Turbulent non-premixed flames - Diffusion flame structure ambiguity

Then, additional information is required: pdf functions depend also on another flame parameter, which is the scalar dissipation rate at flame location (χ_{st}, equivalent to the flame stretch). By using the stoichiometric scalar dissipation value, it is possible to analyse the stretch effects and quenching of a flame, but not to predict the flame stabilization. Consequently to this last statement, pdf functions are redefined as:

$$p(z, \chi_{st}) = p(z) \cdot p(\chi_{st}) \tag{2.4.20}$$

or, in terms of mass-weighted probability density function:

$$\rho \cdot p(z, \chi_{st}) = \overline{\rho} \cdot \tilde{p}(z) p(\chi_{st}) \tag{2.4.21}$$

where statistical independence of mixture fraction and its scalar dissipation rate is assumed in order to decouple the dependence.

Probability density functions are usually presumed, using $\beta - function$ for $\tilde{p}(z)$ (previously defined) and a Dirac-delta function for $\tilde{p}(\chi_{st})$.

$$p(\chi_{st}) = \delta(\chi_{st} - \widetilde{\chi_{st}}) \tag{2.4.22}$$

A more physical approach is to use log normal distributions for $p(\chi_{st})$. It is:

$$p(\chi_{st}) = \frac{1}{\chi_{st}\sigma\sqrt{2\pi}} \cdot exp\left(- \frac{(ln(\chi_{st}) - \mu)^2}{2\sigma^2} \right) \tag{2.4.23}$$

where μ and σ are linked to mean value of χ_{st} and its variance $\widetilde{\chi''^2_{st}}$.

$$\chi_{st} = \int_0^{+\infty} \chi_{st} p(\chi_{st}) d\chi_{st} = exp\left(\mu + \frac{\sigma^2}{2}\right) \tag{2.4.24}$$

$$\widetilde{\chi''^2_{st}} = \widetilde{\chi^2_{st}} \cdot exp(\sigma^2 - 1) \tag{2.4.25}$$

Some examples for pdf functions are shown in Fig. (2.13) (Ref. [3]), whose shapes depend on the parameters that define themselves.

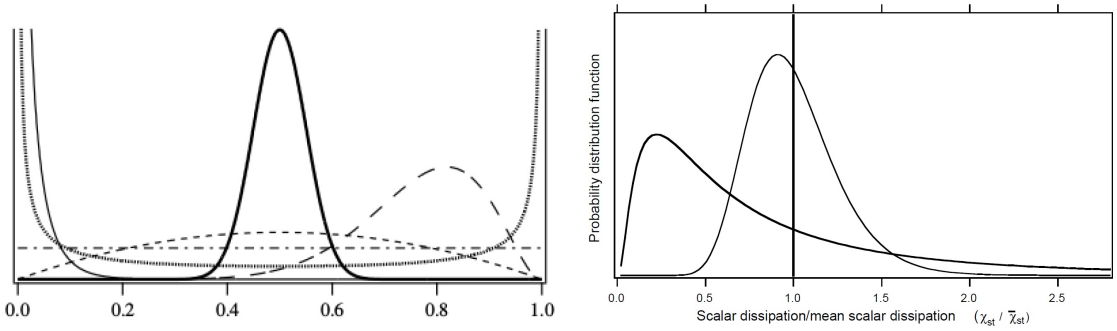

(a) β-function (b) Log normal function

Figure 2.13: Turbulent non-premixed flames - pdf functions

Finally, in order to determine the pdf, it is required to compute the value of the stoichiometric scalar dissipation χ_{st}. For turbulent flames, the total scalar dissipation rate is:

$$\overline{\rho}\tilde{\chi} = 2\overline{\rho D}\left(\frac{\partial z}{\partial x_i}\right)^2 = 2\overline{\rho D}\left(\frac{\partial \tilde{z}}{\partial x_i}\right)^2 + 4\overline{\rho D \frac{\partial z''}{\partial x_i}}\frac{\partial \tilde{z}}{\partial x_i} + 2\overline{\rho D\left(\frac{\partial z''}{\partial x_i}\right)^2} \tag{2.4.26}$$

Considering constant density, the second term of the Eq. (2.4.26) is equal to zero, hence it can be expressed as:

$$\tilde{\chi} = \chi_m + \chi_p \tag{2.4.27}$$

where χ_m is the scalar dissipation rate of the mean $\tilde{z}$ and χ_p corresponds to the scalar dissipation rate due to the turbulent fluctuations of z (i.e. its variance z''). Generally, in RANS computations mean gradients, are negligible. Then, $\chi \approx \chi_p$.

The mean scalar dissipation χ_p is usually modelled from a turbulent time. This means that:

$$\tilde{\chi}_p = c \cdot \frac{\epsilon}{k} \cdot \widetilde{z''^2} \tag{2.4.28}$$

where c is a model constant of order unity. Once $\tilde{\chi}$ is known, $\tilde{\chi}_{st}$ can be obtained as:

$$\tilde{\chi}_{st} = \frac{\tilde{\chi}}{F(\tilde{z}, \widetilde{z''^2})} \quad ; \quad with \quad F(z) = exp(-2 \cdot [erf^{-1}(2z-1)]^2) \tag{2.4.29}$$

In practice, the approximation $\chi = \chi_{st}$ is used.

So, once χ_{st} is obtained, pdf is defined and, consequently, species mass fractions and temperatures can be obtained. The procedure followed by primitive variables approach is summarised in Table (2.4) and Fig. (2.14) (Ref. [3]).

OPERATION	**RESULTS**
STAGNATION POINT FLAMES:	
Store flame structure in library	$T(z,\chi_{st})$; $Y_k(z,\chi_{st})$
IN RANS CODE:	
Solve for mixture fraction and variance	$\tilde{z}$; $\widetilde{z''^2}$
Construct β pdf for z using $\tilde{z}$ and $\widetilde{z''^2}$	$\tilde{p}(z)$
Evaluate $\tilde{\chi}$ from $\widetilde{z''^2}$, k and ϵ	$\tilde{\chi} = c\widetilde{z''^2}\epsilon/k$
Evaluate $\tilde{\chi}_{st}$ from $\tilde{\chi}$ and $F(\tilde{z},\widetilde{z''^2})$	$\tilde{\chi}_{st} = \tilde{\chi}/F(\tilde{z},\widetilde{z''^2})$
Construct log normal pdf for χ_{st} using $\tilde{\chi}_{st}$	$p(\chi_{st})$
Compute mean temperature	$\tilde{T} = \int_0^{+\infty}\int_0^1 T(z,\chi_{st})\tilde{p}(z)p(\chi_{st})dzd\chi_{st}$
Compute mean species mass fractions (if required)	$\tilde{Y_k} = \int_0^{+\infty}\int_0^1 Y_k(z,\chi_{st})\tilde{p}(z)p(\chi_{st})dzd\chi_{st}$
Compute density from $\tilde{T}$	$\overline{\rho}$

Table 2.4: Turbulent non-premixed flames - Principle of a pdf flamelet model using primitive variables

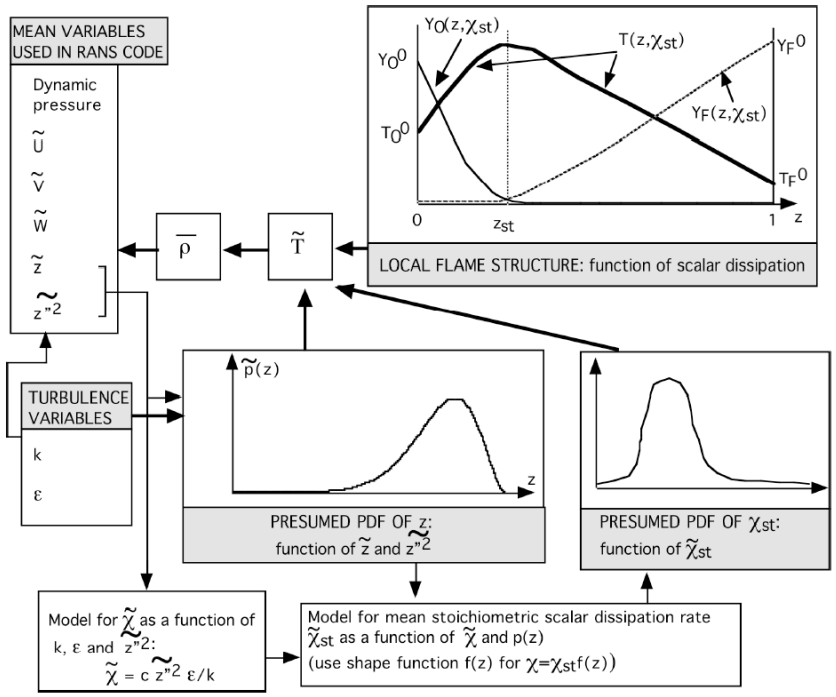

Figure 2.14: Turbulent non-premixed flames - Primitive variables approach

2.5 Swirling flames

Once non-premixed flames and the computational approach used to simulate turbulent combustion problems have been defined, swirling flames are introduced. At this section, the description of a swirling flow and its application in the combustion field is reported.

2.5.1 Introduction to swirling flows

Swirling flows can be defined as a combination of vortex flow and axial velocity, which makes the fluid move in helicoidal trajectories. This is the reason why swirled flows are usually described in cylindrical coordinates (x, r, φ), allowing a better understanding of the flow motion.

In this way, the velocity vector ($\vec{v}$) is decomposed in the following three components, as shown in Fig. (2.15) (Ref. [10]):

- Axial component: It is projected onto the x axis. It allows the flow to advance through the stream tube and it is named as U.
- Radial component: It is projected onto the radial coordinate r, which is giving the relative position of a point with respect the origin in terms of radial distance. Radial velocity is referred as V.
- Tangential component: Known as W, it is projected onto an orthogonal axis to the radial one at a specific φ position.

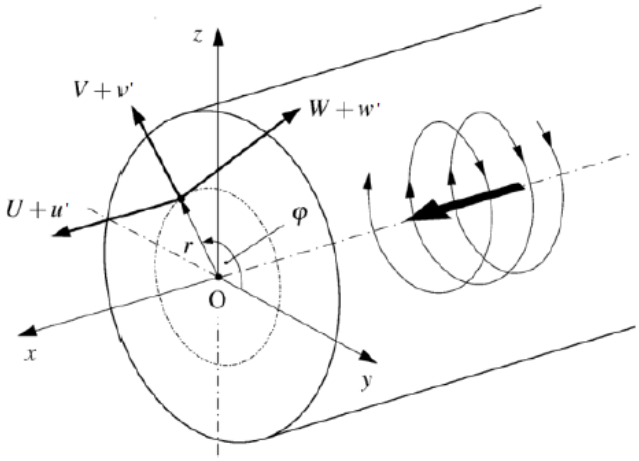

Figure 2.15: Introduction to swirling flows - Velocity components

Some additional comments about the velocity field can be done. The velocity mainly varies along the axial and radial coordinates, while the radial component is usually negligible. [10]

Moreover, swirling flows can be regarded as axisymmetric and, then, the velocity components are modelled as follows:

$$U = U_a \ ; \ V \simeq 0 \ ; \ W = \omega \cdot r \tag{2.5.1}$$

In fact, this will be the modelling adopted when implementing the swirl boundary condition into numerical simulations. This means that a value of axial (U_a) and angular velocity (ω) need to be specified to generate a swirl.

One further comment about axisymmetry assumption should be done. Axisymmetry hypothesis allows to reduce the required computational domain by neglecting all the circumferential gradients ($\partial/\partial\varphi = 0$).

In addition, this swirling flow is characterised by a highly anisotropic turbulence structure as a consequence of additional flow phenomena that are not present in simple shear flow, such as shear component associated to $\partial W/\partial r$; additionally to common mean shear proportional to $\partial U/\partial r$ and streamline curvature. This leads to a perpetual challenge in terms of turbulence modelling.

This turbulent nature is represented by the sum of mean (time-averaged) and fluctuating velocity, as defined with Reynolds statistical description of turbulent flow. As a consequence, velocity components are defined as:

- Axial velocity: u = U+u'
- Radial velocity: v = V+v'
- Tangential velocity: w = W+w'

where U, V and W represent the mean value of the velocity component; while u', v' and w' are the corresponding velocity fluctuations.

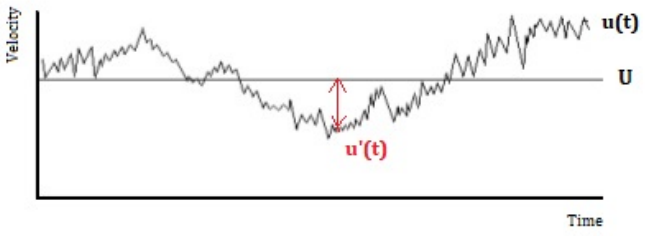

Figure 2.16: Introduction to swirling flows - Velocity fluctuations

2.5.1.1 Governing equations and parameters

Once the swirl phenomenon has been described in terms of velocity field, the governing equations and parameters of a swirling flow are reported. The general conservation equations (only mass and momentum are referred) characterising a swirl read as: [11]

$$Mass \Rightarrow \frac{\partial \rho}{\partial t} + \frac{1}{r}\left(\frac{\partial(\rho r v)}{\partial r} + \frac{\partial(\rho w)}{\partial \varphi} + \frac{\partial(\rho r u)}{\partial x}\right) = 0 \tag{2.5.2}$$

$$Momentum\ r \Rightarrow \rho\left(\frac{\partial v}{\partial t} + v\cdot\frac{\partial v}{\partial r} + \frac{w}{r}\cdot\frac{\partial v}{\partial \varphi} + u\cdot\frac{\partial v}{\partial x} - \frac{w^2}{r}\right) = -\frac{\partial p}{\partial r} + \rho\cdot f_{m_r} + \tag{2.5.3}$$

$$+\frac{1}{r}\cdot\frac{\partial(r\tau_{rr})}{\partial r} + \frac{1}{r}\cdot\frac{\partial\tau_{r\varphi}}{\partial\varphi} - \frac{\tau_{\varphi\varphi}}{r} + \frac{\tau_{xr}}{\partial x}$$

$$Momentum\ \varphi \Rightarrow \rho\left(\frac{\partial w}{\partial t} + v\cdot\frac{\partial w}{\partial r} + \frac{w}{r}\cdot\frac{\partial w}{\partial \varphi} + u\cdot\frac{\partial w}{\partial x} + \frac{wv}{r}\right) = -\frac{1}{r}\cdot\frac{\partial p}{\partial\varphi} + \rho\cdot f_{m_\varphi} + \tag{2.5.4}$$

$$+\frac{1}{r^2}\cdot\frac{\partial(r^2\tau_{r\varphi})}{\partial r} + \frac{1}{r}\cdot\frac{\partial\tau_{\varphi\varphi}}{\partial\varphi} + \frac{\partial\tau_{x\varphi}}{\partial x}$$

$$Momentum\ x \Rightarrow \rho\left(\frac{\partial u}{\partial t} + v\cdot\frac{\partial u}{\partial r} + \frac{w}{r}\cdot\frac{\partial u}{\partial \varphi} + u\cdot\frac{\partial u}{\partial x}\right) = -\frac{\partial p}{\partial x} + \rho\cdot f_{m_x} + \tag{2.5.5}$$

$$+\frac{1}{r}\cdot\frac{\partial(r\tau_{rx})}{\partial r} + \frac{1}{r}\cdot\frac{\partial\tau_{x\varphi}}{\partial\varphi} + \frac{\partial\tau_{xx}}{\partial x}$$

where τ_{ij} represents the viscous stress tensor, which is scaled by the Navier-Poisson law for Newtonian fluids. Then:

$$\tau_{rr} = 2\mu\cdot\frac{\partial v}{\partial r} + \left(\mu_v - \frac{2}{3}\cdot\mu\right)\cdot\nabla\underline{v} \tag{2.5.6}$$

$$\tau_{\varphi\varphi} = 2\mu\cdot\left(\frac{1}{r}\cdot\frac{\partial w}{\partial\varphi} + \frac{v}{r}\right) + \left(\mu_v - \frac{2}{3}\cdot\mu\right)\cdot\nabla\underline{v} \tag{2.5.7}$$

$$\tau_{xx} = 2\mu\cdot\frac{\partial u}{\partial x} + \left(\mu_v - \frac{2}{3}\cdot\mu\right)\cdot\nabla\underline{v} \tag{2.5.8}$$

$$\tau_{r\varphi} = \tau_{\varphi r} = \mu\cdot\left[r\cdot\frac{\partial}{\partial r}\left(\frac{w}{r}\right) + \frac{1}{r}\cdot\frac{\partial v}{\partial\varphi}\right] \tag{2.5.9}$$

$$\tau_{x\varphi} = \tau_{\varphi x} = \mu\cdot\left(\frac{1}{r}\cdot\frac{\partial u}{\partial\varphi} + \frac{\partial w}{\partial x}\right) \tag{2.5.10}$$

$$\tau_{xr} = \tau_{rx} = \mu\cdot\left(\frac{\partial v}{\partial x} + \frac{\partial u}{\partial r}\right) \tag{2.5.11}$$

with μ being the viscosity and μ_v as the volumetric viscosity, which is null for monoatomic gases.

Then, applying the hypothesis previously commented ($v \simeq 0\ ;\ \partial/\partial\varphi = 0$), Navier-Stokes equations could be simplified into:

$$Mass \Rightarrow \frac{\partial\rho}{\partial t} + \frac{1}{r}\left(\frac{\partial(\rho r u)}{\partial x}\right) = 0 \tag{2.5.12}$$

$$Momentum\ r \Rightarrow \rho\left(-\frac{w^2}{r}\right) = -\frac{\partial p}{\partial r} + \rho\cdot f_{m_r} + \frac{1}{r}\cdot\frac{\partial(r\tau_{rr})}{\partial r} - \frac{\tau_{\varphi\varphi}}{r} + \frac{\tau_{xr}}{\partial x} \tag{2.5.13}$$

$$Momentum\ \varphi \Rightarrow \rho\left(\frac{\partial w}{\partial t} + u\cdot\frac{\partial w}{\partial x}\right) = \rho\cdot f_{m_\varphi} + \frac{1}{r^2}\cdot\frac{\partial(r^2\tau_{r\varphi})}{\partial r} + \frac{\partial\tau_{x\varphi}}{\partial x} \tag{2.5.14}$$

$$Momentum\ x \Rightarrow \rho\left(\frac{\partial u}{\partial t} + u\cdot\frac{\partial u}{\partial x}\right) = -\frac{\partial p}{\partial x} + \rho\cdot f_{m_x} + \frac{1}{r}\cdot\frac{\partial(r\tau_{rx})}{\partial r} + \frac{\partial\tau_{xx}}{\partial x} \tag{2.5.15}$$

where:

$$\tau_{rr} = \left(\mu_v - \frac{2}{3} \cdot \mu\right) \cdot \nabla \underline{v} \tag{2.5.16}$$

$$\tau_{\varphi\varphi} = \left(\mu_v - \frac{2}{3} \cdot \mu\right) \cdot \nabla \underline{v} \tag{2.5.17}$$

$$\tau_{xx} = 2\mu \cdot \frac{\partial u}{\partial x} + \left(\mu_v - \frac{2}{3} \cdot \mu\right) \cdot \nabla \underline{v} \tag{2.5.18}$$

$$\tau_{r\varphi} = \tau_{\varphi r} = \mu \cdot \left[r \cdot \frac{\partial}{\partial r}\left(\frac{w}{r}\right)\right] \tag{2.5.19}$$

$$\tau_{x\varphi} = \tau_{\varphi x} = \mu \cdot \left(\frac{\partial w}{\partial x}\right) \tag{2.5.20}$$

$$\tau_{xr} = \tau_{rx} = \mu \cdot \left(\frac{\partial u}{\partial r}\right) \tag{2.5.21}$$

If flow is incompressible, Eqs. (2.5.19), (2.5.20) and (2.5.21) are further simplified by setting $\nabla \underline{v} = 0$.

The equations of motion determine how a swirling flow evolves. It is formed by vortices, whose nature can be classified in: [12] [13]

- Free vortex: It is given by the equilibrium of circumferential forces with the radial pressure gradient. It is:

$$\frac{\partial p}{\partial r} = \frac{\rho w^2}{r} \tag{2.5.22}$$

  At this region, tangential velocity is inversely proportional to the radius ($w = C/r$).

- Forced vortex: It is the case in which the fluid rotates as a solid body, and as a consequence, the tangential velocity is proportional to the radial coordinate ($w = \omega \cdot r$).

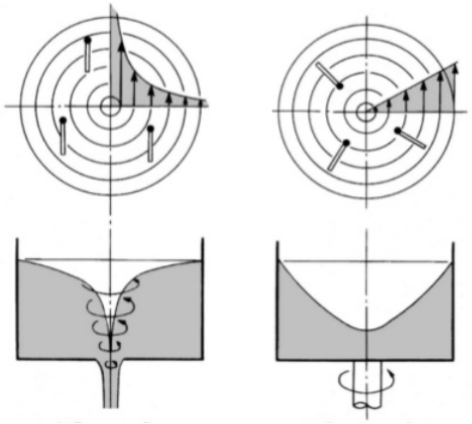

(a) Free vortex (b) Forced vortex

Figure 2.17: Introduction to swirling flows - Water tank analogy

Using the water tank analogy provided by Fig. (2.17), forced vortex is generated by a rotation of the tank around an axis. This motion induces a velocity field that linearly increases as water allocates further from the axis of rotation. On the other hand, free vortex is generated by a sink that sucks the water generating a swirl around the axis. However, in this case, the velocity vanishes as radial coordinate increases, since water is further from the sink. These two effects can be observed for the tangential velocity of a swirling flow in a pipe, as shown in Fig. (2.18) (data from Ref. [14]).

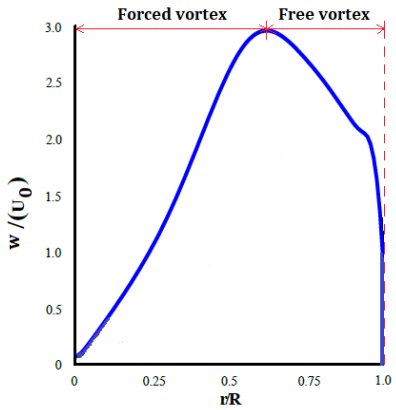

Figure 2.18: Introduction to swirling flows - Tangential velocity profile

Specifically, the whirling of the flow induces a forced vortex governed by the equation of a rigid body rotation. Then, for a certain value of the radial coordinate, the non-slip condition at the pipe wall produces a slow down of the fluid close to the wall. So, due to viscosity effects a free vortex is created, where the sink is given by the tangential velocity peak given by the forced vortex.

To measure the strength of the swirl motion, a parameter is introduced. It is the Swirl Number (S), which is defined as the ratio of axial flux of tangential momentum with respect to the axial flux of axial momentum. [12]

$$S = \frac{\int_A rw\vec{v} \cdot d\vec{A}}{R \int_A u\vec{v} \cdot d\vec{A}} \tag{2.5.23}$$

where: R is the pipe diameter and $d\vec{A}$ refers to the differential of the cross area.

If Eq. (2.5.23) is applied for an axisymmetric flow field, it can be simplified into the following expression:

$$\vec{v} \cdot d\vec{A} = 2\pi rudr \Rightarrow S = \frac{\int_0^R r^2 uwdr}{R \int_0^R ru^2 dr} \tag{2.5.24}$$

Additionally, another parameter is used to completely characterise the swirling flow. It is the Geometric Swirl Number (S_g) [14], whose expression is given by:

$$S_g = \frac{w}{u} = \frac{\omega \cdot r}{u} \tag{2.5.25}$$

Eq. (2.5.25) is mainly introduced when setting the initial state of a swirling flow, while Eq. (2.5.23) can be used to define the Swirl Number at different longitudinal sections.

Depending on the Swirl Number value, swirling flows are classified into low or high swirl. This differentiation would become important when discussing the turbulence model selection. Regarding the definition of the critical value (S_{crit}) that determines the transition between one regime to the another one, several definitions can be found in the bibliographic references. It is ranged between 0.5 and 0.95 [12] [14] and its value plays an important role in the well known free decay phenomenon. It consists on the dissipation of the initial swirl, which could eventually lead to the formation of recirculation zones. Further comments in this sense will be done in next sections.

To sum up, swirl is a whirling flow that induces two different vortices structures (free or forced), whose decay can eventually lead to more complex flow phenomena. These flow structures are controlled by the conservation equations and the swirl intensity.

2.5.2 Applications in the combustion field

Combustors play a crucial role in determining many of the engine operating characteristics, such as fuel efficiency, level of emissions and transient response. A combustor, by definition, must contain and maintain a stable combustion process. To achieve this goal, combustors are carefully designed to first mix and ignite the oxidizer and fuel and, then, mix this mixture in more oxidizer to complete the combustion process. [15]

At this point, swirl injectors, also known as swirlers, can be used to enhance the mixing process. The swirler establishes a local low pressure zone that forces some of the combustion products to recirculate, creating a high turbulence level. Although this fact will improve the combustion kinetics, it can induce higher pressure losses. Then, swirler must be carefully designed so as not to generate more turbulence than needed to sufficiently mix the fuel and oxidizer.

2.5.2.1 Swirl injectors

In a typical swirl injector, the flow is deflected by an array of vanes positioned either axially or radially. Both of them are used to provide the desired fuel/oxidizer distribution that ensures an efficient combustion. [16]

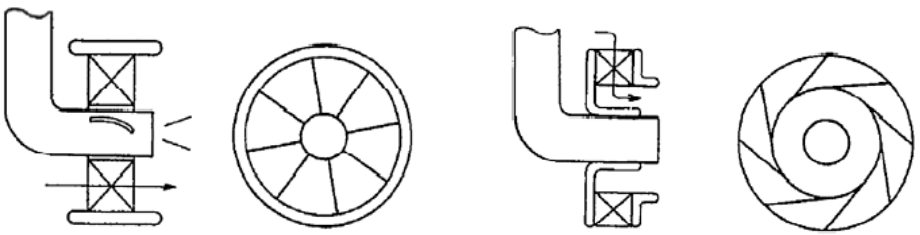

(a) Axial swirler (b) Radial swirler

Figure 2.19: Swirling flames - Blades configuration for a swirl injector

The effects induced by the swirler, whose typologies are shown in Fig. (2.19) (Ref. [16]), depends on the state of the working fluid:

- Liquid phase: For example, when liquid fuels are used as energy sources, they usually need to be atomized, vaporized and mixed with air before burning in the flame zone. Two types of atomization systems are commonly used: pressure and airblast atomizers. The former makes use of pressure and exposes the liquid fuel to an axial or rotating motion. In the latter, atomization of a liquid is achieved by injecting it into a high velocity gas stream, either within the atomizer body or externally.
- Gaseous phase: Swirl injector induces a rotation in the flow motion that contributes to a better fuel to oxidizer mixing. Either the fuel or oxidizer can be the rotating fluid.

Liquid swirl injectors are out of the scope of this thesis project, since we are working with fluids in gaseous phase.

Then, next step consists in commenting the principal advantages provided by this type of injector, as well as noting which are the drawbacks.

2.5.2.2 Expected improvements

The improvements provided by swirl injectors are mainly related with the vortex decay, which leads to the formation of two main flow structures: Vortex breakdown (VB) and Precessing vortex core (PVC), as shown in Fig. (2.20) (Ref. [16]).

- Vortex breakdown: One of the most important flow characteristics of a swirl injector is vortex breakdown, a phenomenon that manifests itself as a sudden change in the core of a vortex, and usually develops downstream in a recirculating bubble or a spiral pattern. The flow region of VB provides the dominant **flame stabilisation mechanism**, and is characterised by the existence of internal stagnation points and reversed flows. [16] In other words, VB is described as the transition from steadily swirling flow with a high axial velocity component and almost laminar flow behaviour at the central axis to a flow with highly turbulent motion in the vicinity of the axis. This breakdown yields a strong deceleration (up to **recirculation**) of the flow along the axis. [17] The local flow development is depending on the swirl intensity of this region. As the Swirl Number increases, the size of the recirculation zone also increases.

  Regarding the benefits associated to VB, these are expected in 2 aspects: firstly, heat and active chemical species would be recirculated to the root of the flame, thus it will reduce velocity requirements for flame. Secondly, low temperature parcels could mix with high temperature parcels and ignite unburned fuel. [18] VB may eventually result in a precessing vortex core.

- Precessing vortex core: It is a three dimensional unsteady asymmetric flow structure, commonly related to turbulent combustion devices. PVC develops when a central vortex core starts to precess around the axis of symmetry at a well-defined frequency. This phenomenon is usually linked to vortex breakdown and the associated recirculation zone in a high Reynolds Number flow. The frequency of precess depends on the Swirl Number and chamber configurations, and increases linearly with flow rate.

PVC strongly affects the flow and flame evolution in combustion systems. It may improve **combustion efficiency** through its enhancement of turbulent intensity and **mixing**, but it also represents a largely undesired characteristic because of the possible resonant coupling low-frequency acoustic oscillations. As previously commented, this effect becomes worse as flow rate increases. [16]

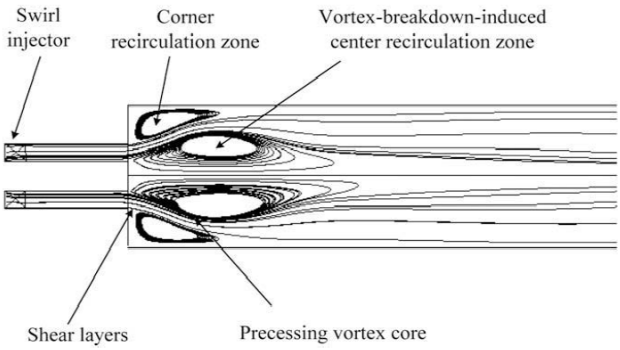

Figure 2.20: Swirling flames - Vortex breakdown and preprocessing vortex core

So, the main advantages provided by swirl injectors are flame stabilization, fast mixing and the creation of recirculation zones that improve the fuel efficiency. These three factors make easier to fulfil some basic combustor requirements such as:

- Complete combustion: The creation of recirculation zones increase the residence time of the fuel and oxidizer, reducing in this way the amount of unburned fuel, as well as the creation of unwanted emissions of unburned hydrocarbons (CO and soot).
- Flame stability: Motion of the flame up and downstream is constrained.
- Small physical size and weight: Since mixing process is accelerated, flame length is reduced. This leads to smaller combustion chambers.

However, there is a main drawback: noise level emissions. The fluctuations induced by PVC should be carefully analysed to avoid aeroacoustic problems.

Chapter 3

Methodology

As already noted in the previous chapter, a computational approach is used to solve turbulent combustion problems. The software used is OpenFoam, whose open source nature allows us implementing new codes in order to solve specific problems. During this work, the main objective is to implement a swirl boundary condition at the inlet. In this way, a swirl injector is simulated.

So, this chapter explains the basics of a Computational Fluid Dynamics simulation, specifically applied to OpenFOAM environment, as well as describes the implementation of a swirling flow.

3.1 Computational Fluid Dynamics

Computational Fluid Dynamics is the science that studies the numerical simulation of fluid flows. It constitutes an interesting tool because it allows obtaining detailed information without using intrusive experimental measurements. In addition, generally it is cheaper than performing its equivalent experiment. [19]

On the other hand, it is difficult to completely control CFD techniques since they require to have a deep knowledge about fluid dynamics, numerical methods and programming. Complex problems also could be a disadvantage due to the need of a very powerful computer, which is not always possible.

CFD can also be used to construct fluid models that reproduce the behaviour provided by experimental data. This application is the one exploited in this thesis project. Another possibility offered by CFD is to perform parametric analysis in order to design a specific geometry that provides the most efficient behaviour for a certain field of application.

In what refers to the working principle, a CFD code decompose the fluid domain in cells (mesh), where the conservation equations are solved. When discretising, the partial differential equations are converted into an algebraic system, which are solved iteratively. In particular, the discretization process adopted for our simulations is the Finite Volume Method (FVM). It is a conservative formulation that sets the conservation equation in integral form for each control volume (cell).

The stages that define a generic CFD simulation are shown in Fig. (3.1).

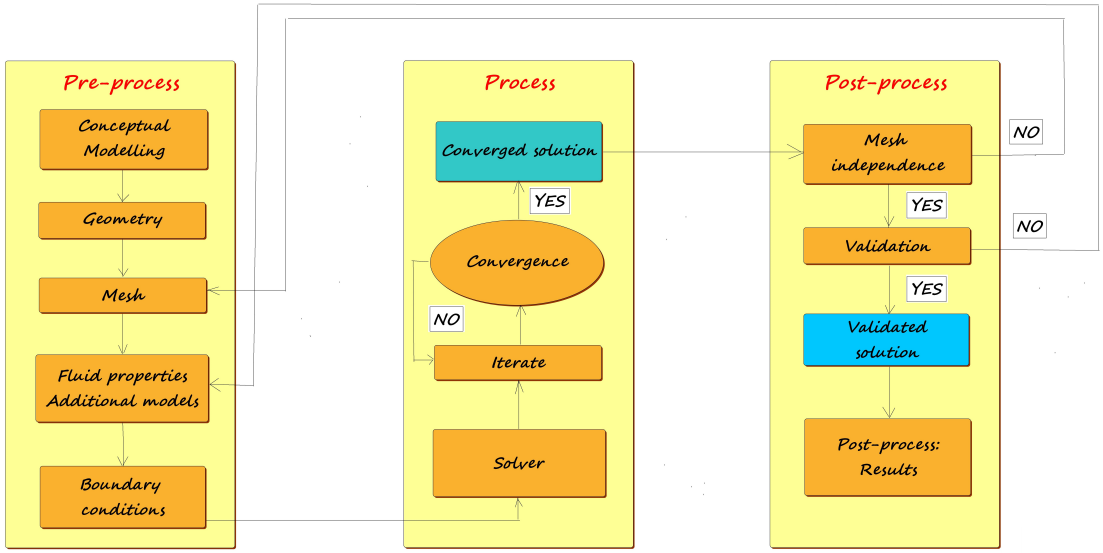

Figure 3.1: Computational Fluid Dynamics - Simulation process

As shown in Fig. (3.1), a CFD simulation can be split in 3 different parts:

1. **Pre-process**. This phase starts with the conceptual modelling. At this point, the objectives of the simulation are defined, as well as the possible simplifications (2D axisymmetric, steady/unsteady phenomena...) are implemented. After that, the geometry is designed according to the simplifications previously introduced. This geometry should be meshed, ensuring a compromise between cells quality and computational cost. In addition, the boundary conditions are set together with the fluid models: compressible/incompressible flow, heat transfer through the walls, ideal/real gases...

   One remaining point is given by the selection of the turbulence model or any additional model. In our case, a combustion model is used, which is the flamelet approach (as already commented).

2. **Process**. This stage is defined by the solver election. The solution should be iterated until convergence is achieved.

3. **Post-process**. The first step of the post-process phase is to check that mesh is independent: it means that the solution is not varying any more when mesh is refined. After that, the solution should be validated by comparing it with either numerical data coming from already validated simulations or reliable experimental data. Note that if it is not possible to validate the solution, the fluid properties and additional models considered should be checked. In most cases, the deviation is due to a wrong turbulence modelling. Finally, in case the solution is validated, the results are presented.

Once the main characteristics of Computational Fluid Dynamics have been introduced, the structure of the simulations carried out on OpenFOAM environment are briefly described.

3.1.1 OpenFOAM environment

OpenFOAM (abbreviation for Open source Field Operation And Manipulation) is a framework for developing application executables that use packaged functionality contained within a collection of approximately 100 C++ libraries. OpenFOAM is shipped with approximately 250 pre-built applications that fall into two categories: **solvers**, which are designed to solve a problem in fluid mechanics; and **utilities**, which are designed to perform tasks that involve data manipulation.

Its big flexibility allows users to extend the collection of solvers, utilities and libraries, using some pre-requisite knowledge of the underlying method, physics and programming techniques involved. [21]

As a generic CFD simulation, an OpenFOAM simulation is composed by pre-process, process and post-process. In particular, when talking about the turbulent combustion processes computed in this thesis project, the following comments can be done:

1. **Pre-process**. [5] A fundamental point is to generate the flamelet libraries, which are defining the fluid properties. They are generated by varying the stoichiometric scalar dissipation rate. Assuming the hypothesis of ideal gas, it is divided into two steps: first of all, to create the laminar flamelet libraries through the *LaminarFlamelet* software and, then, based on the obtained data, to create the turbulent flamelet libraries by the *LookUpTables* software.

   In particular, *LaminarFlamelet* software requires an input dictionary, in which the initial conditions of composition, pressure and temperature on the fuel and oxidizer sides must be specified, as well as the stoichiometric scalar dissipation rate. The *LookUpTables* software is the last step in creating flamelet libraries, where the Favre mean are applied to the flame properties, thus generating turbulent flamelets.

   Another point to consider is the geometry and mesh generation, which are achieved by using the internal mesher provided by OpenFOAM: *blockMesh*.

2. **Process**. The solver used is named flameletSMOKE. It is a CFD solver for turbulent non-premixed flames based on the Steady Laminar Flamelets method and developed by the CRECK Modeling Group of the Politecnico of Milan, Italy. [20] Specifically, flameletPimpleSMOKE is the solver used, which is an application of the flameletSMOKE solver. It implements the PIMPLE loop and includes the low-Mach number formulation.

3. **Post-process**. Once the simulations are done, data should be analysed. To achieve this goal, *paraView* is used. It is open-source visualization application that allows obtaining a huge variety of results such as vector plots, streamlines, contour plots or different property fields. During this thesis project, it is also used to export the numerical data obtained from the simulations. In this way, it is possible to later import this data into Matlab to obtain a wide sort of plots. Matlab is mainly used for the validation process of the numerical results with experimental data.

These specific comments regarding OpenFOAM framework when using a flamelet approach for the simulation of non-premixed turbulent combustion are summarised in Fig. (3.2). (Ref. [5])

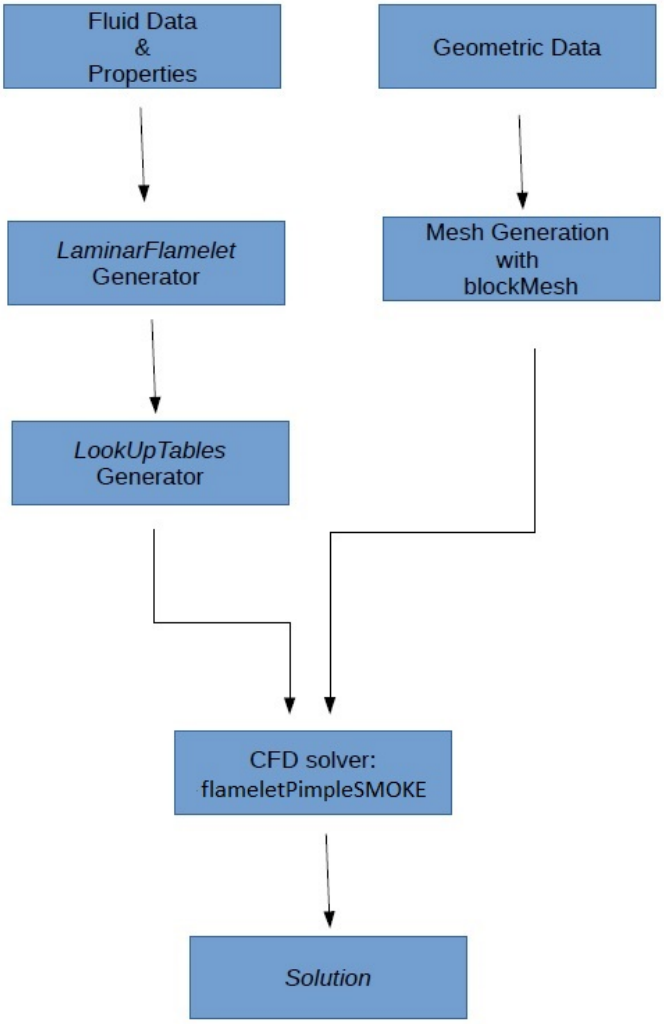

Figure 3.2: Computational Fluid Dynamics - OpenFOAM framework

Apart from the description of the CFD simulations, to define the velocity boundary condition that generates a swirling flow is of utmost importance.

3.2 Swirl boundary condition

After having described and characterised a general CFD simulation as well as having introduced OpenFOAM environment together with the main solver used in this thesis (flameletPimpleSMOKE), it is explained how a new boundary condition that replicates the swirl injector is implemented. Moreover, the complex flow structures generated by the swirl injector require a precise turbulence modelling.

3.2.1 OpenFOAM code

Taking advantage of the versatility provided by OpenFOAM environment, a new boundary condition that simulates a swirling flow is set. OpenFOAM environment has a boundary condition type called *codedFixedValue*, which allows writing your own code to model a specific boundary condition. In our case, a piece of code was found, whose aim is to produce an inflow swirl by defining the velocity field. [22]

```
{
    type            codedFixedValue;
    redirectType    swirl;

    code
    #{
        const vector axis(0, 0, 1);                         // Axis of rotation

        vectorField v = 20.0*this->patch().Cf() ^ axis;     // Angular velocity in rad/s
        v.replace(vector::Z, 1);                           // Velocity of axial flow in m/s
        operator==(v);
    #};
    value           $internalField;
}
```

Note that this code is modelling swirl motion as written in Eq. (2.5.1). As an initial step, the correct functionality of the code lines described by the comments added is checked. A parametric analysis is carried out by changing the axis of rotation, angular and axial velocity values. These modifications provided the expected results at the inlet condition.

Since its authority is unknown, a validation process is required to verify that the results given by this model correspond to the real flow behaviour.

3.2.2 Turbulence model selection

When running simulations that involve complex flow structures, such as a swirl, the selection of a suitable turbulence model becomes a key point. An extensive discussion about turbulence models is found for swirling flows. RANS limitations are exposed in [10].

Although k-ϵ is the most common turbulence model used in CFD for turbulent flow conditions, the physical phenomena presented in a swirl are not correctly described by this model. Even introducing modifications with higher order terms, this k-ϵ is not able to predict the axial and tangential velocity profiles due to the anisotropy nature of a swirling flow.

RNG k-ϵ model was developed using Re-Normalisation Group (RNG) methods to renormalise the Navier-Stokes equations in order to account for the effects of smaller scales of motion. In the standard k-ϵ model, the eddy viscosity is determined from a single turbulence length scale. Then, the calculated turbulent diffusion occurs only at the specified scale, whereas in reality, all scales of motion will contribute to the turbulent diffusion. RNG approach results in a modified form of the ϵ equation, which attempts to account for the different scales of motion through changes to the production term. [23]

It has been proved that RNG k-ϵ model gives better predictions for low Swirl Number values, while Reynolds Stress Models (RSM) are more adequate for high Swirl Number cases. Specifically, Launder and Gibson (LG) and Speziale Sarkar Gatski (SSG) models provide very good results.

In addition, Realizable k-ϵ model can be also considered for low swirl cases. [24] [25] An immediate benefit of this model is that it provides improved predictions for the spreading rate of both planar and round jets. It also exhibits superior performance for flows involving rotation, boundary layers under strong adverse pressure gradients, separation and recirculation. In virtually every measure of comparison, Realizable k-ϵ demonstrates a

superior ability to capture the mean flow of the complex structures.

All these characteristics makes the Realizable k-ϵ model an optimum choice for low swirl cases.

Moreover, RANS-based RNG k-ϵ models are compared with LES in [16]. Both LES and RANS are successfully predicting the presence of recirculation zones but they are oversized by RANS models. This fact leads to a completely different nature of recirculation zones. Regarding the vorticity field, LES shows more fine structure that the RANS result. The RANS only show the ensemble averaged representative turbulent structures while LES show the turbulent structure solved at grid level. In conclusion, LES results outperform RANS results and show a better agreement with the measurements in the statistical results and also better predict the flow pattern of the recirculation zones. RANS fails in the modelling of PVC.

Despite the better performance provided by LES, it is decided to use Realizable k-ϵ model due to the computational cost limitations (as pointed out in the previous chapter). In addition, this choice supposes another constraint: only low swirl cases can be studied.

In fact, real applications usually involve low swirled flows to avoid acoustic problems. So, this restriction is not severe. In case it is desired to increase Swirl Number, LES simulations should be run to ensure a good description of the turbulence behaviour.

Chapter 4

Numerical results

This chapter shows the discussion of the results obtained by the CFD simulations carried out in OpenFOAM environment. As already commented, introducing a swirl boundary condition that perfectly reproduces the flow behaviour imposed by a swirl injector represents the main challenge of the present thesis. As a consequence, the code presented in the previous chapter needs to be validated in order to ensure that it is describing flow motion as expected. This validation is accomplished by successfully reproducing well-known experimental and numerical tests coming from reliable bibliographic sources. Both non-reactive and reactive flow cases are considered in order to obtain a complete validation in terms of fluid dynamics and combustion.

Additionally, the limitations given by the choice of Realizable $k-\epsilon$ turbulence model should be considered and deeply analysed.

4.1 Validation of the swirl boundary condition

An intensive validation process is done, which is split in two parts, whose computational cost and complexity are gradually increased.

- Non-reactive flow: At a first stage, the behaviour of a swirling flow in a pipe is analysed. To achieve that, the simulations carried out at reference [14] are reproduced. Some simplifications are introduced in terms of turbulence model, which are deeply discussed in next sections.
- Reactive flow: The capabilities of swirl boundary condition are finally checked by simulating a well-known case given by the Sidney Burner. [26] In this case, a real combustion problem is simulated. Combustion is previously solved by using the flamelet model.

4.1.1 Non-reactive flow

Reference [14] analyses how a swirling flow evolves through a stationary pipe. Direct Numerical Simulations (DNS) were performed to compare the obtained results with another ones coming from experimental data. Three different cases are studied by varying the Geometric Swirl Number. S_g takes three different values: 1, 4.4 and 8.8.

Then, comparing our simulations with respect to these results will allow us to verify the swirl inlet condition with respect to experimental and numerical data.

4.1.1.1 Numerical settings

Before carrying out the simulations, pre-process stage is performed. The settings used are:

- Conceptual modelling: The objective defined for these simulations is to evaluate the swirl decay and to recognise its behaviour. To achieve this, a 2D axisymmetric model is used, which allows to considerably reduce the computational cost. Although swirled flows are defined as a 3D phenomenon, this assumption is completely valid due to the selection of the longitudinal axis as axis of rotation of the swirl motion. This fact makes the flow be independent of the tangential component φ.
- Geometry: The pipe is represented by a slice of a cylinder, since the case is 2D axisymmetric as just mentioned. In what refers to the dimensions and names given to each face, they are defined in Fig. (4.1).

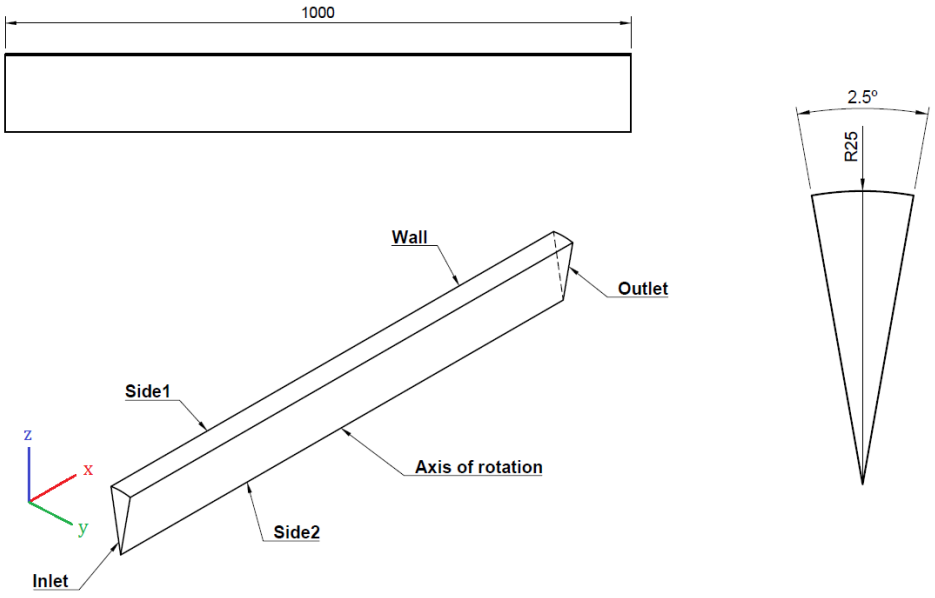

Figure 4.1: Non-reactive flow - 2D axisymmetric geometry

- Mesh: Structured mesh is used for this case. Several meshes are used until mesh convergence is met. No mesh refinements are introduced since wall functions are used to model the flow in the wall vicinity.
- Fluid properties: Flow is incompressible since water is used as working fluid. It is only required to define the kinematic viscosity (ν), which is obtained from the imposed Reynolds Number. Its value is 1730, while the flow velocity in the axial direction is 0.135 m/s and pipe diameter is equal to 0.05 m. Then:

$$Re = \frac{U \cdot D}{\nu} \Rightarrow \nu = \frac{U \cdot D}{Re} = \frac{0.135 \cdot 0.05}{1730} \simeq 10^{-6}\ m^2/s \tag{4.1.1}$$

- Boundary conditions: They are set for the pressure and velocity field at each geometric boundary defined in Fig. 4.1. The most important conditions are reported below.
  - Wall: *noSlip* is used for velocity. In this way, non slip condition is imposed, i.e. flow is slowed down to null velocity as it reaches the wall.

- Side1 and Side2: They are defined as type *wedge*, either for pressure or velocity. This boundary condition is considered for the verification of the conservation equations. wedge specifies these sides as a piece of the whole cylinder.
- Inlet: To implement swirl boundary condition, axial and angular velocity are defined. Axial velocity is kept constant for the 3 values of S_g considered with a value equal to 0.135 m/s. Then, angular velocity is varied and it is 5.4, 23.76 and 47.52 rad/s for S_g = 1, 4.4 and 8.8, respectively.
- Outlet: $fixedValue$ with an uniform field equal to 0 m^2/s^2 is used to define the initial pressure. Note that pressure boundary condition is given by pressure divided density. This fact is due to the solver used.

– Turbulence model: Realizable k-ϵ turbulence model requires to define 3 additional boundary conditions. These are the turbulent kinetic energy (k), the eddy dissipation rate (ϵ) and the turbulent kinematic viscosity (ν_t). Then, they are specified as:

- Wall: Wall functions are used to model flow behaviour in the vicinity of the wall. These are $kqRWallFunction$, $epsilonWallFunction$ and $nutWallFunction$ for k, ϵ and ν_t, respectively.
- Side1 and Side2: As defined for pressure and velocity field, they are of type *wedge*.
- Inlet: k is given by setting a turbulent intensity value. In this case, it corresponds to 5%. This value corresponds to medium-high turbulent cases. [27] The expression that relates turbulent intensity (I) with turbulent kinetic energy is:

$$I = \frac{u'}{U} \Rightarrow u' = \sqrt{\frac{2}{3} \cdot k} \Rightarrow I = \frac{\sqrt{0.667k}}{U} \tag{4.1.2}$$

  Regarding ϵ, a dissipation length is defined, which is equal to half pipe length (i.e. 0.5 m). The turbulent viscosity is set as $calculated$.
- Outlet: Both k and ϵ are defined as $inletOutlet$, while ν_t corresponds to type $calculated$.

– Solver: simpleFoam is the solver used. It is a steady-state solver for incompressible, turbulent flow, which uses the SIMPLE algorithm to solve the p-v coupling.

4.1.1.2 Analysis of results

Once the simulations have been set, the results obtained are analysed. First of all, it should be noted that completely incoherent results were obtained for high swirl flows due to the turbulence model selection. Then, the only case reported is S_g = 1. A mesh independence study is carried out to guarantee the convergence of the simulations.

The criterion established when refining the mesh is that between two successive meshes the number of cells in each dimension should be increased, at least, by 1.5 times. It means that for 2D meshes, the number of cells should be raised 2.25 times as minimum. [28] This second definition is the one adopted, since it allows to modify the aspect ratio of the cells. As a consequence, it is possible to refine more in the regions with higher gradients. Mesh properties are sum up in Table (4.1).

Properties	Coarse	Medium	Refined	Ultrarefined
Number of cells	300 x 15 = 4500	450 x 23 = 10350	675 x 35 = 23625	1200 x 45 = 54000
Cell size (mm^2)	3.33 x 1.66	2.22 x 1.08	1.48 x 0.71	0.83 x 0.55
Aspect ratio	2	2.04	2.07	1.5

Table 4.1: Non-reactive flow - Mesh properties

The mesh is considered to be independent when the variation of the variables of interest is lower than 1 % between two successive meshes. [28] Velocity magnitude and axial velocity are chosen as variables of interest. They are studied at two different sections: x/D = 3 and x/D = 5, since at these positions is where the data to be compared is available. From Figs. (4.2) and (4.3), it can be observed the mesh is independent for 23k.

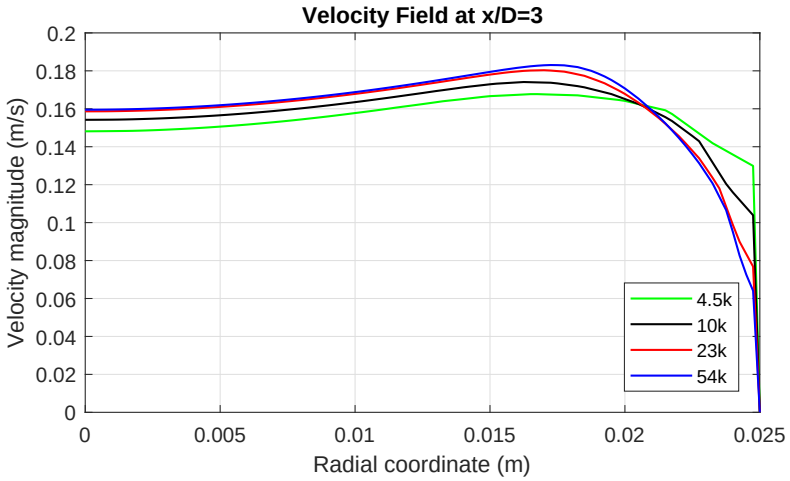

(a) x/D = 3

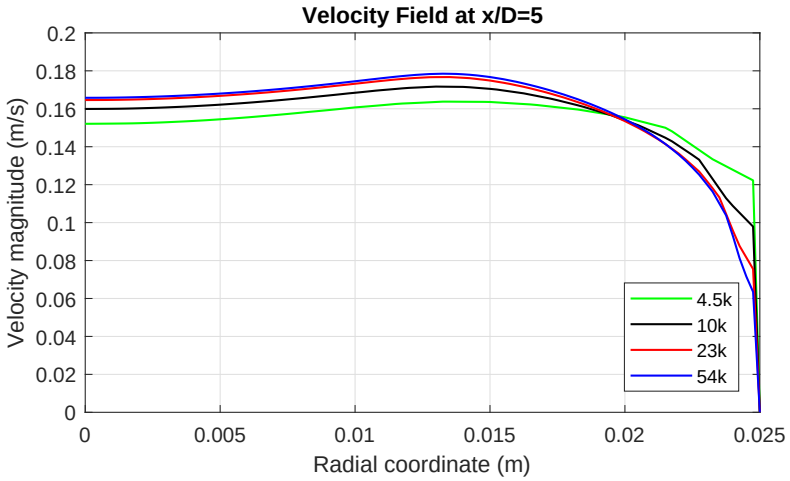

(b) x/D = 5

Figure 4.2: Non-reactive flow - Mesh independence for velocity magnitude

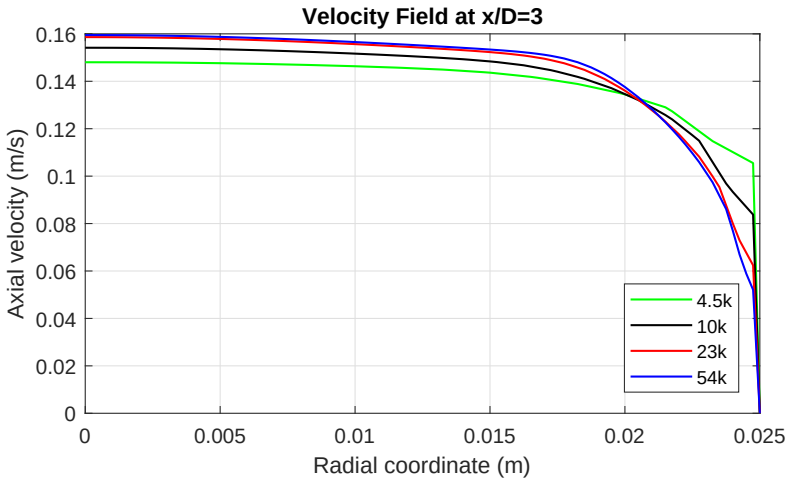

(a) x/D = 3

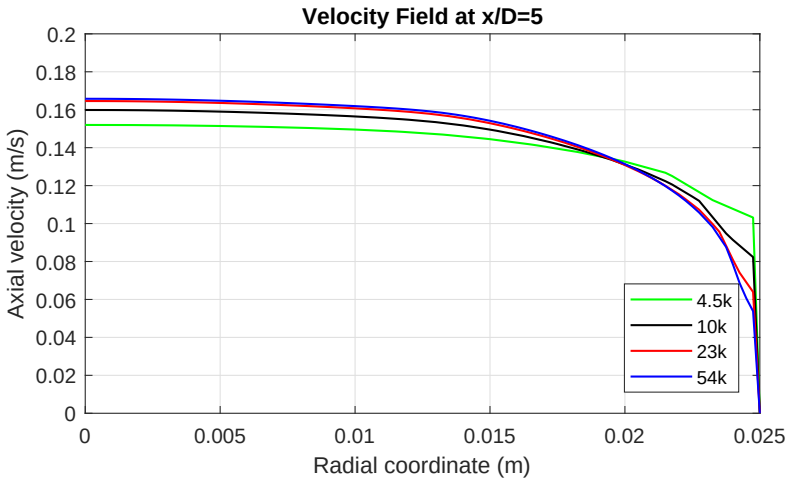

(b) x/D = 5

Figure 4.3: Non-reactive flow - Mesh independence for axial velocity

Finally, the data given by the independent mesh is compared with the numerical DNS and experimental data coming from [14]. This data is given as dimensionless because axial velocity and radial coordinate are divided by initial axial velocity and pipe radius, respectively.

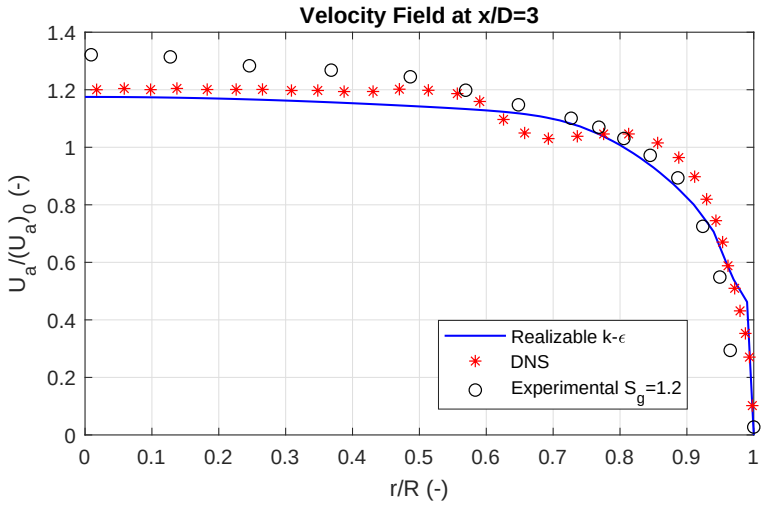

(a) x/D = 3

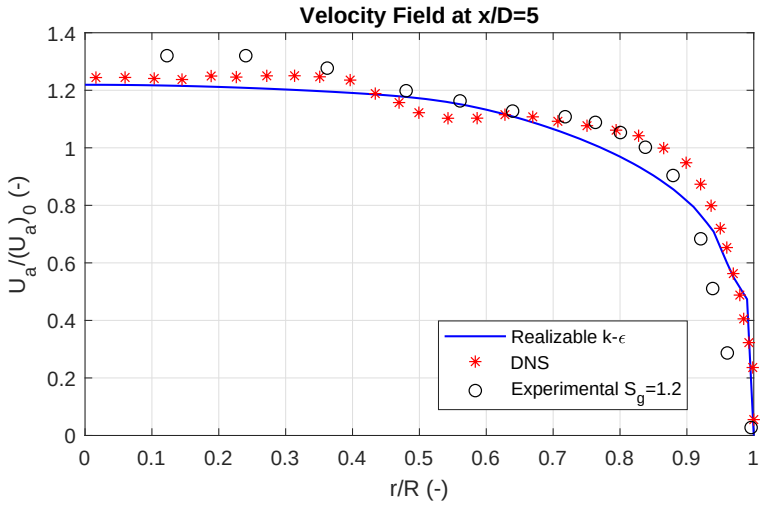

(b) x/D = 5

Figure 4.4: Non-reactive flow - Validation for axial velocity

From Fig. (4.4), it can be observed that Realizable k-ϵ provides a very good fitting with respect to DNS data. There is an undershoot in DNS data before velocity decay close to the wall. This phenomena is not reproduced by Realizable k-ϵ simulation. However, this deviation is not very important and, in general terms, Realizable k-ϵ model is providing a good performance.

In addition, regarding the comparison with respect the experimental data, it should be noted a slight increase in the Geometric Swirl Number, whose value is 1.2. Anyway, the trend described can be studied, which is providing a similar behaviour. Then, swirl boundary condition is verified for low swirl cases and using Realizable k-ϵ as turbulence model.

4.1.2 Non-reactive flow by flamelet model

Before running the reactive flow simulations, which make of use the flamelet model to compute the flow properties coming from the combustion process, another simulation involving non-reactive flow is done. Flamelet model is introduced for calculating the flow properties of a non-reactive flow. It means that constant properties are found for any mixture fraction since only one fluid is used (H_2O in liquid phase). In this way, instead of defining the fluid properties at *transportProperties* file, they are defined through the generated flamelet library, which is called when running flameletSMOKE solvers.

4.1.2.1 Numerical settings

The pre-process is almost equal to the one previously set for simpleFoam simulation. The changes performed are linked to the new solver, which is flameletPimpleSMOKE. It solves the p-v coupling by using the PIMPLE algorithm and it asks for the fluid properties to the generated flamelet library. Regarding the numerical settings, the main modifications introduced are:

- Fluid properties: As already noted, fluid properties are loaded from the flamelet library, whose path is defined in $flameletProperties$ file. Flamelet libraries are composed by 11 thermodynamic properties. These are the mixture fraction (Z), temperature (T), pressure (p), molecular weight (M_w), density (ρ), scalar dissipation rate (χ), enthalpy (h), isobaric heat capacity (c_p), thermal conductivity (λ), thermal diffusivity (α) and dynamic viscosity (μ). Note that all these properties are the turbulent ones, and not the laminar ones.

  Additionally, n mass fractions corresponding to the n elements that compound the mixture. In this case, there is only one specie: H_2O. In the previous simulation (simpleFoam), the only fluid property defined was the kinematic viscosity. However, in this case, it is defined the dynamic viscosity and the density, in such a way that its quotient leads to the same value for ν.

- Boundary conditions: flameletPimpleSMOKE solver requires to define 11 boundary conditions. This fact means that 6 additional properties are introduced with respect to simpleFoam simulation. These are the turbulent thermal diffusivity (α_t), enthalpy (h), turbulent dynamic viscosity (μ_t), temperature (T), mixture fraction (Z) and its variance (Z_{var}). They are defined in correspondence to the values contained in the flamelet library.

  Moreover, it should be pointed out that the actual pressure should be set in this simulation, which is equal to 1 atmosphere.

In what refers to the domain discretization, the independent mesh found in simpleFoam simulation is used. Then, once the setting is completed, the simulation is carried out.

4.1.2.2 Analysis of results

The results obtained with flameletPimpleSMOKE solver are compared with the ones given by simpleFoam solver. This comparison is performed for velocity magnitude and axial velocity, as shown in Figs. (4.5) and (4.6). It can be observed a perfect overlapping between simpleFoam and flameletPimpleSMOKE curves. As a consequence, flameletPimpleSMOKE solver is validated for swirling non reactive flows.

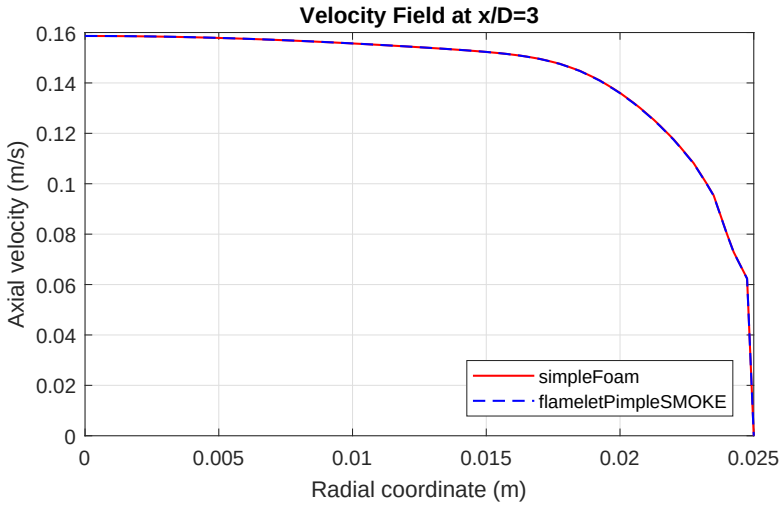

(a) x/D = 3

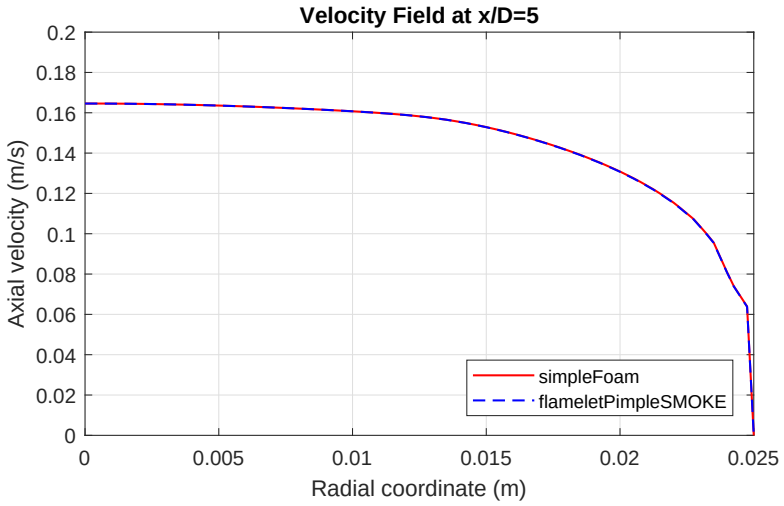

(b) x/D = 5

Figure 4.5: Non-reactive flow - Solvers comparison for axial velocity

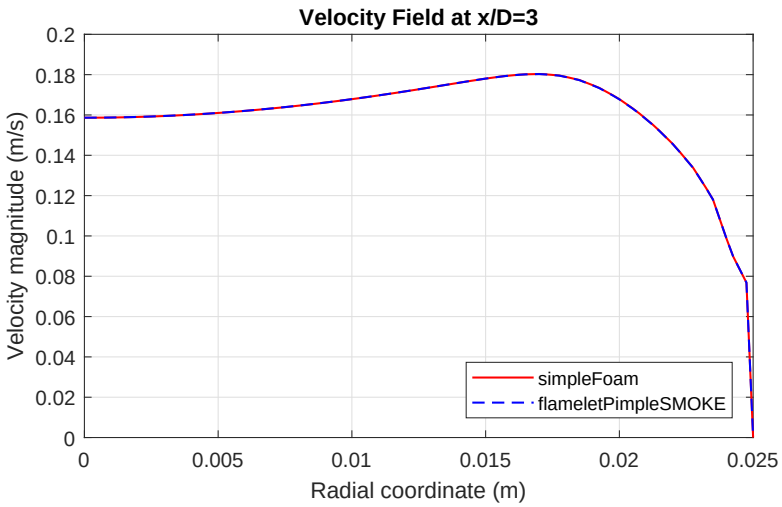

(a) x/D = 3

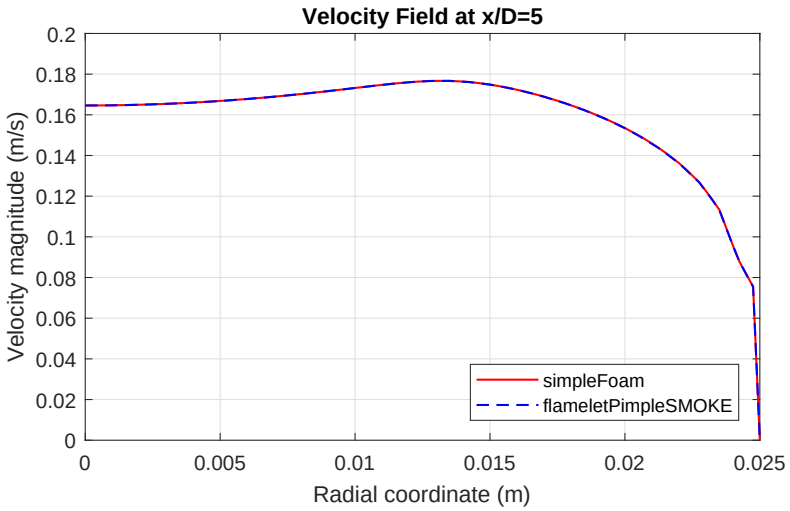

(b) x/D = 5

Figure 4.6: Non-reactive flow - Solvers comparison for velocity magnitude

4.1.3 Reactive flow

Once swirl boundary condition has been satisfactory introduced into non reactive flows, reactive flow is analysed. Sydney burner experiments are taken as reference, considering only low swirl cases. In fact, most of the flames studied by Sydney's university researchers are low swirled. Among the available experimental data, the so-called SM1 flame is chosen as starting point.

4.1.3.1 Sydney burner

The swirl burner shown in Fig. (4.7) is featuring a fuel jet with a diameter equal to 3.6 mm surrounded by a bluff-body of 50 mm diameter. An annular gap (5 mm wide) around the bluff-body provides the swirled primary air. Swirl is introduced aerodynamically by using tangential ports 300 mm upstream of the burner exit. Two diametrically opposed ports, located on the periphery of the burner, but upstream of the tangential inlets, supply the axial air to the swirling stream. The swirled air passes through a tapered neck section that ends 140 mm upstream of the burner exit plane. This promotes uniform boundary conditions at the exit plane by combining the axial and tangential air streams to form an uniform swirling flow. The burner is installed in a wind tunnel which provides a secondary axial air flow. Its objective is to surround the flame and provide well defined outer boundaries and pressure conditions. [29] [30]

Generally, there are four parameters which control the stability characteristics and the flame physical properties. These are:

- Bulk fuel jet velocity (U_j)
- Bulk axial velocity in the primary air stream (U_s)
- Bulk tangential velocity in the primary air stream (W_s)
- Bulk co-flow velocity in the secondary air stream (U_e)

Note that Sydney burner is working with the modelling initially described by Eq. (2.5.1). Additionally, Geometric Swirl number (S_g) should be set. As known, it provides an indication of the intensity of the swirl in the annular flow.

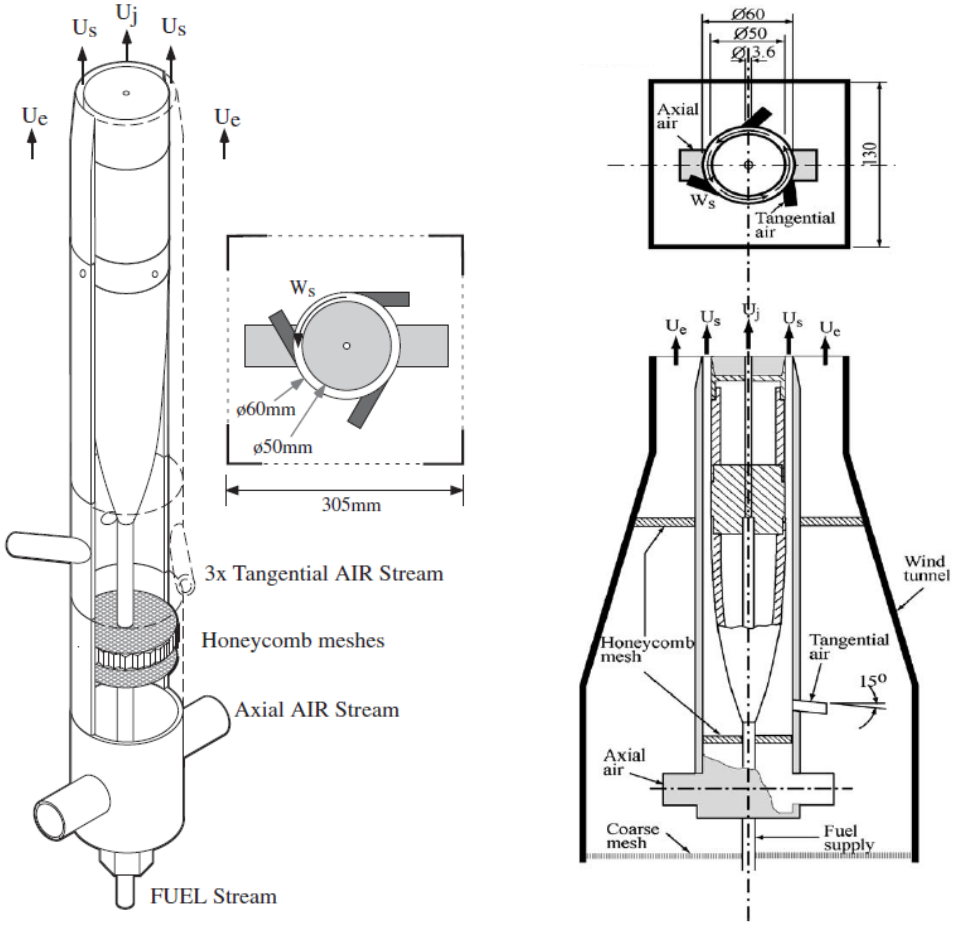

(a) Schematics (b) Dimensions

Figure 4.7: Reactive flow - Sydney burner geometry

Fig. (4.7) (Ref. [29] and [30]) shows Sydney burner geometry, where the different fuel and air streams are reported.

4.1.3.2 SM1 flame

As already said, SM1 flame is a swirling flame. It is a CNG (Compressed Natural Gas) flame, whose composition contains more than 90% methane (CH_4) by volume. The remaining constituents are carbon dioxide ($C0_2$), propane (C_3H_8) and butane (C_4H_{10}). Regarding the oxidizer, air is used. Both fuel and oxidizer are present in gaseous phase. The main flame characteristics are summarised in Table (4.2), where velocities are written in m/s.

To perform the numerical simulations, flames burning pure methane are assumed. Since flamelet model is used as combustion model, initial conditions should be computed from the data coming from Table (4.2) in order to generate the flamelet library corresponding to the combustion of methane into air.

Flame	Fuel mixture	U_s	W_s	U_j	Re_s	Re_{jet}	S_g
SM1	CNG	38.2	19.1	32.7	75900	7200	0.5

Table 4.2: Reactive flow - SM1 flame properties

Initial conditions

The initial flame conditions are computed through a three steps loop:

1. An initial guess for temperature is done. Since dynamic viscosity depends on temperature ($\mu = f(T)$), its value can be computed once the initial temperature is set. Dynamic viscosities can be obtained from reference [31]. Then, using Reynolds number definition, density can be solved. It is:

$$\rho = \frac{Re \cdot \mu}{u \cdot D} \tag{4.1.3}$$

where D is the pipe diameter. In the case of the annular air flow, the diameter of a pipe with equal area should be computed. The governing equation is:

$$\frac{\pi}{4} \cdot D_o^2 - \frac{\pi}{4} \cdot D_i^2 = \frac{\pi}{4} \cdot D_{eq}^2 \tag{4.1.4}$$

where D_o, D_i and D_{eq} are the outer, inner and equivalent diameters, respectively. The value obtained is D_{eq} = 33.16 mm.

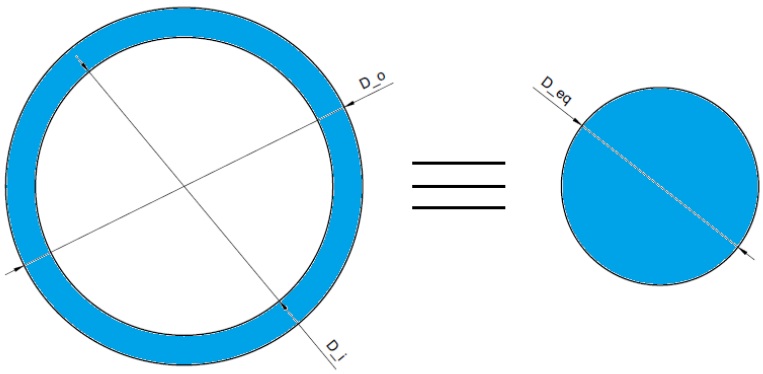

Figure 4.8: Reactive flow - Equivalent pipe

2. Using ideal gas equation, and knowing that the experiments are performed at ambient pressure ($p = 101325\ Pa$), temperature can be solved.

$$p = \rho RT \Rightarrow T = \frac{p}{\rho R} \tag{4.1.5}$$

3. Finally, it is checked if the temperature obtained is corresponding to the value initially guessed ($T_0 = T_1$). If not ($T_0 \neq T_1$), the average temperature is supposed as new initial guess and the process is repeated.

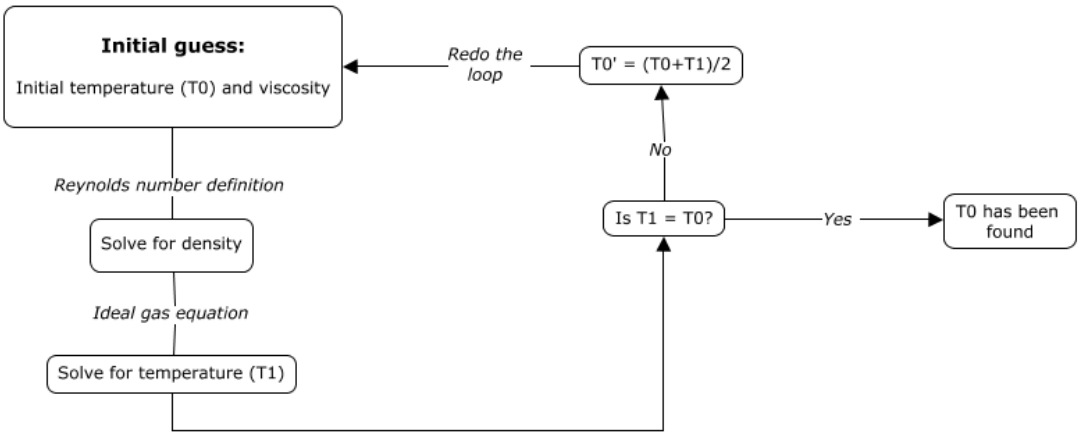

Figure 4.9: Reactive flow - Loop initial flame conditions

This loop is performed for the fuel jet and the air primary flow. 2 iterations are required to obtain fuel initial conditions, while 3 iterations are needed for the air annular flow. The results are shown in Table (4.3):

Fuel (CH_4)				
Iteration	T_0 (ºC)	μ (Pa·s)	ρ (kg/m^3)	T_1 (ºC)
#1	20	$1.1 \cdot 10^{-5}$	0.673	17.47
#2	18.74	$1.09 \cdot 10^{-5}$	0.666	20.4
Oxidizer (Air)				
Iteration	T_0 (ºC)	μ (Pa·s)	ρ (kg/m^3)	T_1 (ºC)
#1	20	$1.82 \cdot 10^{-5}$	1.09	50.69
#2	35.35	$1.89 \cdot 10^{-5}$	1.13	38.55
#3	36.95	$1.90 \cdot 10^{-5}$	1.14	36.92

Table 4.3: Reactive flow - SM1 flame initial conditions

From Table (4.3), it is observed that methane is initially at approximately 18.9 ºC (i.e, average value between the two finals temperatures), while air has an initial temperature equal to 36.95 ºC. Regarding the secondary air flow, it is assumed to be at the same temperature as the annular air flow. Once this data is known, numerical simulations can be carried out.

4.1.3.3 Numerical settings

The pre-process is almost equal to the one previously set for flameletPimpleSMOKE simulation, since the same solver is used for this case. Regarding the numerical settings, the main comments to be done are:

– Geometry: To model Sydney burner, the geometry shown in Fig. (4.7) should be replicated.

To achieve that, 4 coaxial cylindrical wedges are built, each one corresponding to fuel jet, bluff body, primary air stream and air co-flow stream, respectively. Regarding the dimensions of the computational domain, it has been varied between the different meshes, since the initial computational domain set, which was based on the considerations done by [17], was too big. The final geometry is characterised by a length of 10 times the bluff body radius, while external radius of the co-flow is equal to 3 times the bluff body radius. (See Table (4.4)). The final computational domain is reported in Fig. (4.10).

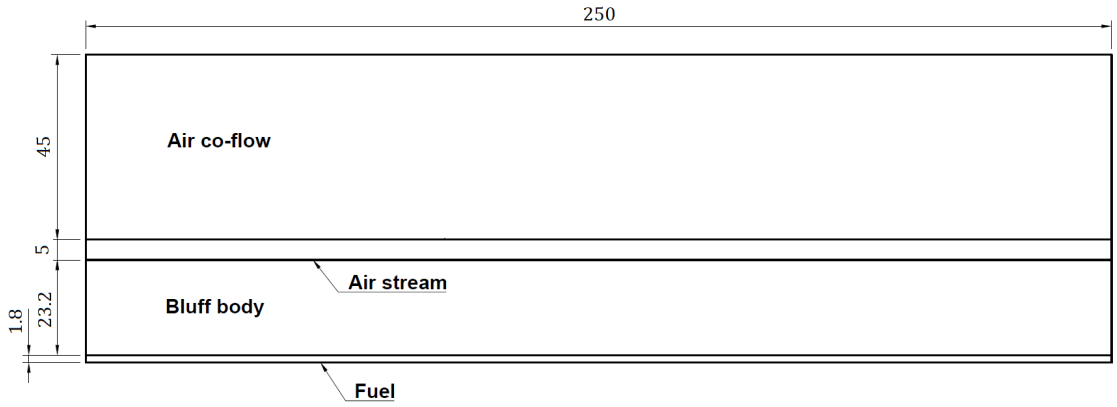

Figure 4.10: Reactive flow - Sydney burner computational domain

- Mesh: In what refers to the domain discretization, several simulations are run to obtain an independent mesh. As in previous cases, structured meshes are used.
- Fluid properties: Fluid properties are loaded from the flamelet library, whose path is defined in $flameletProperties$ file. In this case, the flamelet is containing the chemical information of a methane-air reaction. Further information about the chemical mechanism can be found at [5].
- Boundary conditions: flameletPimpleSMOKE solver requires to define 11 boundary conditions. This fact means that 6 additional properties are introduced with respect to simpleFoam simulation. These are the turbulent thermal diffusivity (α_t), enthalpy (h), turbulent dynamic viscosity (μ_t), temperature (T), mixture fraction (Z) and its variance (Z_{var}). As before, they are defined in correspondence to the values contained in the flamelet library.

Moreover, it should be pointed out that the actual pressure should be set in this simulation, which is equal to 1 atmosphere as used for the initial conditions calculation, while inlet velocities are specified in Table (4.2).

4.1.3.4 Analysis of results

As first step, the mesh independence study is carried out to guarantee the convergence of the simulations. 4 different meshes are considered, whose properties are reported below. Note that for air co-flow, mesh grading has been introduced due to the high computational cost of these simulations (from 40k the order of magnitude for the simulation times is a day). In addition, as already commented, the section of this external air co-flow is reduced since the boundary condition was too far in the coarsest meshes. This means that an excess of computational power was used unnecessarily.

Properties		Coarse	Medium	Refined	Ultrarefined
Fuel	Section (mm^2)	1.8 x 250	1.8 x 250	1.8 x 250	1.8 x 250
	Number of cells	1 x 93 = = 93	2 x 186 = = 372	4 x 372 = = 1488	6 x 372 = = 2232
	Cell size (mm^2)	1.8 x 2.69	0.9 x 1.34	0.45 x 0.67	0.3 x 0.67
	Aspect ratio	1.49	1.49	1.49	2.24
Bluff body	Section (mm^2)	23.2 x 250	23.2 x 250	23.2 x 250	23.2 x 250
	Number of cells	13 x 93 = = 1209	26 x 186 = = 4836	52 x 372 = = 19344	78 x 372 = = 29016
	Cell size (mm^2)	1.78 x 2.68	0.89 x 1.34	0.45 x 0.67	0.3 x 0.67
	Aspect ratio	1.51	1.51	1.51	2.24
Air stream	Section (mm^2)	5 x 250	5 x 250	5 x 250	5 x 250
	Number of cells	3 x 93 = = 279	6 x 186 = = 1116	12 x 372 = = 4464	18 x 372 = = 6696
	Cell size (mm^2)	1.66 x 2.69	0.83 x 1.35	0.42 x 0.67	0.25 x 0.67
	Aspect ratio	1.62	1.62	1.62	2.68
Air co-flow	Section (mm^2)	190 x 250	80 x 250	45 x 250	45 x 250
	Number of cells	106 x 93 = = 9858	89 x 186 = = 16554	81 x 372 = =30132	121 x 372 = = 45012
	Grading	1	1	1.5	2
	Biggest cell size (mm^2)	1.79 x 2.69	0.9 x 1.34	0.67 x 0.67	0.5 x 0.67
	Smallest cell size (mm^2)	1.79 x 2.69	0.9 x 1.34	0.44 x 0.67	0.25 x 0.67
	Biggest Aspect ratio	1.49	1.49	1.52	2.68
	Smallest Aspect ratio	1.49	1.49	1	1.34
Total	Number of cells	123 x 93 = = 11439	123 x 186 = = 22878	149 x 372 = = 55428	223 x 372 = = 82956
	Simulation time (h)	3	7	28	80
	Number CPU	4	4	6	7

Table 4.4: Reactive flow - SM1 mesh properties

The results obtained for mesh independence analysis are reported on Figs. (4.11), (4.12) and (4.13), while the validation plots are given by Figs. (4.14), (4.15) and (4.16).

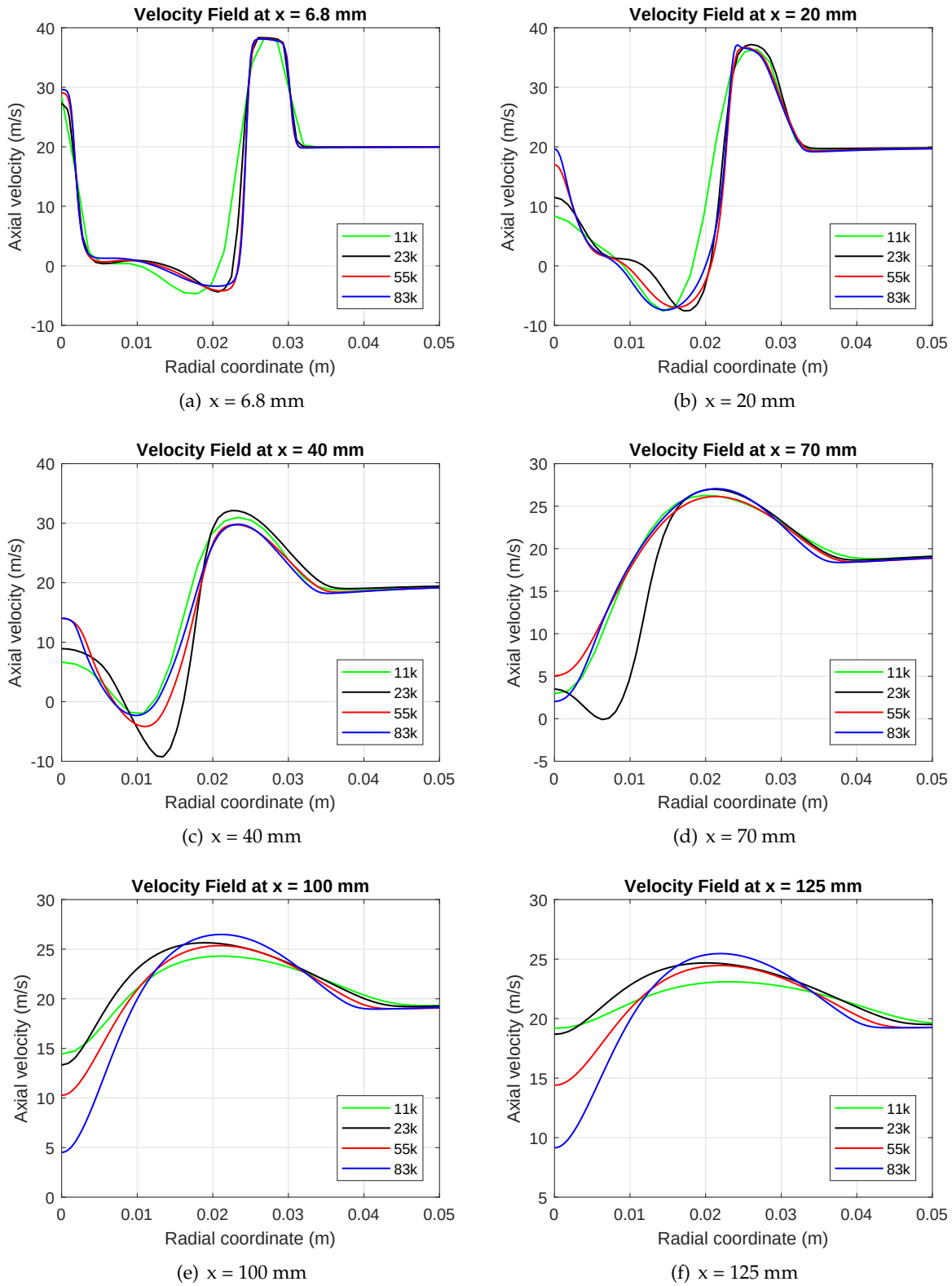

(a) x = 6.8 mm

(b) x = 20 mm

(c) x = 40 mm

(d) x = 70 mm

(e) x = 100 mm

(f) x = 125 mm

Figure 4.11: Reactive flow - SM1 mesh independence for axial velocity

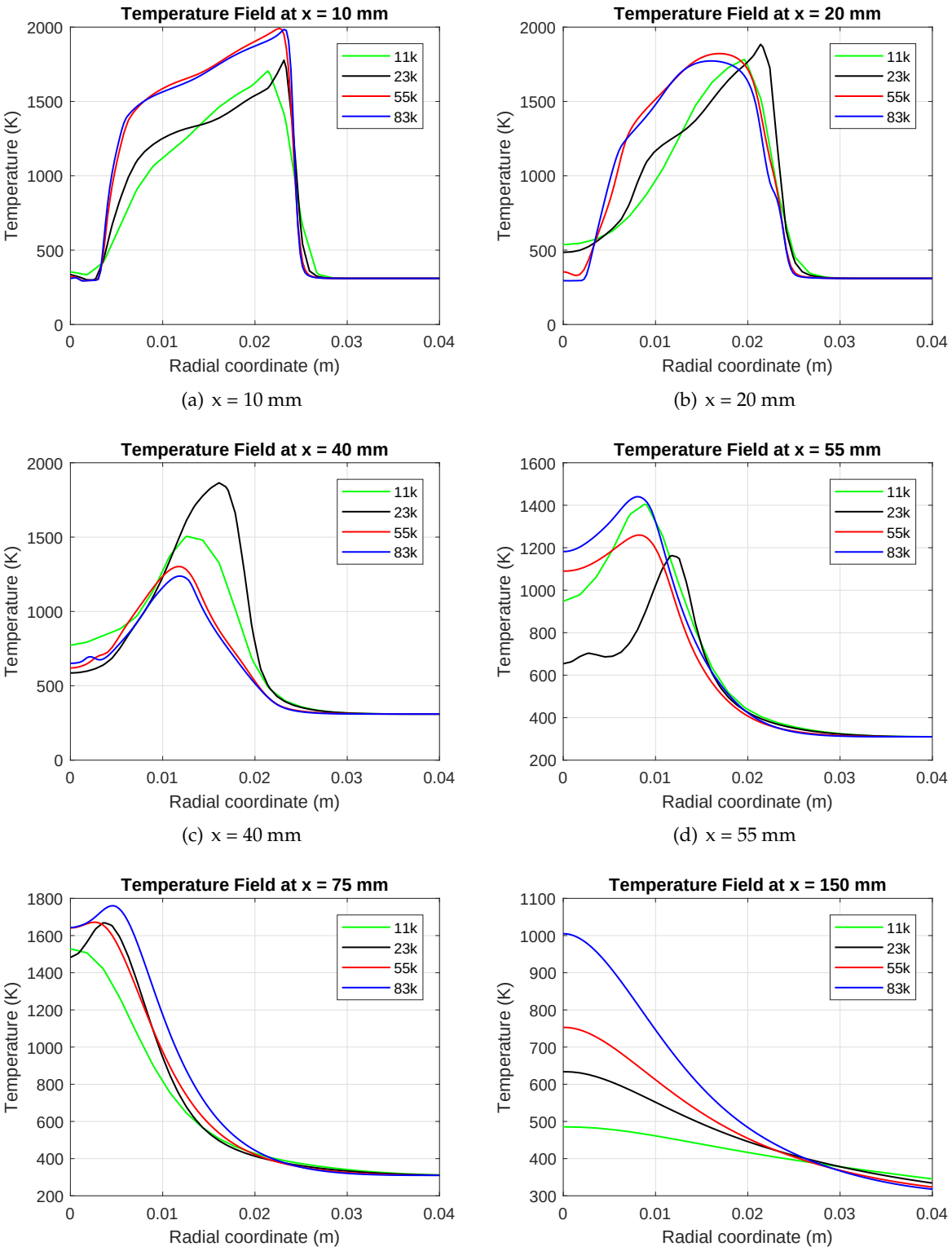

(a) x = 10 mm

(b) x = 20 mm

(c) x = 40 mm

(d) x = 55 mm

(e) x = 75 mm

(f) x = 150 mm

Figure 4.12: Reactive flow - SM1 mesh independence for temperature

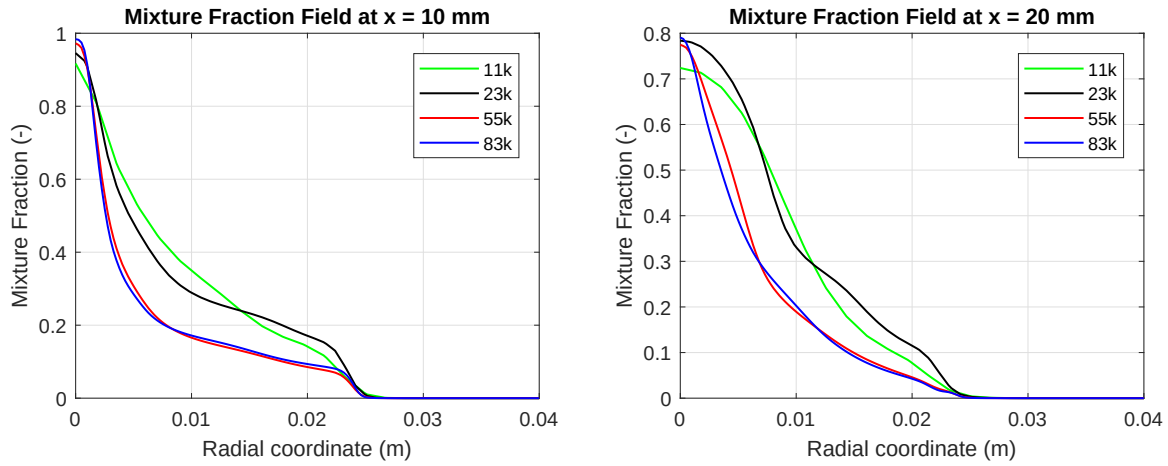

(a) x = 10 mm

(b) x = 20 mm

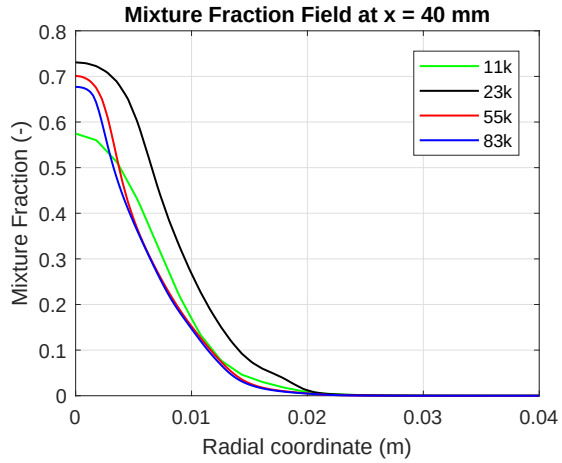

(c) x = 40 mm

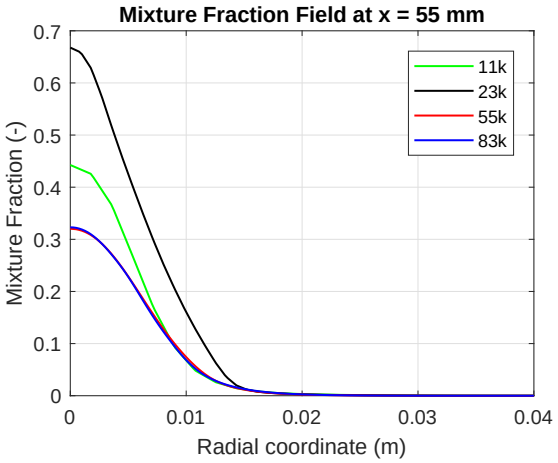

(d) x = 55 mm

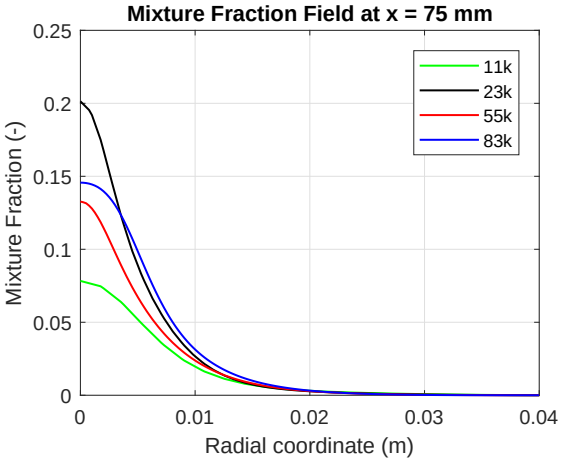

(e) x = 75 mm

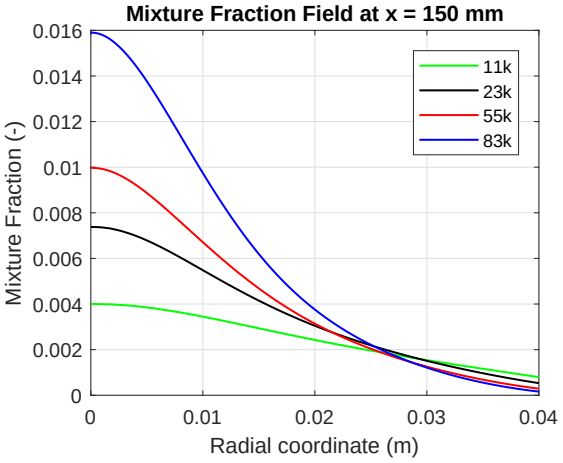

(f) x = 150 mm

Figure 4.13: Reactive flow - SM1 mesh independence for mixture fraction

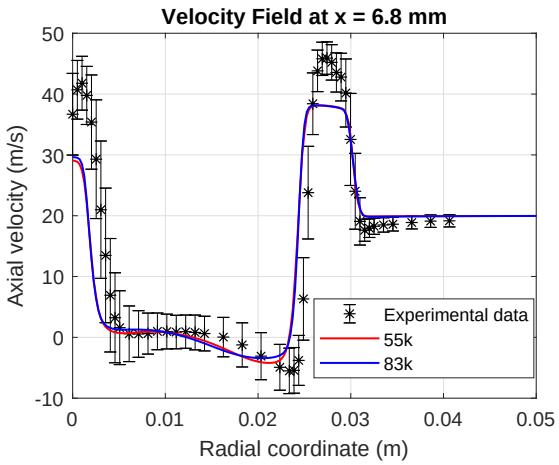

(a) x = 6.8 mm

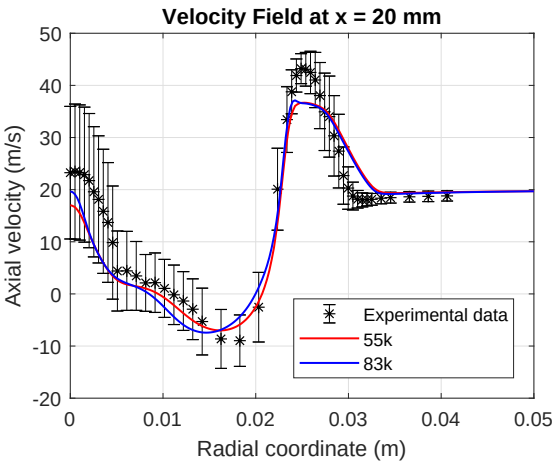

(b) x = 20 mm

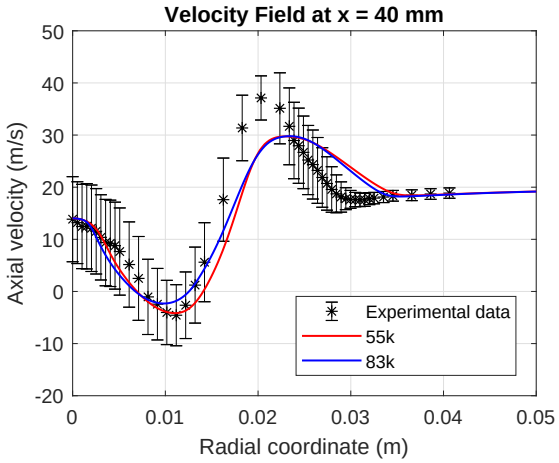

(c) x = 40 mm

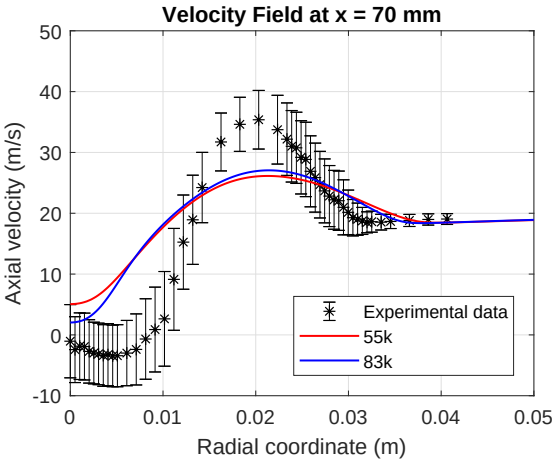

(d) x = 70 mm

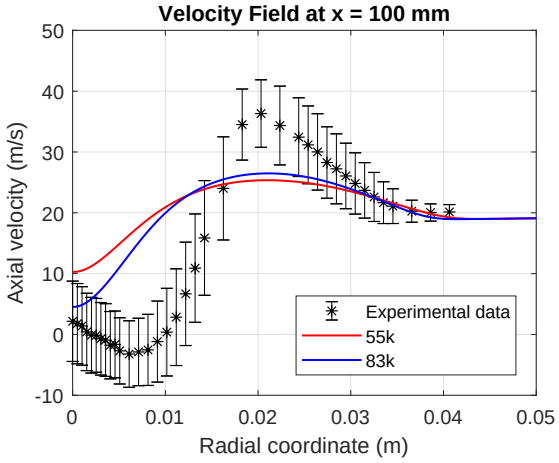

(e) x = 100 mm

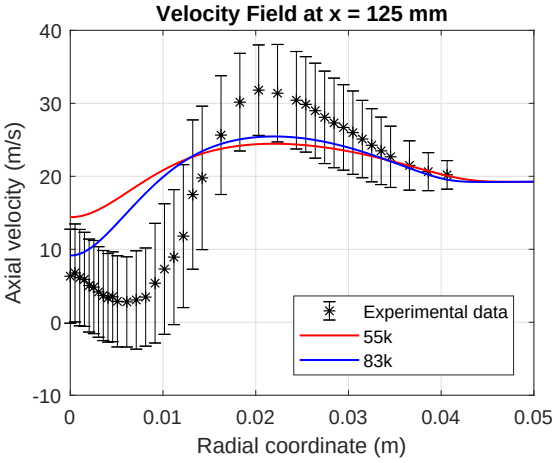

(f) x = 125 mm

Figure 4.14: Reactive flow - SM1 axial velocity

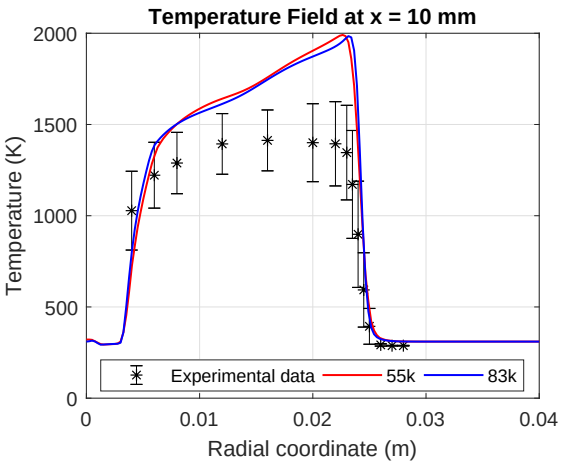

(a) x = 10 mm

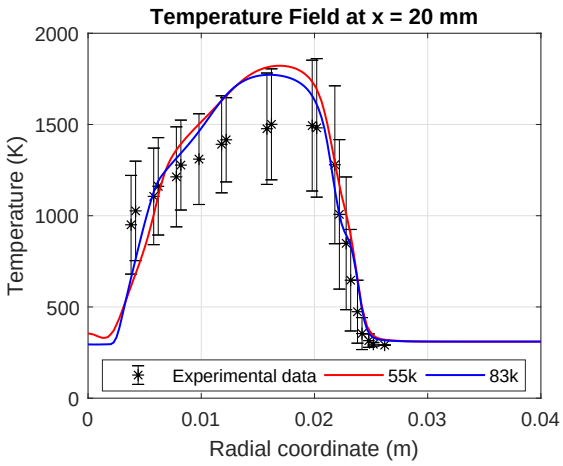

(b) x = 20 mm

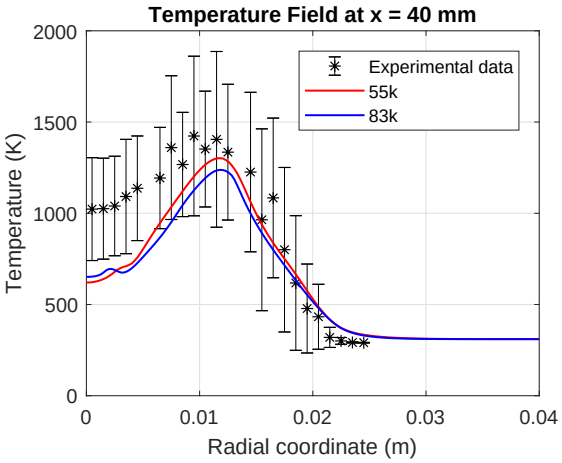

(c) x = 40 mm

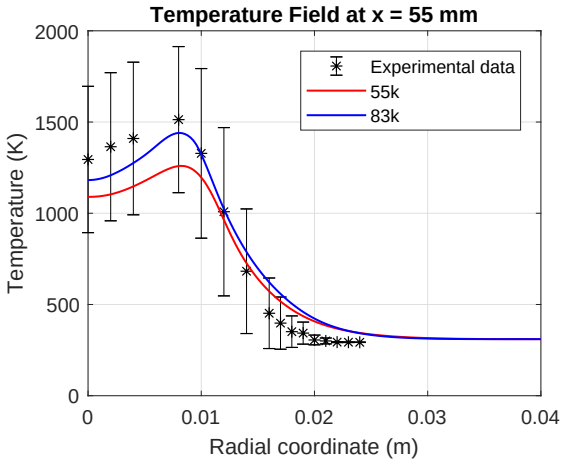

(d) x = 55 mm

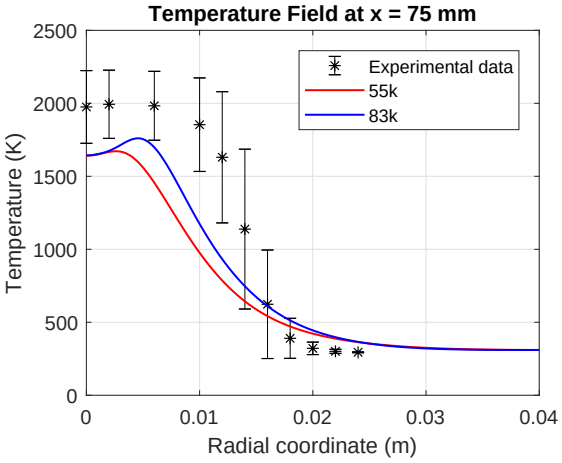

(e) x = 75 mm

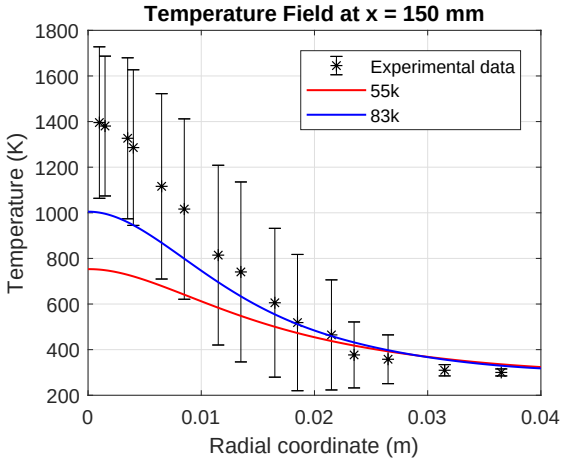

(f) x = 150 mm

Figure 4.15: Reactive flow - SM1 temperature

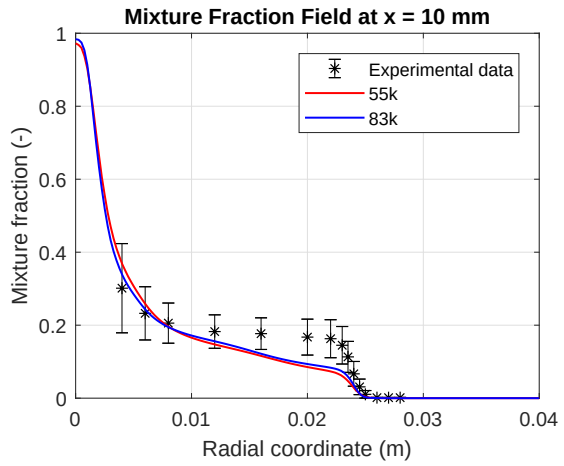

(a) x = 10 mm

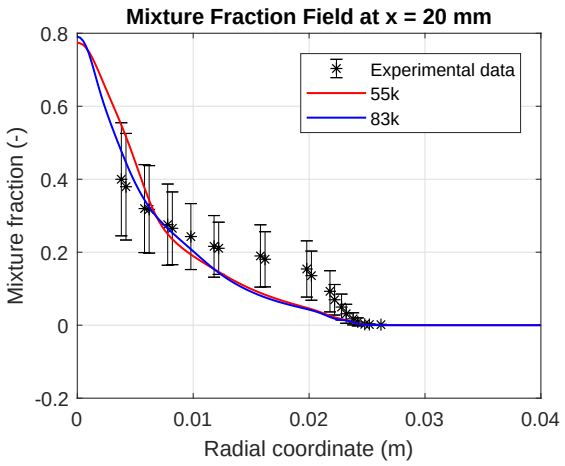

(b) x = 20 mm

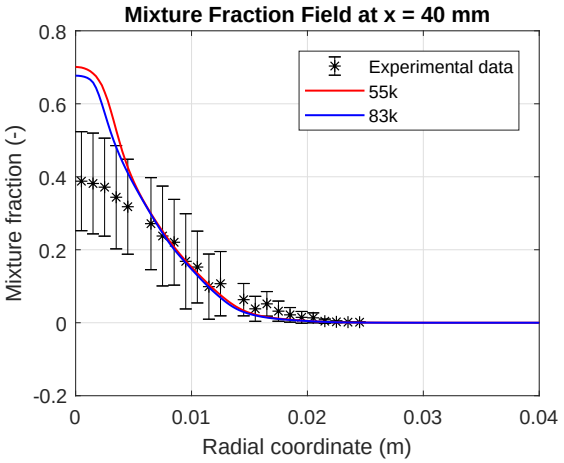

(c) x = 40 mm

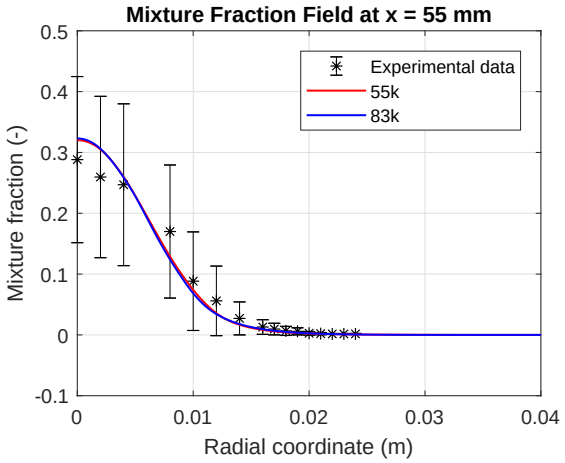

(d) x = 55 mm

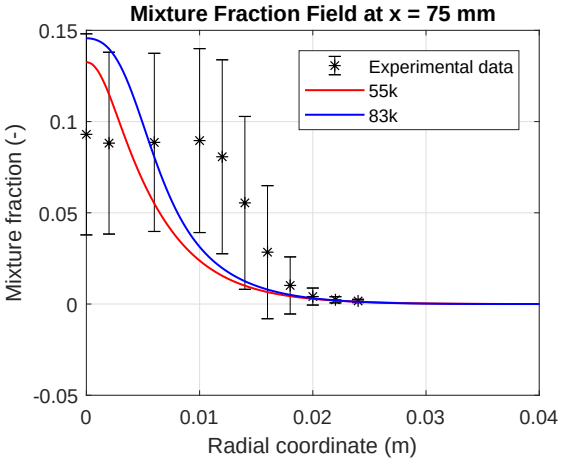

(e) x = 75 mm

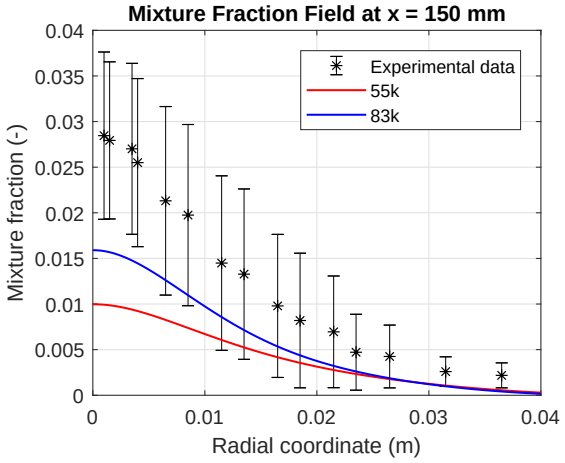

(f) x = 150 mm

Figure 4.16: Reactive flow - SM1 mixture fraction

First of all, it should be commented that velocity field is analysed at x = 6.8 mm, x = 20 mm, x = 40 mm, x = 70 mm, x = 100 mm and x = 125 mm, while temperature and mixture fraction are measured at x = 10 mm, x = 20 mm, x = 40 mm, x = 55 mm, x = 75 mm and x = 150 mm. Properties are calculated at these longitudinal sections since they are the positions where experimental data is provided by [26]. Note that x = 0 mm corresponds to the injectors inlet.

Mesh independence

Regarding **velocity** field (Fig. (4.11)), mesh can be considered as independent for any level of refinement at x = 6.8 mm and x = 20 mm. However, at x = 40 mm and x = 55 mm the only independent mesh in given by 55k. As moving further from injectors inlet, mesh independence cannot even be guaranteed for 55k. Although trends are similar, big deviations are observed at x = 100 mm and x = 125 mm.

In what respect to **temperature** plots (Fig. (4.12)), mesh independence is achieved for 55k at x = 10 mm, x = 20 mm and x = 40 mm. As observed with velocity field, as further moving from the inlet, to reach mesh independence becomes more difficult. As before, trends are quite close but values are different. At x = 150 mm, big deviations are observed, so mesh should be refined.

Finally, **mixture fraction** can also be studied (Fig. (4.13)). It follows an analogous behaviour to temperature field at x = 10 mm, x = 20 mm and x = 40 mm since mesh is independent for 55k. Additionally, at x = 55 mm mesh is also converged, while at x = 75 mm and x =150 mm differences are less important than for temperature field. So, it means that mixing problem is less exigent in terms of level refinement.

So, in general words, 55k mesh can be considered independent at sections close to the injectors inlet ($x < 55$ mm). However, when moving further this condition is not guaranteed.

Due to the high computational cost of the last simulation, which took approximately 80 hours with a mesh of 82956 cells (as reported in Table (4.4)), it is decided to not refine any more the mesh. Increasing the refinement level will mean moving to simulation times in the order of magnitude of weeks, which is not recommended when using RANS models. So, if higher precision was desired, introducing LES turbulence model would be the best option.

Validation SM1 flame

Experimental results are compared with numerical results of the two finest grids. In this way, it is possible to comment if increasing the refinement level makes the numerical solution be closer to the experimental data. This fact would mean that turbulence modelling is not so bad and deviations are mainly due to mesh quality.

Firstly, some comments about the post-processing of experimental data can be done. While velocity data was given with its average and standard deviation, temperature and mixture fraction were given as temporal data. So, time averages are computed for temperature and mixture fraction, obtaining also its standard deviation. It is represented by the error bars presented in Figs. (4.14), (4.15) and (4.16).

In what refers to **velocity** field (Fig. (4.14)), several comments can be done:

- At x = 6.8 mm, numerical data follows experimental data trend. However, it fails at the maximum peaks, which are at r = 0 mm and r = 27 mm. It could be observed that this deviation is bigger at r = 0 mm. Anyway, this behaviour is unexpected: this longitudinal section is very close to the injector and then, it should give as result values very close to the inlet axial velocities. For example, numerical results correspond to axial velocities approximately equal to 30 m/s, 38 m/s and 20 m/s for fuel jet, air primary stream and air co-flow, respectively. Note that these values are very close to the ones reported in Table (4.2). However, experimental data is further from the initial inlet conditions except for the air co-flow.

  In addition, it can be noticed that from r $\approx$ 15 mm to r $\approx$ 23 mm a recirculation bubble is already formed, since there is reverse flow (i.e. negative axial velocity) due to the presence of the bluff body combined with the swirl motion.

- At x = 20 mm, it can be observed a very good fitting between experimental and numerical data. In this case, the underestimation offered by numerical results at r = 0 mm and r = 27 mm is smaller. Again, this deviation can be justified in an analogous way to x = 6.8 mm. At this location, recirculation bubble has moved down in the radial coordinate.

- At x = 40 mm, the fitting is still good. However, the effects of the high diffusivity associated to RANS turbulence model can be slightly appreciated.

- At x = 70 mm, x = 100 mm and x = 125 mm, Realizable $k-\epsilon$ model is not able to accurately reproduce the flow behaviour. As previously commented, RANS models are too diffusive and, as a consequence, flow behaviour is smoothed.

- In general lines, it is observed that the finer mesh provides results closer to the experimental data, so increasing the refinement could slightly improve the quality of the results. However, it would not be possible to fully reproduce the vortex breakdown phenomenon, as reported in [16] and [18].

Temperature field is given by Fig. (4.15). The following comments can be done:

- At x = 6.8 mm, temperature is clearly overestimated in the location where fuel and oxidizer react. However, the general trend is followed and the reaction zone is well defined.

- At x = 20 mm, x = 40 mm and x = 55 mm, numerical data is almost perfectly fitting the experimental one. This means that flame structure is defined properly at these regions. It should be noted that the maximum temperatures are moved to smaller radial coordinates. This feature should be due to the vortex decay.

- At x = 75 mm, maximum temperatures are reached for experimental data, which shows a peak close to 2000 K. Unluckily, this behaviour has not being obtained with the simulations.

- At x = 150 mm, temperatures start to decrease. This plot illustrates the flame quenching once the fuel has been consumed.

– As happened with velocity field, the finest mesh offers more accurate results. In this case, 83k mesh is clearly outperforming at x = 55 mm and x = 150 mm. In this last case, it seems that even a finer mesh would be able to fully reproduce the experimental temperature field.

In what refers to **mixture fraction**, the following aspects can be pointed out:

– At x = 6.8 mm, the initial conditions can be observed. At r = 0 mm, mixture fraction is almost equal to 1 due to the presence of a fuel predominant mixture. As moving away from the fuel jet (z = 1), the mixture fraction is reduced due to its mixing with the oxidizer (z = 0). Once the position of the air co-flow is reached, mixture fraction is set to 0. Regarding the fitting, numerical results are underestimating the experimental data. This behaviour is also found at x = 20 mm.

– At x = 40 mm and x = 55 mm, very good fittings are found except for small values of the radial coordinate at x = 40 mm. Until this point, the 4 sections described are approximately reproducing the mixing in an adequate way.

– At x = 75 mm and x = 150 mm, bigger deviations are found. Note that at x = 150 mm, mixture fraction is very close to 0. This means that fuel has been almost fully consumed.

– Mixture fraction has been found as the less sensible variable to the level of refinement: important differences are not found until x = 75 mm. As happened with velocity and temperature fields, it could be stated the finest mesh offers better results. At x = 75 mm, it is not so evidence, but this trend is clearly observed at x = 150 mm, where the finest mesh provides numerical results that are closer to the experimental data.

So, after having analysed the velocity, temperature and mixture fraction fields, it can be concluded that vortex decay structures have not been fully described. While, in general terms, flow behaviour is perfectly captured for the zones close to the injector, results are not so satisfactory when moving further, i.e. at vortex breakdown and precessing vortex core.

Despite this fact, the mean features regarding swirling flames have been captured: numerical results show a similar trend to experimental data. So, *swirl* boundary condition has been definitely validated.

To conclude this analysis, temperature field can also be compared with respect to the temperature field captured experimentally, reported at [32]. Fig. (4.17) contains this information with numerical data taken from 83k mesh. Note that the scale is expressed in K. It can allows observing the main points described previously: temperature field zone is well described for values of the longitudinal coordinate close to the injectors inlet although their values are different. Note that experimental temperatures are lower than those obtained numerically.

As moving far away from the inlet, it can be noticed that the numerical results are too diffusive compared with experimental data. It can be seen that flame width is clearly smaller and colder (lower temperature).

Analogously, mixture fraction contour plot is reported in Fig. (4.18). In this case, the width is equal to r = 0.075 m, while the length shown is x = 0.25 m.

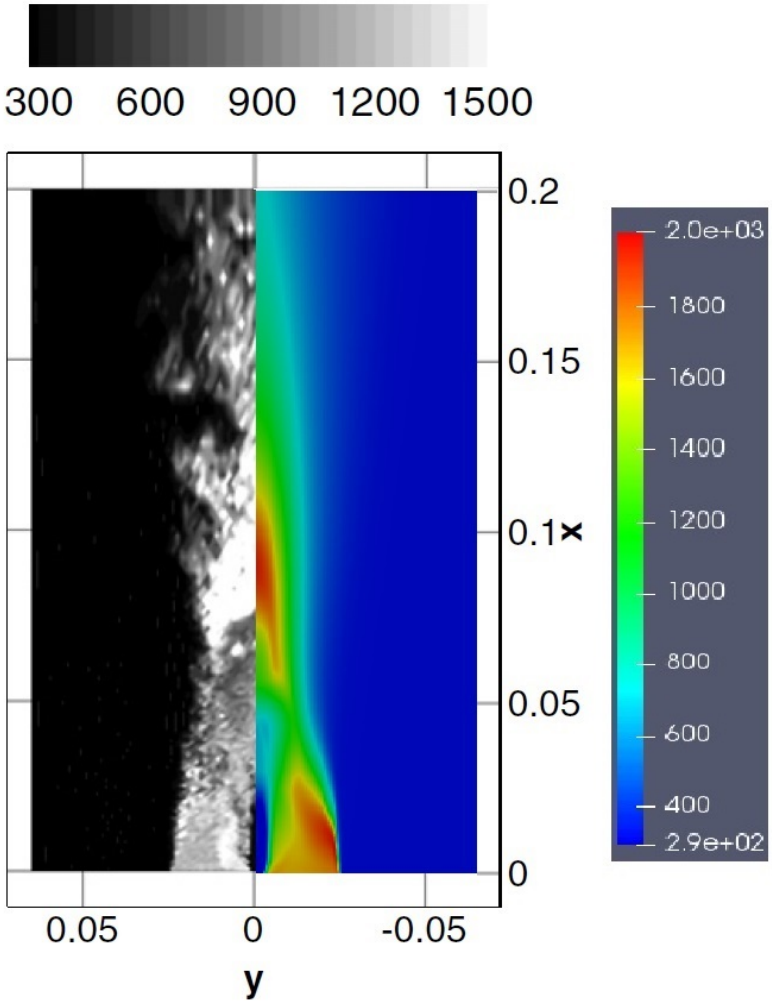

Figure 4.17: Reactive flow - SM1 temperature field comparison

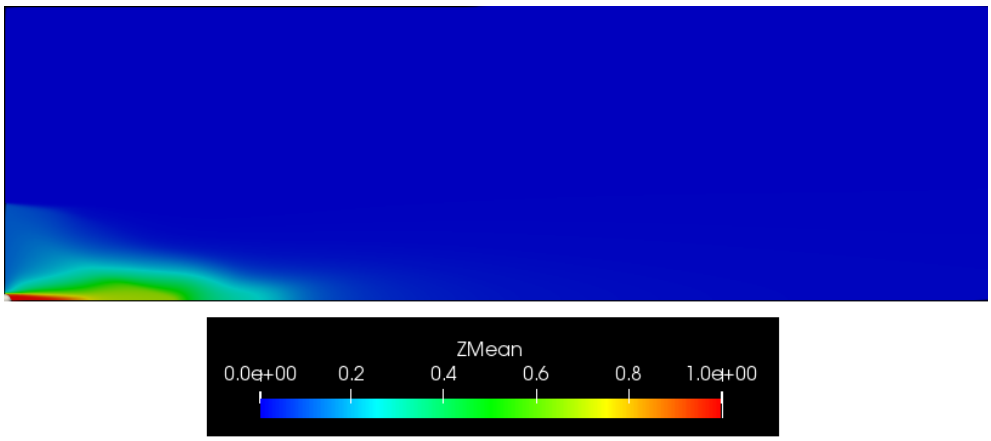

Figure 4.18: Reactive flow - SM1 mixture fraction field

In the case of axial velocity field, contour plot together with vector plot is reported in Fig. (4.19). Scale is given in m/s. Two different vector plots are added in order to recognise the recirculation bubble and the vortex decay structures. They are highlighted.

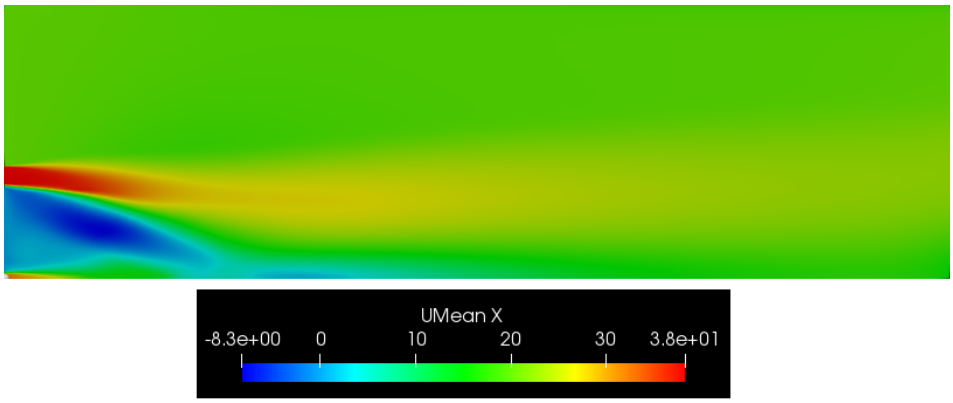

(a) Contour plot

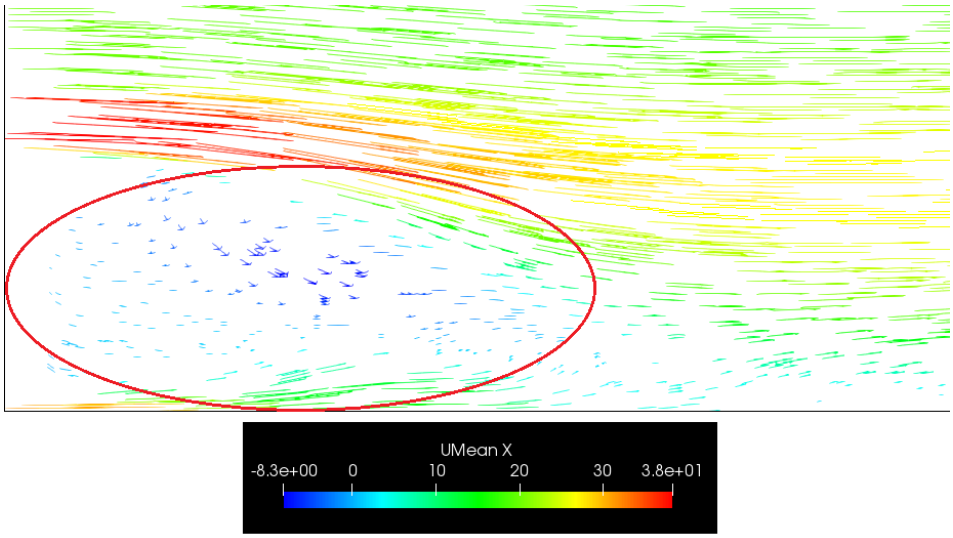

(b) Recirculation bubble

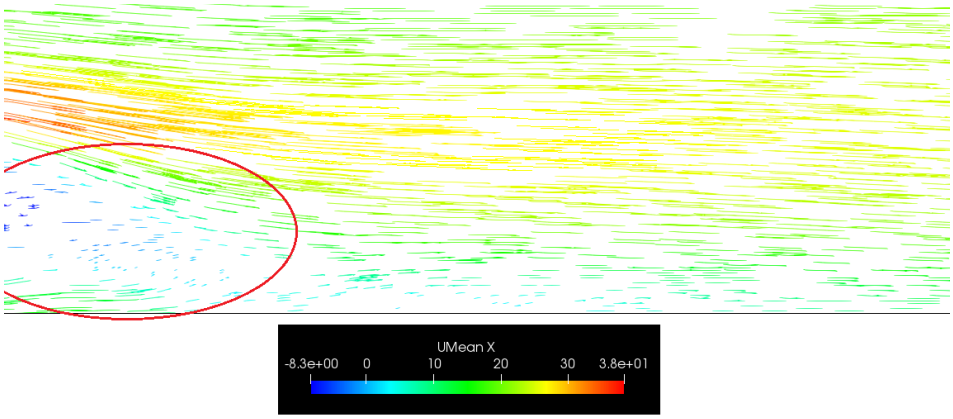

(c) Vortex decay

Figure 4.19: Reactive flow - SM1 axial velocity field

Chapter 5

Conclusions

Swirling flames constitute a growing point of interest for the combustion field, and its study is what has motivated this thesis project. They offer three main advantages: flame stabilization, reduction of unburned gases and mixing enhancement. These features are due to the creation of a recirculation zone, which is related to a complex flow structure derived from the swirl motion.

To capture this flow phenomenon a suitable turbulence modelling should be chosen. This fact raises a detailed discussion in which a compromise between computational cost and accuracy is found by choosing Realizable $k-\epsilon$ as turbulence model (RANS).

Another main point to consider is the strategy followed to solve the combustion. The methodology used is based on Computational Fluid Dynamics techniques which allow solving turbulent combustion problems through the implementation of a numerical approach known as Flamelet approach. It consists on decoupling the combustion process into two subsets: mixing and flame structure. This method is attainable thanks to the introduction of a passive scalar: the mixture fraction z.

Once the theoretical framework required to solve turbulent non-premixed flames is set, it is time to implement a swirling flow in OpenFOAM. This constitutes the main objective of this thesis work. To achieve it, a new boundary condition is set, named *swirl*. A piece of code is added for the velocity inlet condition, whose authority is unknown and, then, a validation process is carried out. Both non-reactive and reactive flow simulations are performed, whose analysis is done by comparing them with experimental data.

Non-reactive flow simulations offer very good results with Realizable $k-\epsilon$ model. However, the flow complexity added when carrying out a simulation regarding SM1 swirling turbulent non-premixed flame of Sydney's burner produces a change of scenario: Realizable $k-\epsilon$ model does not provide so accurate results, as well as computational cost is drastically increased. In fact, mesh independence was not achieved since increasing the level refinement would have mean carrying out computations with time simulations in the order of weeks. This is completely inefficient when using RANS turbulence models, since it is a huge computational cost for the lowest level of turbulence modelling. Once simulations take about a week, introducing LES turbulence model should be considered.

After deeply analysing the results obtained for SM1 flame, it is concluded that further refining the mesh leads to more precise results. However, this numerical results would never perfectly fit the experimental data due to the limitations given by RANS model, which is not able to perfectly capture the flow behaviour derived from the swirl decay.

Despite this fact, *swirl* boundary condition is considered to be validated. This fact opens new possibilities of research.

Chapter 6

Prospective research

This thesis project constitutes a starting point for the study of swirling flames in OpenFOAM environment. So, further research could be done in this field thanks to the validation process accomplished during this thesis project.

Some topics that could be investigated are proposed, such as:

- LES simulations for swirling non-premixed flames. In this way, turbulence will be solved at grid level. This fact will allow capturing vortex breakdown and precessing vortex core phenomena accurately.
- LES simulations for designing high pressure combustion chambers with swirl injector. Since LES turbulence models offer a precise description of the swirl decay, LES simulations can be run to predict combustion chamber performance at a given conditions. In this sense, parametric analysis could eventually be carried out.

Chapter 7

Bibliography

[1] Creta, F. *Combustion course. Lecture notes - The main definitions of Combustion*. Roma.

[2] Creta, F. *Conbustion course. Lecture notes - Rankine Hugoniot Part A*. Roma.

[3] Poinsot, T., & Veynante, D. (2012). *Theoretical and numerical combustion.* Toulouse. Cedex: The authors.

[4] Müller, H., Niedermeier, C., Pfitzner, M., & Hickel, S. (2019). *Steady Laminar Flamelet Modeling for turbulent non-premixed Combustion in LES and RANS Simulations.* München. Retrieved from `https://www.sfbtr40.de/fileadmin/Annual-Reports/annualreport2013/c1-2013.pdf`

[5] Caputo, M. (2019). *A Flamelet Approach for High Pressure Diluted Non-Premixed Flames* (Laurea Magistrale in Ingegneria Spaziale e Astronautica). Sapienza Università di Roma.

[6] Burke–Schumann flame. (2013). Retrieved from `https://en.wikipedia.org/wiki/Burke%E2%80%93Schumann_flame`

[7] Martí Gómez-Aldaraví, P. *Unidad 4 - Turbulencia.* Valencia.

[8] Teorema π de Vaschy-Buckingham. (2019). Retrieved from `https://es.wikipedia.org/wiki/Teorema_%CF%80_de_Vaschy-Buckingham`

[9] Martí Gómez-Aldaraví, P. *Tema 11 - Ecuaciones del flujo medio.* Valencia.

[10] S. Cocic, A., R. Lecic, M., & M. Cantrak, S. (2014). *Numerical analysis of axisymmetric turbulent swirling flow in circular pipe.* Retrieved from `https://www.researchgate.net/publication/274505291_Numerical_analysis_of_axisymmetric_turbulent_swirling_flow_in_circular_pipe`

[11] Dolz, V., Hoyas, S., Pla, B., & Fajardo, P. (2012). *Mecánica de Fluidos.* Valencia: Editorial Universitat Politècnica de València.

[12] Unknown. *Swirling flows.* Retrieved from `http://www.dartmouth.edu/~cushman/courses/engs250/Swirling-flows.pdf`

[13] *Vortex.* (2019). Retrieved from `https://en.wikipedia.org/wiki/Vortex`

[14] H. A. Vaidya et al. (2011). *Numerical simulations of swirling pipe flows- decay of swirl and occurrence of vortex structures.* J. Phys.: Conf. Ser. 318 062022. Retrieved from `https://iopscience.iop.org/article/10.1088/1742-6596/318/6/062022`

[15] Valorani, M. *Corso di Motori Aeronautici. Appunti - Gas Turbines Combustion Chamber*. Roma.

[16] Huang, Y., & Yang, V. (2009). *Dynamics and stability of lean-premixed swirl-stabilized combustion.* Retrieved from https://www.sciencedirect.com/science/article/pii/S0360128509000094

[17] Stein, O., & Kempf, A. (2006). *LES of the Sydney swirl flame series: A study of vortex breakdown in isothermal and reacting flows.* Retrieved from https://www.sciencedirect.com/science/article/pii/S1540748906002598

[18] Yang, Y., & Kaer, S.K. (2012). *Comparison of Reynolds Averaged Navier-Stokes Based Simulation and Large-eddy Simulation for One Isothermal Swirling Flow.* Retrieved from https://link.springer.com/article/10.1007/s11630-012-0530-9

[19] Martí Gómez-Aldaraví, P. *Tema 6 - Introducción al CFD.* Valencia.

[20] Cuoci, A., Frassoldati, A., Faravelli, T., Ranzi, E., OpenSMOKE++. *An object-oriented framework for the numerical modeling of reactive systems with detailed kinetic mechanisms (2015) Computer Physics Communications, 192, pp. 237-264* DOI: 10.1016/j.cpc.2015.02.014

[21] OpenFOAM v6 User Guide: 2 OpenFOAM Tutorials. (2019). Retrieved from https://cfd.direct/openfoam/user-guide/v6-tutorials/

[22] Swirled inlet – CFD Online Discussion Forums. (2015). Retrieved from https://www.cfd-online.com/Forums/openfoam-solving/162659-swirled-inlet.html

[23] RNG k-epsilon model – CFD-Wiki, the free CFD reference. Retrieved from https://www.cfd-online.com/Wiki/RNG_k-epsilon_model

[24] K-epsilon turbulence model. Retrieved from https://en.wikipedia.org/wiki/K-epsilon_turbulence_model

[25] FLUENT 6.3 User's Guide - 9.5.3 Turbulence Modeling in Swirling Flows. Retrieved from https://www.sharcnet.ca/Software/Fluent6/html/ug/node397.htm

[26] Aerospace Mechanical and Mechatronic Engineering - The University of Sydney. Retrieved from http://web.aeromech.usyd.edu.au/thermofluids/swirl.php

[27] Turbulence intensity – CFD-Wiki, the free CFD reference. Retrieved from https://www.cfd-online.com/Wiki/Turbulence_intensity

[28] Martí Gómez-Aldaraví, P. *Tema 7 - Preproceso en CFD.* Valencia.

[29] Kempf, A., Malalasekera, W., Ranga-Dinesh, K., & Stein, O. (2007). *Large Eddy Simulations of Swirling Non-premixed Flames With Flamelet Models: A Comparison of Numerical Methods.* Retrieved from https://link.springer.com/article/10.1007/s10494-008-9147-1

[30] KALT, P., AL-ABDELI, Y., MASRI, A., & BARLOW, R. (2002). *Swirling turbulent non-premixed flames of methane: Flow field and compositional structure.* Retrieved from https://www.sciencedirect.com/science/article/pii/S1540748902802322

[31] Wolfram—Alpha: Making the world's knowledge computable. Retrieved from https://www.wolframalpha.com/

[32] James, S., Zhu, J., & Anand, M. (2007). *Large eddy simulations of turbulent flames using the filtered density function model.* Retrieved from https://www.sciencedirect.com/science/article/pii/S1540748906001684